DESIGN AND FABRICATION OF MILLIMETER WAVE ANTENNA FOR FUTURE WIRELESS APPLICATIONS

Thesis Submitted for the Award of the Degree of

DOCTOR OF PHILOSOPHY

in

Electronics and Communication Engineering

By

Reena Aggarwal

41800516

Supervised By

Dr. Ajay Roy (22652)

ECE (Professor)

Lovely Professional University

Co-Supervised By

Dr. Rajeev Kumar

ECE (Associate Professor)

Chitkara University

LOVELY PROFESSIONAL UNIVERSITY, PUNJAB

2026

DECLARATION

I, hereby declare that the presented work in the thesis entitled "Design and Fabrication of Millimeter Wave Antenna for Future wireless Applications" in fulfilment of degree of **Doctor of Philosophy (Ph.D.)** is outcome of the research work carried out by me under the supervision of Dr. Ajay Roy, working as Professor, in the School of Electronics and Electrical Engineering of Lovely Professional University, Punjab, India, and Dr. Rajeev Kumar, working as Associate Professor in the Department of Electronics and Communication Engineering of Chitkara University Institute of Engineering and Technology, Punjab, India. In keeping with general practice of reporting scientific observations, due acknowledgements have been made whenever work described here has been based on findings of other investigator. This work has not been submitted in part or full to any other University or Institute for the award of any degree.

(Signature of Scholar)

Name of the scholar:	Reena Aggarwal
Registration No.:	41800516
Department/School:	School of Electronics and Electrical Engineering
Lovely Professional University	
Punjab, India	

CERTIFICATE

This is to certify that the work reported in the Ph.D. thesis entitled "Design and Fabrication of Millimeter Wave Antenna for Future Wireless Applications" submitted in fulfillment of the requirement for the award of degree of **Doctor of Philosophy (Ph.D.)** in the School of Electronics and Electrical Engineering, is a research work carried out by Reena Aggarwal, 41800516, is bonafide record of her original work carried out under my supervision and that no part of thesis has been submitted for any other degree, diploma or equivalent course.

(Signature of Supervisor)
Name of Supervisor:
Designation:
Department/school:
University:

(Signature of Co-Supervisor)
Name of Co-Supervisor:
Designation:
Department/school:
University:

कर्मण्येवाधिकारस्ते मा फलेषु कदाचन।
मा कर्मफलहेतुर्भूर्मा ते सङ्गोऽस्त्वकर्मणि।। २-४७

Abstract

The exponential growth in data demand, driven by applications such as cloud computing, social networking, e-commerce, and high-definition video streaming, has placed immense pressure on existing wireless communication networks. As 4G *LTE* networks struggle with congestion and bandwidth limitations, the transition to fifth generation (5G) and future wireless systems necessitates the development of high-performance *Millimeter Wave* (*mmWave*) antennas that can support ultra-high data rates, minimal latency, and enhanced spectral efficiency. The mmWave spectrum (30–300 GHz) offers significant advantages, including wider bandwidth availability and reduced signal congestion. However, challenges such as high propagation losses, *Non-Line of Sight* (*NLoS*) limitations, mutual coupling, and design constraints hinder the full potential of mmWave *Multiple-Input Multiple-Output* (*MIMO*) antennas.

This research focuses on the design, fabrication, and performance evaluation of a compact 4×4 *MIMO* antenna for 5G mmWave applications, n261 frequency band (27.5–28.35 GHz), with a bandwidth of 850 MHz. The proposed antenna features a rectangular patch with four diamond-shaped slots to enhance impedance matching, along with a dumbbell-shaped *Defected Ground Structure* (*DGS*) to minimize mutual coupling. Fabricated on an ultra-thin Rogers RT/Duroid 5880 substrate (0.254 mm thick), the design maintains a compact footprint of 20 mm × 19 mm × 0.254 mm, making it suitable for next-generation wireless devices. The study is structured around four key objectives to ensure a comprehensive exploration of the topic. First, it conducts comparative analysis of planar *MIMO* antenna technologies, where a wide range of existing planar antenna architectures is critically evaluated, including slot/patch-based antennas, *Defected Ground Structure* (*DGS*), *Dielectric Resonator Antenna* (*DRA*), metasurface-based designs, and *MIMO* antenna arrays. The performance of these antennas is assessed based on critical parameters such as operating frequency, bandwidth, gain, isolation, diversity gain, radiation efficiency, and the number of antenna elements. This comparative analysis helps identify gaps in current designs and highlights potential areas for performance improvement. Second, the research presents the development of single-element and four-element *MIMO* antenna designs, engineered to operate efficiently within the mmWave spectrum. A special emphasis

is placed on improving radiation efficiency, bandwidth, and isolation to meet the stringent requirements of next-generation communication systems. The proposed designs incorporate novel slot geometries, enhanced feed structures, and engineered ground plane configurations to enhance overall performance. Third, extensive parametric studies are conducted to fine-tune various antenna parameters, including feed and ground plane dimensions, slit lengths, slot widths, and decoupling structures. These optimizations contribute to improvements in impedance matching, bandwidth, gain, and inter-element isolation, ensuring that the antennas meet the required performance standards for *MIMO*-based mmWave communication. The final stage involves the realization of the optimized designs through fabrication and rigorous experimental testing. The antennas are fabricated using state-of-the-art techniques and tested under real-world conditions to validate their performance. Simulations are conducted using Ansys HFSS, while fabricated prototypes are evaluated at leading research facilities. The following experimental setups are used: S-parameter measurements are performed using a *Vector Network Analyzer* (*VNA*) at the Microwave and Antenna Research Laboratory, Thapar Institute of Engineering and Technology (TIET), Patiala. Radiation pattern assessments are conducted in an anechoic chamber at Banasthali Vidyapith, Jaipur, ensuring accurate characterization of the antennas' radiation properties.

The results obtained from both simulations and experimental validations show a strong correlation, confirming the effectiveness of the proposed designs. The developed antennas exhibit low *Envelope Correlation Coefficient* (ECC $<$ 0.011), high *Diversity Gain* (DG $>$ 9.90 dB), and excellent isolation performance (better than -19.5 dB). These features make them highly suitable for 5G and beyond communication networks, including applications in *Internet of Things* (*IoT*), *Vehicle-to-Everything* (*V2X*) communication, and next-generation wireless systems.

By integrating advanced fabrication techniques, rigorous experimental verification, and novel design strategies, this research significantly contributes to the field of mmWave *MIMO* antenna technology. The findings from this work provide valuable insights for the development of compact, high-efficiency antennas capable of supporting high-data-rate wireless communication systems, paving the way for advancements in 6G and future wireless networks.

Acknowledgements

High achievement always takes place in the framework of high expectation. The expectation was there and I begin with determined resolve and put in sustained hard work. It has been rightly said that every successful individual knows that his or her achievement depends on a community of persons working together but the satisfaction that accompanies the successful completion of any task would be incomplete without mentioning those people who made it possible.

This is to acknowledge with gratitude the guidance and suggestions from my supervisor, **Dr. Ajay Roy**, and co-supervisor **Dr. Rajeev Kumar** and my former co-supervisor **Dr. Gurpreet Kumar** for their support and motivation throughout the thesis work.

I am grateful to the members of the School of Research Degree Programme (RDP) for being in my entire research progress review panel, providing useful suggestions during the period. I am indeed thankful to all anonymous reviewers of my research papers submitted to various international journals and international conferences, due to which I was able to improve upon the work containing herein.

I am indebted to Honorable Chancellor, Worthy Pro-Chancellor, the Pro-Vice-Chancellor, and the successive Deans, LPU, for facilitating the administrative issues involved and encouraging me throughout. I express my heartfelt gratefulness to Head of School, School of Electronics and Electrical Engineering, and the staff for their cooperation and support. I am also thankful to NITTTR, Chandigarh, Banasthali Vidyapith, Jaipur, and Thapar Institute of Engineering and Technology, Patiala for their help in the simulation, fabrication, and testing process of the work.

I express my deepest gratitude to my husband Mr. Pardeep Mittal, my parents, grandparents, for their cooperation, support, and encouragement in this endeavor and my kids Urvi Mittal and Vivan Mittal for their wholehearted, and endless support and patience. No words of thanks are enough to express my deepest gratitude and sincerest love to my in-laws whose rock-solid faith in me kept me strong in all circumstances. They always stood by me in all difficult times and reinforced my confidence. I would also like to pay my sincere regards to my relatives for their constant motivation and support. Their words of encouragement made this journey easier.

I express my special thanks to **Dr. Akanksha Sharma**, for helping and guiding me in writing thesis and preparing presentation using LaTex. I express my gratitude to all those whom I have worked, interacted, and whose thoughts have helped me in furthering my grasp and understanding of the subject.

Last but not the least, I bow in reverence to *Almighty* who has always showered blessings on me at each and every step to complete this Thesis.

Reena Aggarwal

(41800516)

Contents

Abstract ..... **ii**

Acknowledgements ..... **iv**

Contents ..... **vi**

List of Figures ..... **ix**

List of Tables ..... **xiii**

Abbreviations ..... **xv**

1 Introduction **1**

1.1 Overview *1*

1.2 Millimeter Wave System *2*

1.3 Importance of MIMO Antennas in mmWave Communications *6*

1.4 Challenges in MIMO Antenna Design *6*

1.5 Motivation of Thesis *7*

1.6 Research Gaps *9*

1.7 Research Objectives *10*

1.8 Research Contribution *10*

1.9 Research Methodology *11*

1.10 Thesis Organization *11*

2 Literature Survey **14**

2.1 Introduction *14*

2.2 Sub-6 GHz and UWB (3 - 12 GHz) *14*

2.3 Literature Review of Single-Port Antenna for 5G Applications *15*

2.4 Study of 2-Port Antenna for 5G Applications *16*

2.5 Study of 4-Port Antenna for 5G Applications *20*

2.6 Study of 8-Port Antenna for 5G Applications *25*

2.7 Summary *30*

3 Comparative Analysis of various Planar MIMO Antennas operating in Millimeter Frequency range. 31

3.1 Overview ***31***

3.2 Classification of Planar MIMO Antennas for mmWave Applications ***32***

3.3 MIMO Antenna Performance Metrics for Comparison ***32***

3.3.1 Envelope Correlation Coefficient (ECC) *33*

3.3.2 Diversity Gain (DG) *33*

3.3.3 Total Active Reflection Coefficient (TARC) *34*

3.3.4 Channel Capacity Loss (CCL) *35*

3.3.5 Radiation pattern *36*

3.3.6 Bandwidth (BW) *38*

3.3.7 S-Parameters *39*

3.3.8 Directivity (D) *40*

3.3.9 Antenna Gain (G) *40*

3.3.10 Efficiency *41*

3.4 Comparative Analysis of Planar MIMO Antennas for mmWave Range ***42***

3.4.1 Slot/Patch MIMO Antennas *42*

3.4.2 Defected Ground Plane MIMO Antennas *47*

3.4.3 MIMO Antenna Array *52*

3.4.4 Dielectric Resonator Antennas (DRAs) *59*

3.4.5 Metamaterial/Metasurface Structures *67*

3.5 Chapter Summary ***72***

4 Design of a Planar Antenna for Millimeter Wave (mmWave) band 73

4.1 Introduction ***73***

4.2 Design Configuration of a Proposed Single Antenna ***73***

4.3 Evolution of Proposed Antenna Design ***78***

4.3.1 Antenna Feeding Techniques and Rationale for Microstrip Line Feed Selection *82*

4.4 Parametric Analysis ***84***

4.5 Results and Discussion ***92***

4.5.1 Return Loss Performance of Single Planar Antenna at 28 GHz *92*

4.5.2 Radiation and Total Efficiency *93*

4.5.3 Directivity *94*

4.5.4 Gain *95*

4.5.5 Effect of Gain with and without DGS *96*

4.5.6 Effect of Return Loss with and without DGS *97*

4.5.7 Radiation Pattern *98*

4.5.8 Surface Current *100*
4.6 Summary ***102***

5 Design of a Planar MIMO Antenna for Millimeter Wave (mmWave) band. 103
5.1 Introduction ***103***
5.2 MIMO Antenna Design ***104***
5.3 Parametric Study of Proposed 4 x 4 MIMO Antenna ***107***
5.3.1 Spatial Configuration and Decoupling *107*
5.3.2 Frequency Domain Characteristics (S-Parameters) *107*
5.3.3 Mutual Isolation vs. Inter-element Gap *109*
5.3.4 ECC vs. Inter-element Gap *110*
5.3.5 Effect of Increasing Edge-to-Edge Spacing to 5 mm *111*
5.3.6 Final Optimized Configuration *112*
5.3.7 Conclusion *112*
5.4 Fabrication and Prototyping of the Proposed MIMO Antenna ***113***
5.4.1 Measurement Setup *115*
5.5 Results and Discussion ***116***
5.5.1 S-Parameters *116*
5.5.2 Radiation Characteristics *121*
5.5.3 MIMO Parameters *129*
5.5.4 Surface Current *132*
5.6 Summary ***137***

6 Conclusions and Future Scope 138
6.1 Conclusion ***138***
6.2 Future Work ***139***

List of Publications 141

References 142

List of Figures

Fig. 1.1 ***Internet usage statistics given by Extremely High Frequency (EHF)****. Source: Mane et al. (2023), as reproduced in Design and Fabrication of Millimeter Wave Antenna for Future Wireless Applications (2024, p. 2)* *2*

Fig. 1.2 ***Internet usage statistics of top 15 countries with the largest internet users as of October 2025*** *(Source: Statista)* *3*

Fig. 1.3 ***Advantages of millimeter wave*** *4*

Fig. 1.4 ***Millimeter wave's applications*** *4*

Fig. 1.5 ***Regional Allocation of 5G mmWave Spectrum in the 24–30 GHz Range, Highlighting Key Bands for FR2 Deployment (Source: Telecom Gurukul, "5G NR Frequency Bandwidth: Everything You Need to Know," May 2023)*** . . *8*

Fig. 3.1 ***Types of MIMO antenna for Millimeter Wave (mmWave)*** *32*

Fig. 3.2 ***Radiation characteristics of the MIMO antenna, depicting The direction of the power's radiation.*** *37*

Fig. 3.3 ***Figure illustrates the process of determining the bandwidth of the MIMO antenna system based on the S-parameters.*** *39*

Fig. 3.4 ***Scattering parameter illustrations with a two-port network*** *40*

Fig. 3.5 *Fabricated slot/patch MIMO design. Source: (a) Kobal et al. (2022), (b) Wang et al. (2022), (c) Jabeen & Khan (2022), (d) Usman et al. (2022), (e) Sehrai et al. (2020), (f) Patel et al. (2022), (g) Jetti et al. (2023), (h) El-Nady & Attiya (2022), (i) Ali et al. (2021), as reproduced in Design and Fabrication of Millimeter Wave Antenna for Future Wireless Applications (2024, p. 45).* . . . *44*

Fig. 3.6 *Fabricated defected ground plane MIMO design. Source: (a) Farooq & Lokam (2023), (b) Khalid et al. (2020), (c) Abdullah et al. (2021), (d) Patel et al. (2022), (e) Sharma & Arora (2022), (f) Joseph et al. (2023), (g) Abbas et al. (2023), as reproduced in Design and Fabrication of Millimeter Wave Antenna for Future Wireless Applications (2024, p. 52).* *51*

Fig. 3.7 *Fabricated MIMO array design. Source: (a) Kumar & Kumar (2023), (b) Hussain et al. (2022), (c) Tahat et al. (2020), (d) Yang et al. (2017), (e) Kamal et al. (2021), (f) Bilal et al. (2022), (g) Malviya & Gupta (2023), (h) Khan et al. (2022), (i) Ud Din et al. (2023), (j) Mandloi et al. (2023), as reproduced in Design and Fabrication of Millimeter Wave Antenna for Future Wireless Applications (2024, p. 57).* *55*

Fig. 3.8 *Fabricated DRA array antennas. (a) Source: Pan et al. (2019), (b) Source: Zhang et al. (2019), as reproduced in Design and Fabrication of Millimeter Wave Antenna for Future Wireless Applications (2024, p. 66).* *64*

Fig. 3.9 ***Fabricated Metamaterial Inspired antennas. Source: (a) Singh et al. (2022), (b) Tadesse et al. (2022), (c) Esmail & Koziel (2023), (d) Tariq et al. (2021), (e) Hussain et al. (2020), (f) Kumar & Dixit (2021), as reproduced in Design and Fabrication of Millimeter Wave Antenna for Future Wireless Applications (2024, p. 70).*** *68*

Fig. 4.1 ***Top view of the feed plane of the proposed single-element antenna, showing the inset-fed rectangular patch with integrated circular and diamond-shaped slots for impedance tuning and bandwidth enhancement.*** *75*

Fig. 4.2 ***Top view of the ground plane featuring a dumbbell-shaped Defected Ground Structure (DGS) composed of two circular slots connected by a rectangular slot, with embedded circular patches to improve impedance matching and radiation efficiency.*** *77*

Fig. 4.3 ***Progressive evolution of single element antenna design showing systematic modifications to feed and ground planes across four design iterations (a-d) for performance enhancement.*** *79*

Fig. 4.4 ***Return loss (S_{11}) comparison across four design iterations for the n261 band (27.5–28.35 GHz).*** *81*

Fig. 4.5 ***Parametric analysis of the circular slot radius (R_s) on the feed plane, showing its influence on the resonant frequency and impedance matching of the antenna.*** *84*

Fig. 4.6 ***Effect of varying the feed-plane circular slot radius (Rs) on the Return Loss (S_{11}) of the designed antenna.*** *85*

Fig. 4.7 ***Effect of Length of slit along the Feed-line (Ls) on antenna frequency tuning.*** *86*

Fig. 4.8 ***Effect of varying the Length of slit along the Feed-line (Ls) on the return loss (S_{11}) of the designed antenna*** *87*

Fig. 4.9 ***Parametric analysis of the circular slot radius (R_c) in the ground-plane Defected Ground Structure (DGS), demonstrating its role in tuning the resonant frequency and bandwidth of the antenna.*** *88*

Fig. 4.10 ***Simulated S_{11} response for varying circular slot radii (R_c) in the DGS, illustrating frequency tuning and impedance matching improvement within the 5G n261 band.*** *89*

Fig. 4.11 ***Parametric study of the interconnecting rectangular slot width (W_{id}) in the dumbbell-shaped Defected Ground Structure (DGS), showing its impact on the antenna's resonant frequency.*** *91*

Fig. 4.12 ***(S_{11}) characteristics for different widths (W_{id}) of the rectangular slot in the DGS, highlighting bandwidth control and resonance alignment with the n261 band.*** *91*

Fig. 4.13 ***Simulated Return Loss (S_{11}) of single planar antenna vs. Frequency.*** *93*

Fig. 4.14 ***Simulated results of single planar antenna in terms of Radiation and Total Efficiency vs. Frequency*** *94*

Fig. 4.15 ***Simulated results of single planar antenna in terms of Directivity vs. Frequency*** *95*

Fig. 4.16 ***Simulated results of single planar antenna in terms of Gain vs.Frequency*** . . *96*

Fig. 4.17 ***Simulated results representing the effect of Gain with and without DGS vs.Frequency*** *97*

Fig. 4.18 ***Simulated results representing the effect of Return loss (S_{11}) with and without DGS vs.Frequency*** *98*

Fig. 4.19 ***Simulated results of Radiation pattern for single planar antenna.*** *99*

Fig. 4.20 ***Surface current distribution for single planar antenna*** *101*

Fig. 5.1 ***Structural design of a proposed MIMO Antenna (a) Feed Plane (Top view) (b) Ground Plane (Top View)*** *106*

Fig. 5.2 ***Parametric study of Mutual Isolation (S_{21}) versus Frequency for different edge-to-edge spacings between antenna elements.*** *108*

Fig. 5.3 ***Parametric variation of Return Loss (S_{11}) with Frequency for different edge-to-edge spacings between antenna elements.*** *109*

Fig. 5.4 ***Variation of mutual isolation (S_{21}) with inter-element spacing at the operating frequency of 28 GHz.*** *110*

Fig. 5.5 ***Parametric study of Envelope Correlation Coefficient (ECC) against inter-element spacing, illustrating how increased separation reduces correlation between antenna elements for improved MIMO performance.*** . . *111*

Fig. 5.6 ***Fabricated prototype of proposed MIMO antenna a) Feed Plane (Top view) b) Ground Plane (Bottom View)*** *114*

Fig. 5.7 ***Measurement setup (a) Prototype Testing under Anechoic chamber (b) Prototype Testing under Vector Network Analyzer (VNA)*** *116*

Fig. 5.8 ***Calculated Reflection Co-efficient for different elements of a proposed MIMO antenna (a) Represents Simulated values (b) Represents Measured values*** . . *117*

Fig. 5.9 ***Calculated Isolation among different elements of a proposed MIMO antenna (a) Represents Simulated values (b) Represents Measured values*** *120*

Fig. 5.10 ***Radiation Characteristics (dB)*** *122*

Fig. 5.11 ***Radiation pattern representing the Co and Cross-polarization behavior of Ant-1 at different frequency range (a) 27.7 GHz (b) 28 GHz (c) 28.25 GHz*** . . *124*

Fig. 5.12 ***Radiation pattern representing the Co and Cross-polarization behavior of Ant-2 at different frequency range (a) 27.7 GHz (b) 28 GHz (c) 28.25 GHz*** . . *126*

Fig. 5.13 ***Radiation pattern representing the Co and Cross-polarization behavior of Ant-3 at different frequency range (a) 27.7 GHz (b) 28 GHz (c) 28.25 GHz*** . . *128*

Fig. 5.14 ***Radiation pattern representing the Co and Cross-polarization behavior of Ant-4 at different frequency range (a) 27.7 GHz (b) 28 GHz (c) 28.25 GHz*** . . *129*

Fig. 5.15 ***Performance metrics of proposed MIMO antenna in terms of Envelope Correlation Coefficient (ECC)*** *130*

Fig. 5.16 ***Performance metrics of proposed MIMO antennain terms of Diversity Gain (DG)*** *131*

Fig. 5.17 ***The proposed MIMO antenna's surface current distribution at 27.8 GHz when Antenna-1 is excited (a) A feed plane that depicts the top view (b) The ground plane, which depicts the bottom view*** *133*

Fig. 5.18 ***Surface current distribution for the proposed MIMO antenna at 27.8 GHz when Antenna-2 is energized. Top view represents (a) the feed plane and (b) the ground plane. (c) Ground surface represents the bottom view.*** *135*

List of Tables

Tab. 1.1 Design Requirements for Millimeter-Wave Antennas 5

Tab. 1.2 Downlink and Uplink Frequencies for NR Operating Bands 9

Tab. 3.1 Comparison between the Performances of Slot and Patch MIMO antennas . . . 48

Tab. 3.2 Comparison between the Performances of the Defected Ground Structure (DGS) MIMO antenna. 53

Tab. 3.3 Comparison of the performance of MIMO design 58

Tab. 3.4 Comparison of Performance for Millimeter Wave DRAs 61

Tab. 3.5 Comparison of Performance for DRA Arrays 63

Tab. 3.6 Comparison performances of Circularly Polarized DRAs. 66

Tab. 3.7 Comparison of the performances of Metamaterial/Metasurface structures. . . . 71

Tab. 4.1 Dimensional Specifications of the Feed Plane for a Single Antenna 76

Tab. 4.2 Dimensional Specifications of the Ground Plane for a Single Antenna 78

Tab. 4.3 Resonant Frequency and Bandwidth for Different Values of Rs 85

Tab. 4.4 Resonant Frequency and Bandwidth for Different Values of Ls 87

Tab. 4.5 Parametric analysis of the circular slot radius (R_c) in the ground-plane Defected Ground Structure (DGS): resonant frequency, bandwidth, and fractional bandwidth for 5G n261 band optimization. 90

Tab. 4.6 Impact of rectangular slot width (W_{id}) in the Defected Ground Structure (DGS) on resonant frequency, bandwidth, and fractional bandwidth, demonstrating precise tuning for mmWave 5G operation. 92

Tab. 5.1 Dimensions of proposed MIMO antenna parameters in mm 106

Tab. 5.2 Comparing Measured Radiating Frequency Ranges with Simulated Ranges and Fractional Bandwidth 118

Tab. 5.3 Comparison of Simulated and Measured Reflection Coefficient S_{11} (dB) 118

Tab. 5.4 Comparing Measured and Simulated Isolation (dB) 120

Tab. 5.5 Performance comparison of the proposed MIMO antenna with recent state-of-the-art designs 136

Abbreviations

ADS	Advanced Design System
AVA	Antipodal Vivaldi Antenna
CCL	Chammel Capacity Loss
CP	Circularly Polarized
CPW	Co-Planar Waveguide
CSR	Circular Split Ring
CSRR	Complementary Split Ring Resonator
CST	Computer Simulation Tool
DB-DGS	Dumbbell Shaped-Defected Ground Structure
D2D	Device-to-Device
DG	Diversity Gain
DGS	Defected Ground Structure
DR	Dielectric Resonator
DRA	Dielectric Resonator Antenna
EBG	Electromagnetic Band Gap
ECC	Envelope Correlation Coefficient
EHF	Extremely high Frequency
FCC	Federal Communications Commission
FR2	Frequency Range 2
FSS	Frequency Selective Surface
HFSS	High Frequency Structure Simulator
IBFD	In Band Full Duplex

IEEE	Institute of Electrical and Electronics Engineers
IoT	Internet of Things
ITU	International Telecommunication Union
LCP	Liquid Crystal Polymer
LHCP	Left-Handed Circular Polarization
LoS	Line of Sight
LPF	Low Pass Filter
LTE	Long Term Evolution
MEG	Mean Effective Gain
MIMO	Multiple-Input Multiple-Output
mmWave	Millimeter Wave
MPA	Microstrip Patch Antenna
MSA	Microstrip Slot Antenna
NIM	Negative Index Metamaterial
NLoS	Non-Line of Sight
NR	New Radio
PD	Power Divider
PIFA	Planar Inverted-F Antenna
RHCP	Right-Handed Circular Polarization
RF	Radio Frequency
Rx	Receiver
SIC	Successive Interference Cancellation
SIW	Substratte Integrated Waveguide
SNR	Signal-to-Noise Ratio

SRR	Split Ring Resonator
STAR	Simultaneous Transmit and Receive
TARC	Total Active Reflection Coefficient
TDD	Time Division Duplex
TRAI	Telecommunication Regulatory Authority of India
TSA	Tapered Slot Antenna
Tx	Transmitter
UHF	Ultra High Frequency
VNA	Vector Network Analyzer
VSWR	Voltage Standing Wave Ratio
V2X	Vehicle-to-Everything
Wi-Fi	Wireless Fidelity
WiGig	Wireless Gigabit
WLAN	Wireless Local Area Network

Chapter–1

Introduction

1.1 OVERVIEW

With the constant demand for data, network providers must work harder to provide high-speed mobile internet. Most apps are hosted in the cloud or online, which demands continuous data speeds and low latency [1]. 5G technology makes this possible. Many nations are building 5G infrastructure to better serve their customers. The *Telecommunications Regulatory Authority of India (TRAI)* just released 26 GHz mmWave spectrum for 5G in India, so vendor services may start soon [2].

The *International Telecommunication Union (ITU)* predicts almost five billion internet users by 2023. This group comprises 67 percent of the global population. The world will have 5.4 billion internet users by December 31, 2023. Figure 1.1 shows average consumption of data over the past two decades and Figure 1.2 shows, as of February 2025, India has over 806 million internet users, as noted by Statista, thereby placing it just behind China (1.11 billion) and well ahead of the United States (322 million). Due to its limited bandwidth and growing user base, 4G *Long Term Evolution (LTE)* data support capability is at capacity. Despite its limits, mmWave for 5G could improve data throughput due to its large bandwidth [3]. Most nations are deploying 5G in Group 30 and 40 channels at mmWave, per WRC recommendations [4]. Forge et al. in [5] presented the 5G deployment plans and policies for the low income countries based on research on 5G-enabled states. This research focused on 5G-implemented nations.

This chapter is organized into seven sections. Section 1.1 describes the brief overview of the area under study. Section 1.2 and Section 1.3 give the introduction to mmWave systems and the importance of antennas in mmWave systems respectively. Further, Section 1.4 provides the

motivation of the research, and Section 1.5 represents the various research gaps. Finally, Section 1.6 and Section 1.7 hold the objectives and thesis organization of the work respectively.

1.2 MILLIMETER WAVE SYSTEM

Wireless communication technology is expanded by the mmWave's large bandwidth at 30-300 GHz [6]. The mmwave wavelength is 1–10 mm, which is *Extremely High Frequency (EHF)* according to *International Telecommunication Union (ITU)* regulations. The *Federal Communications Commission (FCC)* improved the least mmWave spectrum to 400 MHz [7] because of the longer wavelength and wider spectrum, compared to 4G *Long Term Evolution (LTE)*. Figure 1.3 shows mmWave benefits.

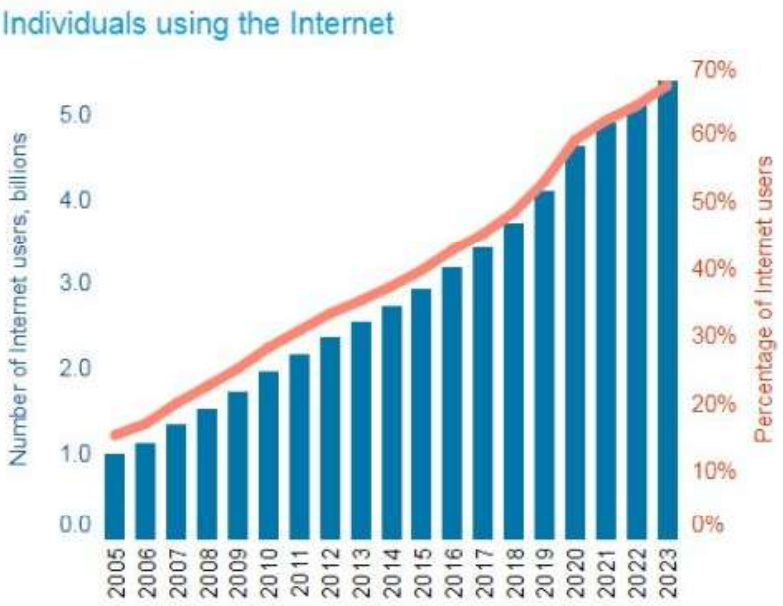

Fig. 1.1: Internet usage statistics given by Extremely High Frequency (EHF). Source: Mane et al. (2023), as reproduced in Design and Fabrication of Millimeter Wave Antenna for Future Wireless Applications (2024, p. 2)

The signal baud rate may transport more information due to mmWave's high carrier frequency, resulting in a higher rate of data (bits/sec/Hz) & reduced the time of buffering while producing high-quality films [2]. Cellular communication exploits frequency reuse through cell

splitting and sectoring to expand network coverage due to the mmWave's limited range [8]. As shown in Figure 1.4, other mmWave applications include 5G and small cell concept, HD video, Satellite Communication, Automotive, Body Scanner, Radar and image sensing, headsets of virtual reality, medical-mmWave therapy, military, *Institute of Electrical and Electronics Engineers (IEEE)* 802.11ad *Wireless Gigabit (WiGig)* technology and IoT [9].

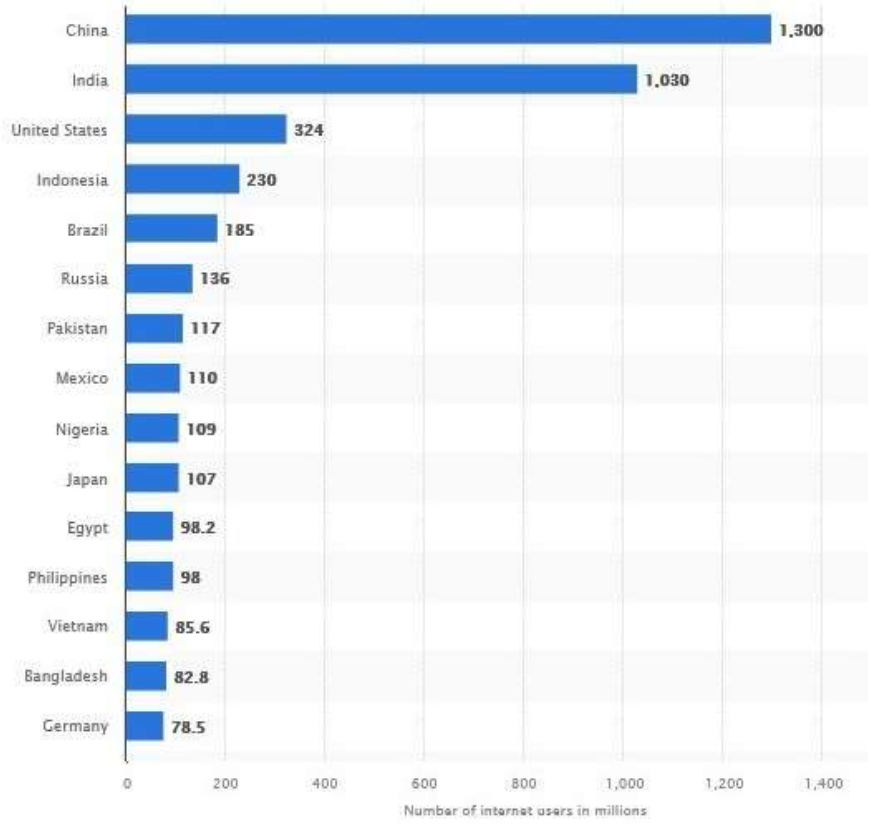

Fig. 1.2: Internet usage statistics of top 15 countries with the largest internet users as of October 2025 (Source: Statista)

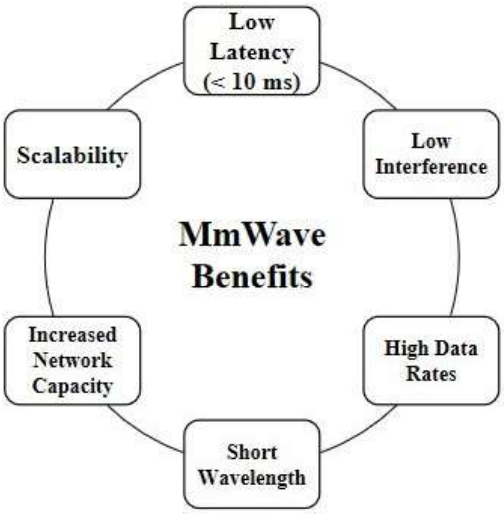

Fig. 1.3: Advantages of millimeter wave

Fig. 1.4: Millimeter wave's applications

Besides its benefits, mmWave has numerous limitations, including air attenuation from gaseous losses (such as water vapor and oxygen absorption of radio signals) rain, and propagation

path losses [10]. Above 10 GHz, atmospheric H_2O and O_2 molecules impede mmWave signals. The signal is greatly attenuated by H_2O at the frequencies of 20 GHz, 200 GHz, and 250 GHz and O_2 at 4 GHz and 100 GHz. Due of its shorter wavelength than rainfall or plants, mmWave signals scatter. Another drawback of mmWave is that its shorter wavelength prohibits it from traveling through dense structures, limiting it to *Line of Sight (LoS)* communication [11]. *Non-Line of Sight (NLoS)* mmWave channel measurement studies in (urban/suburban) areas have given low route loss exponent and signal spread, making it popular for 5G applications. High gain and directivity are dependent on the antenna in wireless communication systems [12, 13, 14]. An early mmWave study [15] suggested a reflector design, lenses, arrays, and horn technique to boost antenna gain.

Table 1.1: Design Requirements for Millimeter-Wave Antennas

Parameter	**Desired Value**
Bandwidth	$>$ 500 MHz (24 GHz - 100 GHz)
Radiation Efficiency	$>$ 70%
Phase Response	Linear or Circular (for MIMO and CP Applications)
Radiation Pattern	Directional or Beamforming
Gain	$\geq$ 8 dBi for mobile; $\geq$ 20 dBi for fixed applications
Substrate Material	Low-loss dielectric (e.g., Rogers RT/Duroid 5880, Taconic)
Physical Size	Compact

Table 1.1 illustrates the different parameters vital for designing a mmWave antenna. *Millimeter Wave (mmWave)* antennas play an important function in modern radio transmission, particularly in 5G and forthcoming networks. To effectively support high-speed data transmission and low-latency communication, these antennas must meet several key design criteria. One of the primary requirements is wide bandwidth, typically exceeding 500 MHz within the 24 GHz–100 GHz range, to accommodate the increasing data demands of wireless applications. Additionally, achieving high radiation efficiency above 70% is essential to minimize power loss and maximize signal strength. The specified gain refers to the total realized gain of the antenna system (array), necessary to overcome mmWave path loss and meet application-specific link budgets. These

requirements are grounded in real-world propagation physics, regulatory constraints, and industry standards for 5G, WiGig, and fixed wireless access systems. The choice of substrate material is equally important, with low-loss dielectric materials like Rogers RT/Duroid 5880 and Taconic being preferred due to their minimal signal attenuation at high frequencies. Finally, compact size is crucial for easy integration into modern wireless devices, including smartphones, base stations, and IoT sensors.

1.3 IMPORTANCE OF MIMO ANTENNAS IN MMWAVE COMMUNICATIONS

As the need for higher throughput and lower latency continues to grow, *Millimeter Wave (mmWave)* communication, particularly in the 24–300 GHz range, has emerged as a critical technology for next-generation wireless networks [16]. Compared to single-antenna systems, *Multiple-Input Multiple-Output (MIMO)* device shows a primary role in mitigating issues like signal fading, atmospheric absorption, and path loss, making it essential for modern cellular communication. *Multiple-Input Multiple-Output (MIMO)* enables simultaneous data propagation across multi-element antennas, ranging from 2×2 and 4×4 configurations to massive *MIMO* systems with hundreds or thousands of elements, ensuring significantly higher data rates, which is crucial for cellular communication.

1.4 CHALLENGES IN MIMO ANTENNA DESIGN

Millimeter Wave (mmWave) communication is crucial for applications like broadband cellular networks, wireless backhaul, and *Device-to-Device (D2D)* communication. On October 22, 2015, the *Federal Communications Commission (FCC)* proposed new rules (FCC 15138) allocating mmWave bands at 28 GHz, 37 GHz, 39 GHz, and 64–71 GHz that are part of the 5G spectrum [17]. However, the high propagation and atmospheric losses at these frequencies necessitate high-gain antenna designs. Unlike low-frequency antennas, mmWave antennas must be compact while offering strong performance. To counteract the path loss, antenna arrays are essential for achieving high gain, but integrating multiple antennas in a compact space leads to challenges like mutual coupling, which degrades efficiency and bandwidth.

The short wavelength of mmWave frequencies allows for miniaturized antenna structures, making it feasible to incorporate multiple elements within a small footprint. However, designing such compact *MIMO* antennas requires careful consideration of mutual coupling and isolation to streamline performance. Reducing mutual coupling not only enhances overall system efficiency but also contributes to higher gain and better signal quality. Additionally, antenna decoupling is crucial for base station antennas in space-constrained environments.

Since microstrip antennas experience higher losses at mmWave frequencies, selecting low-loss substrates is essential. Materials like Rogers substrates, which have low dielectric loss and high efficiency, are widely preferred for high-frequency 5G applications to ensure better signal integrity and performance [16].

1.5 MOTIVATION OF THESIS

The shift from 4G to 5G technology has driven an increasing need for faster internet speeds, calling for the development of advanced radio systems. *Multiple-Input Multiple-Output (MIMO)* antenna systems have proven to be an effective solution, offering enhanced network capacity and supporting high data rate requirements. With 5G communication extending into new frequency bands, including those below 6 GHz and mmWave frequencies beyond 24 GHz, innovative antenna designs are essential to accommodate these high-frequency ranges. For instance, the n261 band, functioning between 27.5 GHz and 28.35 GHz as illustrated in the Figure 1.5, is tailored for short-range communication while maintaining high data rates. The 24.25–29.5 GHz mmWave spectrum is allocated differently across key regions: the USA utilizes 27.5–28.35 GHz, Europe focuses on 24.25–27.5 GHz, South Korea employs 26.5–29.5 GHz, Japan uses 27.5–29.5 GHz, and China has allocated 24.75–27.5 GHz for 5G NR deployments, as summarized in industry overviews including the Telecom Gurukul article "5G NR Frequency Bandwidth: Everything You Need to Know." All these mmWave bands fall under FR2 (24–100 GHz) and operate exclusively in Time Division Duplex (TDD) mode, consistent with 3GPP specifications. To meet the requirements of contemporary *MIMO* systems, antennas need to be compact and low-profile, enabling multifunctional, aesthetically pleasing designs. However, incorporating multiple antenna elements in *MIMO* configurations can lead to performance issues, such as mutual coupling, which affects overall system efficiency. This challenge has been addressed

by employing defected structures to enhance isolation between antenna elements, improving overall performance. Table 1.2 presents *New Radio (NR)* operating bands for *Millimeter Wave (mmWave)* 5G communications, detailing the corresponding uplink and downlink frequency ranges. All listed bands operate in *Time Division Duplex (TDD)* mode, with frequencies between 24.25 GHz and 71 GHz, supporting high-speed and low-latency 5G applications. In 5G NR, Frequency Division Duplex (FDD) is used only in sub-6 GHz bands (FR1) such as n1, n3, n7, and n28 where separate frequency channels are allocated for uplink and downlink. In contrast, all millimeter-wave bands in FR2 (24–100 GHz), including n257 through n263 (notably n261 covering 27.5–28.35 GHz), operate exclusively in Time Division Duplex (TDD) mode. The 5G NR mmWave bands (n257–n263, 24.25 to 71 GHz) operate in TDD mode only, as the unpaired spectrum allocation at these frequencies makes FDD impractical. TDD supports flexible slot allocation for asymmetric traffic and enables efficient beamforming through channel reciprocity. While FDD offers lower latency and better coverage in sub 6 GHz bands, TDD is the preferred and necessary scheme for mmWave 5G due to its spectral efficiency and feasibility. As confirmed by 3GPP standards and industry references like Telecom Gurukul, there are no FDD allocations above 6 GHz. This is because TDD better supports the high directionality, channel reciprocity, and efficient spectrum use required at mmWave frequencies, making it the only practical and standardized duplexing approach for such bands.

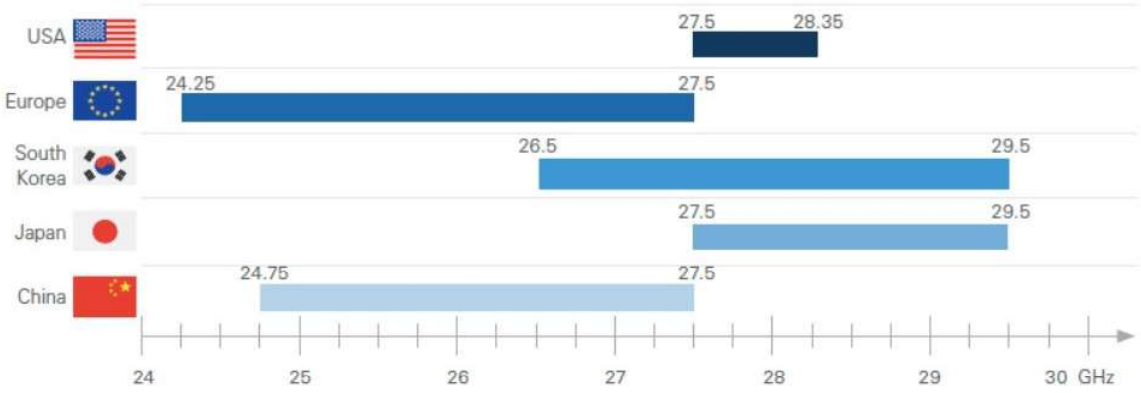

Fig. 1.5: Regional Allocation of 5G mmWave Spectrum in the 24–30 GHz Range, Highlighting Key Bands for FR2 Deployment (Source: Telecom Gurukul, "5G NR Frequency Bandwidth: Everything You Need to Know," May 2023)

Table 1.2: Downlink and Uplink Frequencies for NR Operating Bands

NR Operating Band	Uplink (UL) and Downlink (DL) Frequencies	Duplex Mode
n257	26.5 GHz – 29.5 GHz	TDD
n258	24.25 GHz – 27.5 GHz	TDD
n259	39.5 GHz – 43.5 GHz	TDD
n260	37 GHz – 40 GHz	TDD
n261	27.5 GHz – 28.35 GHz	TDD
n262	47.2 GHz – 48.2 GHz	TDD
n263	57 GHz – 71 GHz	TDD

1.6 RESEARCH GAPS

In recent years, researchers have actively explored and developed antenna designs for future 5G devices, focusing on frequency bands above 6 GHz. Various antenna structures have been proposed, studied, and analyzed such as Abbas et al. in [18] proposed a tapered slot *MIMO* antenna with end-fire radiation for 5G applications, covering 27.5–40 GHz, and successfully achieved isolation enhancement of over 25 dB using a *Low Pass Filter (LPF)* with a stepped impedance method. However, the proposed quad antenna has a relatively large footprint (158 × 77.8 mm^2), making it impractical for compact 5G devices. The need for miniaturized MIMO antennas with high isolation and reduced size remains an important challenge. Similarly, Marzouk et al. in [19] designed a *DGS*-based two-element dual-band *MIMO* antenna achieving -27 dB mutual coupling, but the increased inter-element spacing ($0.87\lambda_0$ or 9.41 mm) makes it less suitable for compact applications.

The ten-element slot-loop *MIMO* antenna with *Split Ring Resonator (SRR)*-based metamaterials [20] operates at 28–36 GHz on an FR4-epoxy substrate, achieving -17.5 dB mutual coupling at 34.6 GHz. While the design improves isolation, there is still room to further reduce mutual coupling, especially for compact arrays. Additionally, the FR4 substrate's higher dielectric losses could affect millimeter-wave performance. Future research should explore

low-loss materials, miniaturized designs, and broadband isolation techniques to improve overall efficiency and versatility.

Additionally, in [21] a miniaturized two-element microstrip antenna array using *Electromagnetic Band Gap (EBG)* ground provided only 15 dB isolation in the 26.5–29.5 GHz range, indicating the necessity of enhancing antenna diversity techniques. These findings highlight a critical research gap in developing compact, high-isolation *MIMO* antenna designs that maintain strong isolation while addressing size constraints, fabrication challenges, and improved mutual coupling techniques for efficient 5G mmWave applications. Addressing these gaps will lead to more efficient, compact, and high-capacity *MIMO* antenna designs for future applications.

1.7 RESEARCH OBJECTIVES

The research work entitled ***Design and Fabrication of Millimeter wave Antenna for Future Wireless Applications*** have been carried out with the following objectives:

1. To do comparative analysis of various planar *MIMO* antennas operating in millimeter frequency range.
2. To design a new *MIMO* antenna in millimeter frequency range for future wireless applications.
3. To perform a parametric analysis of the designed antenna.
4. To do fabrication and perform testing of the designed antenna for validation of results.

1.8 RESEARCH CONTRIBUTION

This work introduces a compact quad antenna designed for mmWave 5G applications, specifically operating in the n261 band at 28 GHz. A slotted patch antenna with a *Dumbbell Shaped Defected Ground Structure (DB-DGS)* is implemented to improve isolation, ensuring improved performance in dense wireless environments. The use of Rogers 5880 substrate (ε_r = 2.2, thickness = 0.254 mm) ensures low loss and efficient radiation characteristics at mmWave

frequencies. To validate its real-world feasibility, the design is manufactured and experimentally checked, with measured values closely aligning simulated values. As opposed to existing *MIMO* antenna designs, the proposed structure offers better isolation, compactness, and overall efficiency, indicating its potential for use in radio communication systems of the future.

1.9 RESEARCH METHODOLOGY

The research will be carried theoretically and through simulations using commercial software simulation package such as *High Frequency Structure Simulator (HFSS)*, *Computer Simulation Tool (CST)*. These softwares will be used for design and simulation of proposed antenna structures. Then analysis and optimization of the antenna structures is done to achieve desirable antenna characteristics and performance Following methodology is followed to achieve objectives of the research work:

- To review planar antennas operating at millimeter wave frequency .
- To review best suitable antenna design system for the performance enhancement of *MIMO*.
- To design and simulate *MIMO* antenna using *HFSS*/*CST* software with optimized parameter.
- Analysis of various antenna performance parameter such as reflection coefficient (S_{11}), isolation, correlation, gain, efficiency, etc.
- Lastly, using printed circuit board technique, fabrication of the designed antenna is completed, and followed by measurement of antenna parameters using VNA and Anechoic chamber.

1.10 THESIS ORGANIZATION

There are six chapters in the thesis summarizing the specific contributions directed in achieving the above objectives. These Chapters are briefed herewith as:

Chapter-1: Introduction

This chapter sets the context by introducing millimeter wave technology and its relevance to

next-generation wireless systems. It outlines the motivation behind the study, defines the research objectives, and highlights the identified gaps. It also describes the methodology and scope of the work.

Chapter-2: Literature Survey

A detailed review of recent work on MIMO antenna designs operating at mmWave frequencies is presented. The chapter discusses different types of antenna structures, coupling reduction strategies, and key performance parameters. It concludes by identifying the limitations in existing studies, forming the basis for the proposed work.

Chapter-3: Comparative Analysis of various Planar MIMO Antennas operating in Millimeter Frequency Range

This chapter presents a categorized analysis of existing planar MIMO antennas based on design types such as patch, array, DGS, and DRA-based structures. Key performance indicators like bandwidth, gain, ECC, and diversity gain are compared to evaluate the strengths and trade-offs of each approach.

Chapter-4: Design of a Planar Single Element Antenna for Millimeter Wave (mmWave) band

A single antenna element's design and optimization for use in the 28 GHz band are highlighted in this chapter. Performance measures including gain, return loss, and the impact of DGS on radiation characteristics are covered, along with parametric studies and the evolution of the antenna shape.

Chapter-5: Design of a Planar MIMO Antenna for Millimeter Wave (mmWave) band

This chapter details evolution of a compact 4-port array antenna. It includes simulation and fabrication steps, followed by experimental testing. The effectiveness of the antenna is verified by comparing measured findings, including S-parameters, gain, ECC, surface current distribution, and radiation patterns with simulations.

Chapter-6: Conclusions and Future Scope

The final chapter outlines the outcomes of the research, connecting them back to the defined

objectives. It also outlines the main contributions of the work and provides suggestions for future exploration in areas like material choice, miniaturization, and wideband operation.

Chapter–2

Literature Survey

2.1 INTRODUCTION

This chapter offers a thorough examination of prior research related to *MIMO* antenna design for 5G applications. The need for effective and small antennas in communication devices is growing as 5G technology develops. The development of different 5G antennas is examined in this chapter, including single-element designs and *MIMO* configurations with two, four, and eight elements. Integrating several antennas in a constrained area while preserving high performance is a significant challenge in 5G antenna design. New methods for increasing bandwidth, optimizing gain, and improving isolation have been made possible by recent developments in antenna technology. This chapter presents a variety of antenna types created by researchers in recent years, highlighting their benefits and drawbacks as well as methods for improving antenna performance. Lastly, the chapter discusses various approaches adopted in the literature to reduce mutual coupling, which is a key factor in improving overall *MIMO* system performance.

2.2 SUB-6 GHZ AND UWB (3 - 12 GHZ)

The development of MIMO antenna systems for 5G has followed divergent paths in sub-6 GHz and mmWave domains. In the sub-6 GHz and UWB regimes (3–12 GHz), research has emphasized wideband operation, mutual coupling suppression, and interference resilience to support coexistence with WiMAX, WLAN, and satellite services. Zhang *et al.* in [22] pioneered wideband isolation using a tree-like ground structure, achieving > 20 dB isolation across the full FCC UWB band (3.1–10.6 GHz) in a compact layout. This approach was later miniaturized by Luo *et al.* in [23], who employed dual defected ground structures (DGS) to attain > 18 dB

isolation in a 22 mm x 26 mm footprint demonstrating the efficacy of ground-plane engineering for decoupling.

Band-notching further enhanced spectral selectivity: Jetti *et al.* in [24] integrated C-shaped slots and U-shaped ground strips to realize triple-band rejection (3.3–3.7, 5.15–6, and 7.8–8.4 GHz), while Chandel *et al.* in [25] used inverted L-shaped slits to suppress WLAN and INSAT C-band (6.3–7.27 GHz), both reporting envelope correlation coefficient (ECC) < 0.013 and $S_{21} < -25$ dB. Multi-standard integration was advanced by Zhu *et al.* in [26], whose CPW-fed UWB antenna combined split-ring resonators for dual band-notching and isolation, and by Al-Saif *et al.* in [27], who covered 2–12 GHz encompassing global sub-6 GHz 5G bands (n77/n78) with > 20 dB isolation and 143 % fractional bandwidth.

Architectural innovation continued with Patre *et al.* in [28], who proposed a shared-radiator MIMO topology that eliminated inter-element decoupling structures while maintaining 136.6 % bandwidth, and Feng *et al.* in [29], who demonstrated a 3D metasurface-integrated magneto-electric dipole MIMO system with ECC $< 5 \times 10^{-4}$, 7.6 dBi gain, and omnidirectional coverage across 5G, WiMAX, WLAN, and X-band.

However, these sub-6 GHz/UWB strategies do not scale to mmWave frequencies. Unlike planar UWB designs, mmWave MIMO performance depends on array geometry, feeding networks, and substrate integration. Preliminary works such as Chen *et al.* in [30] have demonstrated 28 GHz 2×2 MIMO antennas with > 12 dB isolation using edge-coupled patches, but often rely on high-cost substrates (e.g., Rogers RO4003) and lack the compactness and fabrication scalability needed for consumer devices.

2.3 LITERATURE REVIEW OF SINGLE-PORT ANTENNA FOR 5G APPLICATIONS

Aziz Elfatimi *et al.* in [31] proposed a compact single-feed patch antenna tailored for 5G mmWave opeartion, specifically targeting the 28 GHz frequency. The design is fabricated on a Rogers RT5880 substrate (dielectric constant 2.2, thickness 0.508 mm), offering low loss and high-frequency support. This small design offers consistent radiation properties and good impedance matching. Despite its simplicity and ease of fabrication, the study highlights a

key limitation; while suitable for single-element operation, the design lacks scalability for multi-element (*MIMO*) configurations, and mutual coupling is not addressed. This identifies a research gap in extending compact mmWave designs to *MIMO* systems with improved isolation and performance.

Circular patch antennas for 5G at 28 GHz were examined in [32] by Sundeep Kumar and Arvind Kumar (2019) using RT/Duroid 5880 ($\varepsilon_r = 2.2$, loss tangent = 0.0009). They discovered that the coaxial-fed antenna had a greater bandwidth (0.792 GHz vs. 0.660 GHz) when they compared coaxial and microstrip line feeds. Rectangular patch antennas, however, have been demonstrated in earlier research to provide better bandwidth and directivity. To improve efficacy, study emphasized the necessity of optimizing antenna arrays and investigating substitute substrates.

In [33], Saleh *et al.* (2021) suggested a dual U-slot microstrip patch antenna for 5G applications operating in the frequency range of 25.5-31.2 GHz. The antenna, which was fed by a coaxial probe and had a circular patch with two U-shaped slots, was constructed on a FR-4 substrate. The design achieved a return loss below -15 dB across the operating band, with a gain ranging from 10.5 dBi to 12.2 dBi, peaking at 30 GHz. The design can be extended to MIMO configurations in the mmWave frequency range.

For 5G millimeter wave use, Pavithra *et al.* (2022) in [34] created a high-gain circular and rectangular microstrip patch antenna that operates at a resonant frequency of 3 GHz. The antennas were made on a FR4 substrate with a thickness of 3.18 mm and a dielectric constant of 2.2. With a gain of 10.0 dB, the circular patch antenna outperformed its rectangular counterpart, which had a gain of 5.0 dB. Even though the study concentrated on single-element antennas, future research should investigate compact *MIMO* configurations with multiple elements to fulfill the requirements of future wireless networks. This will ensure high isolation, reduced mutual coupling, and improved bandwidth.

2.4 STUDY OF 2-PORT ANTENNA FOR 5G APPLICATIONS

Ying Liu *et al.* suggested a two-element *MIMO* antenna designed to operate at 5.8 GHz in 2019 [35]. The antenna is constructed on a 1.5 mm thick substrate with a dielectric constant of

2.65. Each antenna element measured 25 mm × 30 mm, with an edge-to-edge spacing of 0.13 λ (approximately 6.7 mm at 5.8 GHz). The design incorporated hybrid *Electromagnetic Band Gap (EBG)* structures and a *DGS* to achieve low mutual coupling. While effective for two-element configurations, the study identified a research gap in extending these techniques to larger *MIMO* systems with more elements, where maintaining low mutual coupling and correlation remains a challenge.

Muhammad Usman *et al.* presented a small dual-port annular slot *MIMO* antenna for mmWave 5G applications in 2022 at 28 GHz [36]. A gain of 6.9 dBi per port and over 20 dB port isolation were used to obtain a 10 dB impedance bandwidth of 400 MHz. Its exceptional *MIMO* performance was proved by a *ECC* of 0.065 and a *DG* of 9.98 dB. At only $33 \times 27.5 \times 0.76$ mm^3, the design is remarkably small and can be integrated into 5G devices with little space. However, the design operated within a single frequency band, future work can focus on enhancing compactness further by leveraging advanced materials or integration techniques such as metasurfaces or electromagnetic/defected ground structures (EBG/DGS), potentially enabling multiband support without compromising isolation or gain, thus improving applicability for next-generation compact wireless systems.

This year, Ameen *et al.* [37] proposed a compact antenna tailored for millimeter wave 5G applications. The antenna operated over broad bandwidth of impedance of 34.1% reached high reparation over 30 dB and had a peak gain of 11 dBi at 26.1 GHz, extending from 23.61 to 33.3 GHz. The design integrated a staircase-shaped metasurface for circular polarization and a modified mushroom metasurface for isolation enhancement. The antenna employed an aperture-coupled structure and a stacked configuration to realize high performance. The work highlighted the need for further miniaturization for better integration into compact 5G millimeter wave systems, indicating a research gap in size-efficient, high-gain MIMO solutions with polarization diversity at mmWave bands.

Also in 2022, Manirathnam C. et *et al.* [38] proposed a compact two-port *MIMO* antenna for 5G communication, specifically targeting the 28 GHz frequency. The antenna was constructed on a Rogers RT/Duroid 5880 substrate, which was 0.8 mm thick and had a dielectric constant of 2.2. With a bandwidth of 1.48 GHz and a peak gain of 6.82 dB, the design operated between 27.25 GHz and 28.73 GHz. The two antenna components were positioned perpendicular to one

other to provide strong isolation, surpassing 30dB, with a small footprint of 22 mm × 12 mm × 0.8 mm. The configuration demonstrated strong *MIMO* performance, including low *Envelope Correlation Coefficient (ECC)*, high diversity gain, and minimal channel capacity loss. The design was simple and effective, but future improvements were suggested to enhance bandwidth and reconfigurability.

In 2023, Jetendra Jakhar *et al.* [39] suggested an asymmetric flare-shaped patch for 5G millimeter wave application in a small two-port *MIMO* antenna. The design operated across a broad frequency spectrum from 20 to 40 GHz, providing an impedance bandwidth exceeding 66.66%.By manufacturing the antenna on a Rogers RT Duroid 5880 substrate, which had a dielectric constant of 2.2 and a thickness of 1.6 mm, an overall compact size of 26 mm × 19.2 mm was attained. Above 20dB, the structure achieved a peak gain of 8.17dBi and good isolation between the ports. The incorporation of a *Defected Ground Structure (DGS)* helps improve radiation efficiency and reduce mutual coupling. While the proposed design fulfilled essential requirements for Ka-band 5G applications, future improvements could focus on flexibility or reconfigurability to further enhance its usability in modern wireless systems.

In 2024, V. Koushick *et al.* [40] proposed a compact wideband antenna with two ports that is appropriate for 5G wireless system, particularly targeting the n79 band focused at 4.75 GHz. The design featured circular slots along with a *Defected Ground Structure (DGS)*, contributing to improved bandwidth and port isolation. It showed a directivity of 7.2 dB, a maximum gain of 6.5 dB, and a strong isolation of more than -32 dB. FR-4, the substrate material, had a loss tangent of 0.018 and a relative permittivity (ε_r) of 4.4. The antenna was able to fit into contemporary smartphones while maintaining a small form factor of $30 \times 30 \times 0.8$ mm^3. While the design shows promising performance in a mid-band 5G range, it remains limited to a single band. The antenna was not applicable to mmWave bands. The study suggested future work on miniaturization and multi-band capability.

Also in 2024, Suresh Angadi *et al.* [41] designed a metasurface-based dual-band circularly polarized antenna for sub-6 GHz frequency. The antenna operated at 3.27 GHz and 4.78 GHz, using X-shaped radiators and a metasurface for circular polarization and high isolation (up to -30.01 dB). The antenna had a compact size of 30×23 mm^2 and achieved a peak gain of 7.57 dBi. However, the work focused on sub-6 GHz, and extension to mmWave bands is needed.

Also in 2024, A compact dual-band two-port circularly polarized MIMO antenna was proposed by Suresh Angadi *et al.* in [41] for 5G NR sub-6 GHz applications in bands n48 and n79. The antenna integrates closely spaced mirror-symmetrical X-shaped radiators with a metasurface placed $0.27\lambda_0$ above them to enhance gain and isolation. Operating over 3.03–3.44 GHz and 4.01–5.87 GHz, it achieves resonance at 3.27 GHz and 4.78 GHz, with peak realized gains of 7.57 dBi and 5.60 dBi, respectively. The antenna shows improved isolation of –30.01 dB and –21.00 dB due to metasurface loading. It maintains low ECC values and exhibits circular polarization. The antenna size is 30×23 mm^2. While the design is effective for sub-6 GHz, the current configuration limits its applicability to mid-band frequencies. Future work could focus on enhancing compactness further while extending functionality to mmWave bands (above 24 GHz), where size constraints and high integration are more critical for next-generation 5G and 6G applications.

In the same year, Mya Sandar Aung and T. Hla [42] presented a small, two-port wideband *MIMO* antenna for frequency bands below 6 GHz , with a focus on 5 GHz WiFi applications and the n77/n78/n79 bands. The antenna is made up of two circular slot monopole elements that are symmetrical and measure $36 \times 18 \times 1.6$ mm^3. A T-shaped ground stub was implemented between the radiating elements to enhance isolation and bandwidth. The design achieved a wide impedance bandwidth ranging from 3.3 GHz to 6 GHz with mutual coupling maintained below -18 dB. Additional performance metrics included a low *Envelope Correlation Coefficient* (ECC < 0.006), a peak gain of 2.1 dBi, and a radiation efficiency of approximately 82%. Although the antenna demonstrated excellent performance in the lower 5G bands, future work could aim to reduce the physical size further and extend operation into the mmWave frequency spectrum for next-generation compact wireless devices.

In another 2024 study, a compact dual-band boat-shaped *MIMO* antenna was presented by Cholavendan Munusami *et al.* [43] for 5G and *WLAN* applications. The antenna consisted of two diagonally placed identical rectangular patches on FR-4 substrate with a total size of 56×48 mm^2. It operated over two frequency bands: 2.22–2.42 GHz and 5.142–5.706 GHz, covering key 5G and WLAN spectrums. A ladder-shaped hybrid decoupling unit, combined with a shorting pin and neutralization line, significantly improved isolation. To improve performance, a split ring resonator inspired by metamaterials was incorporated into a defected ground structure.

The work was suitable for low-frequency 5G and *WLAN* but not for mmWave applications. Future work could explore mmWave extensions.

Finally, in 2024, TTzouras Hlias and Stavros Koulouridis (2024) [44] proposed a compact dual-port antenna integrated with a metamaterial surface for applications including 5G millimeter waves. The antenna, fabricated on a Rogers RT/Duroid 5880 substrate ($\varepsilon_r = 2.2$, thickness = 0.78 mm), occupies a compact size of $10 \times 20 \times 0.78\,\text{mm}^3$. It operated in the Ka-band with a measured impedance bandwidth of 3.37 GHz and achieved a maximum gain of 10.02 dB. The inclusion of three metasurface arrays, composed of 8×2 modified H-shaped unit cells, enhances both bandwidth and isolation, which exceeds 20 dB. While the current design successfully addressed performance at mmWave frequencies in a compact footprint, further scope exists in reducing the size even more by optimizing the metasurface layout, adopting higher-permittivity materials, or exploring flexible substrate technologies for integration into smaller or conformal 5G devices.

2.5 STUDY OF 4-PORT ANTENNA FOR 5G APPLICATIONS

For 5G portable and Internet of Things applications, Chattha *et al.* [45] presented a compact, two-element, four-port *MIMO* antenna in 2019. The design was arranged orthogonally on a 50×100 mm^2 ground plane to achieve polarization and spatial diversity. The antenna covered the 2.7–3.6 GHz band, achieving isolation below –25 dB and an *Envelope Correlation Coefficient (ECC)* under 0.009. Although the antenna performed well for sub-6 GHz applications, extending its compact structure to mmWave frequencies remained a research challenge.

In 2020, Khalid *et al.* [46] developed a small, four-port *MIMO* antenna that operates between 25.5 and 29.6 GHz for 5G millimeter wave applications. This design featured slotted rectangular patches and a *DGS* to improve element separation and radiation performance. The antenna achieved a peak gain of 8.3 dBi with Rogers RO4350B substrate. While the compact $30 \times 35 \times 0.76$ mm^3 structure was well-suited for 5G devices, further miniaturization was identified as an area for improvement.

In the same year, Naqvi *et al.* [47] proposed an integrated *MIMO* antenna system supporting both 4G *LTE* and 5G mmWave applications. The design, fabricated on a Rogers RO4350B

substrate ($\varepsilon_r = 3.6$, thickness = 0.76 mm), featured a top-edge array with two elements: *LTE MIMO* and a four-element mmWave *MIMO* array along the elongated edge, operating at 28 GHz. The LTE module supported bands 46 and 47 with an 830 MHz bandwidth, while the 5G module covered a 3.5 GHz bandwidth. The inclusion of a *Defected Ground Structure (DGS)* helped achieve isolation values above 25 dB and 22 dB for *LTE* and 5G, respectively. Despite the effective dual-band operation, further work was needed to enhance miniaturization and integration in compact devices.

In 2022, Patel *et al.* [48] designed a compact *Ultra Wide Band (UWB)* four-port *MIMO* antenna targeting the NR n257/n258/n261 bands for sub-millimeter wave 5G applications. The antenna was built on a Rogers RT/Duroid 5880 substrate ($\varepsilon_r = 2.2$, thickness = 0.8 mm), with a compact size of 24×24 mm^2. A connected ground structure with a circular ring improved isolation above 20 dB. While the antenna balanced compactness and performance, further miniaturization through metamaterials or flexible substrates was suggested for better integration in next-generation communication systems.

A MIMO antenna with four ports and a compact size of 30×35 mm^2 was proposed by Muhammad Bilal *et al.* [49] in the same year 2022 utilizing a Rogers RT/Duroid 5880 substrate ($\varepsilon_r = 2.2$). The antenna operated within the 27.5–28.5 GHz range, achieving significant isolation (>40 dB) through a *Defected Ground Structure (DGS)* with a zigzag decoupling structure. While the study optimized antenna isolation and gain, future work could focus on achieving ultra-wideband performance, integrating beam steering, and incorporating sub-6 GHz bands for broader 5G compatibility.

In 2023, Güler and Keskin [50] introduced a four-port *MIMO* antenna for mmWave 5G applications, focusing on improved isolation and bandwidth. The antenna, produced on an a substrate of RT/Duroid 5880 ($\varepsilon_r = 2.2$, thickness = 0.787 mm), measured $25 \times 25 \times 0.787$ mm^3 and operated in the 25.28–28.02 GHz range. It used a *Defected Ground Structure (DGS)* with semi-circular slots to obtain a minimum isolation of 23.2 dB and a peak gain of 8.72 dBi. Although the antenna demonstrated promising characteristics, further research was needed to enhance bandwidth and radiation patterns for broader 5G applications.

Also in 2023, Abbas *et al.* [51] suggested a small *Ultra Wide Band (UWB) MIMO* antenna covering 25–50 GHz for 5G mmWave applications. Using an RO4003C substrate with dimensions

of $33 \times 33 \times 0.203$ mm^3, the design incorporated a *DGS* to enhance isolation and minimize mutual coupling. Performance evaluations demonstrated an *ECC* below 0.005, a *DG* of 9.999 dB, and less than -10 dB for the mutual coupling. While the antenna accomplished excellent diversity performance, further optimization was suggested to enhance gain and reduce size for next-generation 5G applications.

For mmWave 5G communication, Ghosh *et al.* [52] created a small four-port *MIMO* antenna in 2024. It operates in bands n257, n258, and n261 and has a bandwidth of 3.9 GHz (26.5–30.4 GHz). Constructed on a Rogers RT/Duroid 5880 substrate ($\varepsilon_r = 2.2$, thickness = 0.508 mm), the antenna included a *Complementary Split Ring Resonator (CSRR)* and a *DGS* to improve isolation. With a radiation efficiency of 96% and a peak gain of 11 dBi at 28 GHz, it also had a *ECC* < 0.0001. While the design met key performance criteria, further miniaturization was recommended by refining the feed structure and employing metamaterials.

Most recently, in 2025, Du *et al.* [53] designed a flexible, tri-band four-port *Co-Planar Waveguide (CPW)*-fed slot *MIMO* antenna for multi-standard wireless communication, covering 5G, *Wi-Fi* 6/6E, and X-band satellite applications. Built on a *Liquid Crystal Polymer (LCP)* substrate ($\varepsilon_r = 2.9$, thickness = 0.1 mm), the antenna occupied a 65×65 mm^2 area. It supported three bands: 3.0–4.46 GHz (5G N77/N78), 5.07–7.15 GHz (*Wi-Fi* 6/6E), and 8.01–12 GHz (X-band). High isolation (>25 dB) was achieved through crossed and circular isolation branches. While the antenna performed well for wearable and conformal applications, future work was needed to further miniaturize and integrate it into 6G communication systems.

H. Chattha et al. in [45] propose a low-profile, compact four-port, two-element MIMO antenna tailored for 5G portable and IoT applications. The antenna structure uses two planar inverted-F antenna (PIFA) elements, arranged orthogonally to achieve polarization diversity. Spatial diversity is achieved by placing these elements diagonally across a $50 \times 100\,\text{mm}^2$ ground plane. The design employs an FR-4 substrate with a relative permittivity (ε_r) of 4.4, thickness of 1.5 mm, and a total antenna height of 3.0 mm. Each radiating plate of the PIFA measures $16 \times 33\,\text{mm}^2$. The antenna operates from 2.7 GHz to 3.6 GHz, effectively covering the 3.3–3.6 GHz band for 5G applications. Measured results show isolation between ports reaching below -25 dB, with an envelope correlation coefficient (ECC) under 0.009, confirming excellent MIMO performance. To reduce mutual coupling, etched rectangular slots are included on the ground

plane beneath each radiating element. While the antenna offers good isolation and diversity performance, it is limited to sub-6 GHz bands. A notable research gap exists in extending such compact designs to mmWave frequencies, as well as optimizing integration into more compact device layouts without sacrificing isolation or bandwidth. Further investigation into alternative substrates or techniques such as electromagnetic bandgap (EBG) or defected ground structure (DGS) could support these advancements.

Syeda Iffat Naqvi *et al.* (2020) in [47] developed an integrated MIMO antenna system designed to support both 4G LTE and 5G mmWave applications within a single structure. The antenna is fabricated on a Rogers RO4350B substrate with a dielectric constant of 3.6 and a thickness of 0.76 mm, and occupies a compact area of 75×110 mm^2. The structure consists of a two-element MIMO antenna for LTE placed on the top edge and a four-element mmWave MIMO array along the elongated edge, operating at the 28 GHz band. The LTE antenna supports bands 46 and 47 with a measured bandwidth of 830 MHz, while the 5G module covers a 3.5 GHz bandwidth. To improve performance, a defected ground structure (DGS) is incorporated. High isolation values exceeding 25 dB and 22 dB were achieved for the LTE and mmWave modules respectively, along with peak gains of 5.13 dB (LTE) and 9.53 dB (5G). While the integration demonstrates effective dual-band operation, further miniaturization and flexible deployment remain key areas for improvement in compact terminal devices.

Chengzhu Du *et al.* (2025) in [53] designed a flexible, tri-band 4-port CPW-fed slot MIMO antenna tailored for multi-standard wireless communication, including 5G, WiFi 6/6E, and X-band satellite applications. The antenna supported three frequency bands: 3.0–4.46 GHz (5G N77/N78), 5.07–7.15 GHz (WiFi 6/6E), and 8.01–12 GHz (X-band). It was constructed on a flexible Liquid Crystal Polymer (LCP) substrate with a dielectric constant of 2.9 and a thickness of 0.1 mm, occupying an overall area of 65 mm $\times$ 65 mm. To achieve high isolation, greater than 25 dB, the four slot antennas were placed orthogonally and enhanced with crossed and circular isolation branches. The antenna demonstrated excellent MIMO characteristics with envelope correlation coefficients (ECC) below 0.01 and diversity gain (DG) exceeding 9.995. While the design showed strong performance in conformal and wearable scenarios, especially in bending and human body tests, future scope lies in further miniaturization and integration for next-generation 6G communication platforms.

Amit Patel et al. (2022) in [48] designed a compact UWB CPW-fed 4-port MIMO antenna for sub-millimeter-wave 5G applications, specifically covering the NR n257/n258/n261 bands. The antenna was fabricated on a Rogers RT/Duroid 5880 substrate ($\varepsilon_r = 2.2$, thickness = 0.8 mm) and had a compact size of 24 $\times$ 24 mm^2. To enhance isolation, a connected ground structure with a circular ring was incorporated, achieving isolation levels above 20 dB. The antenna operated over a wide bandwidth of 24.8–44.45 GHz (79.35%) and provided a peak gain of 8.6 dBi with a minimum radiation efficiency of 85%. The design featured a modified CPW feed and an elliptical slot to improve performance. The 4-port MIMO configuration was arranged in a rotational orthogonal manner to minimize mutual coupling and improve diversity characteristics, resulting in an envelope correlation coefficient (ECC) below 0.008 and a diversity gain (DG) above 9.5 dB. While the antenna achieved a balance between compactness and performance, further size reduction could have been explored through optimization of the ground structure, use of metamaterials, or adoption of flexible substrates for better integration into next-generation communication systems.

Ghosh *et al.* (2024) in [52] developed a compact four-port MIMO antenna designed for millimeter-wave 5G communication. The antenna was fabricated on a Rogers RT/Duroid 5880 substrate with a dielectric constant of 2.2 and a thickness of 0.508 mm, resulting in an overall size of 28.3 mm × 28.3 mm × 0.508 mm. It operated within the 5G bands n257, n258, and n261, covering a bandwidth of 3.9 GHz from 26.5 GHz to 30.4 GHz. The design featured two rectangular patch elements connected through a corporate feed network and incorporated complementary split-ring resonators (CSRRs) on the ground plane to enhance isolation. A defected ground structure (DGS) further reduced coupling between antenna elements. The antenna achieved a peak gain of 11 dBi and a radiation efficiency of 96% at 28 GHz, with excellent MIMO performance, including an envelope correlation coefficient (ECC) below 0.0001 and diversity gain (DG) exceeding 9.999 dB. While the design met key performance criteria for 5G applications, there was potential for further miniaturization by refining the feed structure and exploring advanced metamaterial techniques to improve integration in compact wireless devices.

Güler and Keskin (2023) in [50] developed a compact four-port MIMO antenna for millimeter-wave 5G applications, emphasizing improved isolation and bandwidth. Fabricated on an RT/duroid 5880 substrate ($\varepsilon_r = 2.2$, thickness = 0.787 mm), the antenna measured 25 $\times$ 25 $\times$ 0.787 mm^3. It operated within the 25.28–28.02 GHz range, achieving a peak gain of

8.72 dBi and a minimum isolation of 23.2 dB. To enhance performance, a defected ground structure (DGS) with semi-circular slots was incorporated, reducing mutual coupling and improving impedance bandwidth. The four radiating elements were positioned orthogonally to enhance spatial diversity. Performance analysis confirmed low envelope correlation coefficient (ECC), high diversity gain, and effective isolation. While the antenna demonstrated promising characteristics, further research could explore improvements in bandwidth and radiation patterns for broader 5G applications.

Abbas et al. (2023) in [51] developed a compact Ultra-Wideband (UWB) Multiple-Input Multiple-Output (MIMO) antenna for 5G millimeter-wave applications, covering a frequency range of 25–50 GHz. The design incorporated a Defected Ground Structure (DGS) to enhance isolation and minimize mutual coupling between antenna elements. The antenna was fabricated on an RO4003C substrate with dimensions of $33 \times 33 \times 0.203$ mm^3, making it suitable for integration into various telecommunication devices. Performance evaluations demonstrated excellent diversity characteristics, including an Envelope Correlation Coefficient (ECC) below 0.005, a Diversity Gain (DG) of 9.999 dB, and mutual coupling of less than -10 dB. Simulated and measured results exhibited close agreement, validating the antenna's effectiveness. While the design achieved a wide bandwidth and high isolation, future improvements could focus on further enhancing gain and minimizing size to better meet the requirements of next-generation 5G applications.

2.6 STUDY OF 8-PORT ANTENNA FOR 5G APPLICATIONS

For 5G millimeter wave applications, Mahnoor Khalid *et al.* [54] suggested an eight-port *MIMO* antenna in 2021. It operates in the 23.5–27.45 GHz band, which covers the crucial 26 GHz spectrum. With a corporate feed network and an inverted T-shaped array, the antenna achieved a peak gain of 11.5 dBi. The design employed a Rogers RO4350B substrate with a 0.76 mm thickness, a 3.6 dielectric constant, and a 0.0037 loss tangent. Despite its advantages, research gaps remain in further improving isolation, miniaturization, and optimizing the feeding structure for enhanced efficiency in compact wireless devices.

In the same year, Yong Qiang Hei *et al.* [55] created a 5G mobile terminal antenna with eight elements that covers the 5 GHz WLAN range as well as the n77, n78, and n79 frequency

bands. An FR-4 substrate ($\varepsilon_r = 4.4$) with a thickness of 0.8 mm was used to manufacture the antenna. The design incorporated L-shaped feeding branches and a T-shaped slot with a decoupling strip to enhance isolation, achieving a minimum isolation of 15 dB. Despite its advantages, further research could focus on miniaturization and adaptation for mmWave applications.

The dual-polarized eight-port *MIMO* antenna was suggested by Fawad *et al.* [56] in 2024. It uses a central frequency of 3.6 GHz and operates between 3.3 and 4.1 GHz. The FR-4 substrate used for the antenna's design had a loss tangent of 0.025 and a relative permittivity of 4.3. To mitigate mutual coupling, a *Defected Ground Structure (DGS)* was employed, while the design improved isolation, bandwidth, and efficiency, further work is needed to reduce antenna size for more compact smartphone integration.

In the same year, Brijesh Mishra *et al.* [57] created a Rogers RT/Duroid 5870 ($\varepsilon_r = 2.33$) based 8-port annular ring *MIMO* antenna for 5G NR-n260 applications. The antenna covered a wide bandwidth ranging from 34.2 to 40.3 GHz while operating at 36.4 GHz. with isolation exceeding 40 dB and a peak gain of 8.3 dB. While achieving advancements in bandwidth, isolation, and efficiency, future work should focus on miniaturization and real-world integration for next-generation 5G systems.

For sub-6 GHz and New Radio applications of 5G, Srinubabu and Rajasekhar [58] created a small *MIMO* antenna in 2025, combining both frequency bands into a single design. The antenna featured elliptical-shaped monopole antennas and semi-circular monopole antennas when constructed using FR-4 substrate, covering 3.15–5.35 GHz and 23.20–29.90 GHz, respectively. The design maintained peak gains of 11.75 dBi (sub-6 GHz) and 12 dBi (mmWave), with efficiencies ranging from 88% to 96%. While the antenna achieved high isolation and wide bandwidth, further research could focus on reducing the antenna size for smartphone and IoT device integration.

In the same year, Anupma Gupta *et al.* [59] designed an 8-port *MIMO* antenna for 5G body-centric communication in the n261 band at 27 GHz. The antenna features a T-shaped radiator and a ring-shaped ground plane, offering a 2 GHz bandwidth (26–28 GHz). To minimize mutual coupling, slotted structures were introduced in the ground plane, achieving over 20 dB isolation. Tested on various tissue models and pork samples, the antenna showed stable

performance with a low SAR of 0.00427 W/kg and a peak gain of 4.64 dB with an input power of 0.01 mW. With an *ECC* of 0.005 and *DG* of 9.97, it proved effective for wearable *MIMO* applications. While previous studies focused on either free-space or body-centric designs, this work successfully integrates both. Future improvements could focus on flexible materials and enhanced efficiency for real-world use.

Mahnoor Khalid et al. (2021) in [54] proposed an eight-port MIMO antenna for 5G millimeter-wave applications, operating within the 23.5–27.45 GHz band, covering the critical 26 GHz spectrum. The antenna employed an inverted T-shaped array with a corporate feed network, achieving a peak gain of 11.5 dBi. The design utilized a Rogers RO4350B substrate with a thickness of 0.76 mm, a dielectric constant of 3.6, and a loss tangent of 0.0037. Initially, a single-element antenna with dimensions of 2.5×3.7 mm^2 was designed, followed by a two-element array with a parallel feed network. The final configuration evolved into an eight-element MIMO system arranged along the edges of a $45 \times 50 \times 0.76$ mm^3 board, maintaining an inter-element spacing of 1.7 mm ($\sim \lambda/7$ at 26 GHz). The proposed antenna exhibited a wide impedance bandwidth of 4 GHz (23.75–27.75 GHz), with ECC and diversity gain values within acceptable limits. Despite its advantages, research gaps remain in further improving isolation, miniaturization, and optimizing the feeding structure for enhanced efficiency in compact wireless devices.

Yong Qiang Hei et al. in [55] proposed an eight-element MIMO antenna designed for 5G mobile terminals, covering the n77, n78, and n79 frequency bands along with the 5 GHz WLAN band. The antenna was fabricated using an FR-4 substrate with a dielectric constant of 4.4 and a thickness of 0.8 mm. Each antenna pair consisted of F-shaped radiators with dimensions of $75 \times 6 \times 0.8$ mm^3, positioned on the side frames of a $75 \times 37.5 \times 0.8$ mm^3 main board. The design incorporated L-shaped feeding branches and a T-shaped slot with a decoupling strip to enhance isolation, achieving a minimum isolation of 15 dB. The complete MIMO array was formed by arranging four antenna pairs along the side frames, maintaining an 84 mm spacing between pairs and a 15 mm $\times$ 1.2 mm etched gap in the ground plane to further reduce coupling. Experimental validation demonstrated high efficiency, low envelope correlation, and strong MIMO performance. Despite its advantages in wideband coverage and isolation, further research could focus on miniaturization and adaptation for mmWave applications to support future 5G communication systems.

Fawad et al. (2024) in [56] proposed a dual-polarized eight-port MIMO antenna for 5G smartphones, operating from 3.3 GHz to 4.1 GHz with a center frequency of 3.6 GHz. The antenna was designed on an FR-4 substrate with a relative permittivity of 4.3 and a loss tangent of 0.025. It had overall dimensions of $150 \times 75 \times 1.6$ mm^3. To mitigate mutual coupling, a defected ground structure (DGS) was employed, achieving an isolation level of more than 30 dB. The antenna demonstrated an average gain above 3.8 dBi and radiation efficiency exceeding 80%, while in MIMO configuration, the gain surpassed 6 dB with over 85% efficiency. Performance metrics such as envelope correlation coefficient (ECC < 0.001), diversity gain (DG), and total active reflection coefficient (TARC) met 5G standards. The fabricated and tested prototype showed good agreement with simulated results. While the design improved isolation, bandwidth, and efficiency compared to existing models, further research is needed to reduce antenna size for more compact smartphone integration.

Srinubabu and Rajasekhar (2025) in [58] developed a compact 8-port MIMO antenna for sub-6 GHz and mm-wave 5G-NR applications, integrating both frequency bands into a single design. The antenna was built on an FR-4 epoxy substrate ($\varepsilon_r = 4.5$, $\tan\delta = 0.002$) with a compact size of $70 \times 70 \times 1.2$ mm^3. For sub-6 GHz operation, it featured an elliptical-shaped monopole antenna with a CPW-fed structure, achieving a bandwidth of 2.2 GHz (3.15–5.35 GHz). The mmWave design incorporated semi-circular monopole antennas with circular slits, covering 23.20–29.90 GHz with a 6.7 GHz bandwidth. A triangular etching and 45° orientation helped reduce size, improve spatial diversity, and enhance isolation beyond -25 dB. The design maintained peak gains of 11.75 dBi (sub-6 GHz) and 12 dBi (mmWave), with efficiencies ranging from 88% to 96%. Additionally, the envelope correlation coefficient (ECC) remained low at 0.004, ensuring strong diversity performance. The X-shaped branching element, acting as a shared ground, further optimized radiation characteristics. While the antenna achieved high isolation, wide bandwidth, and compactness, further research could focus on reducing the antenna size even more, addressing a key challenge in modern smartphone and IoT device integration.

Brijesh Mishra et al. in [57] developed an 8-port annular ring MIMO antenna for mmWave 5G NR-n260 applications, addressing the scarcity of high-performance, high-isolation MIMO antennas in this frequency range. Fabricated on a Rogers RT/Duroid 5870 substrate ($\varepsilon_r = 2.33$, thickness = 0.508 mm), the compact $52 \times 52 \times 0.508$ mm^3 design incorporated an annular ring

on the radiating plane and a novel isolator structure on the ground plane to minimize mutual coupling. The antenna operated at 36.4 GHz, covering a broad bandwidth of 6.1 GHz (34.2–40.3 GHz) with isolation exceeding 40 dB, a peak gain of 8.3 dB at 39 GHz, and radiation efficiency above 85%. MIMO performance metrics such as envelope correlation coefficient (ECC), total active reflection coefficient (TARC), mean effective gain (MEG), and channel capacity loss (CCL) remained within acceptable limits. To enhance capacity and spatial diversity in mmWave communication, the study further introduced a 16-port massive MIMO antenna with dual-band operation (30–33 GHz and 33.5–40.9 GHz) and isolation over 22 dB. A fabricated prototype validated the design with experimental results closely aligning with simulations. While achieving significant advancements in bandwidth, isolation, and efficiency, future work should focus on miniaturization, real-world integration, multi-band adaptability, and dynamic beamforming for next-generation 5G systems.

Muhammad Bilal et al. in [49] designed a four-port MIMO antenna using a Rogers RT/Duroid 5880 substrate ($\varepsilon_r = 2.2$, thickness = 0.787 mm) with a compact size of 30×35 mm^2. The antenna operated within the 27.5–28.5 GHz range, achieving significant isolation (>40 dB) through a zig-zag decoupling structure and a Defected Ground Structure (DGS). A high gain of 12 dBi and low envelope correlation coefficient (ECC $<$ 0.0003) demonstrated its effectiveness for 5G applications. While the study successfully optimized antenna isolation and gain, future work could focus on achieving ultra-wideband performance, integrating beam steering for enhanced coverage, and incorporating sub-6 GHz bands for broader 5G compatibility. The research highlighted the need for further improvements in miniaturization, multi-band operation, and real-world integration challenges to meet evolving communication demands.

Anupma Gupta et al. (2025) in [59] designed an 8-port MIMO antenna for 5G body-centric communication in the n261 band at 27 GHz. Built on an FR4 substrate ($\varepsilon_r = 4.2$) with a compact size of 23.375 mm^3, the antenna features a T-shaped radiator and a ring-shaped ground plane, offering a 2 GHz bandwidth (26–28 GHz). To minimize mutual coupling, slotted structures were introduced in the ground plane, achieving over 20 dB isolation. Tested on various tissue models and pork samples, the antenna showed stable performance with a peak gain of 4.64 dB and a low SAR of 0.00427 W/kg for 0.01 mW input power. With an ECC of 0.005 and DG of 9.97, it proved effective for wearable MIMO applications. While previous studies focused on either

free-space or body-centric designs, this work successfully integrates both. Future improvements could focus on flexible materials and enhanced efficiency for real-world use.

2.7 SUMMARY

This chapter summarizes the previous work carried out by several researchers in designing the *MIMO* antennas. *MIMO* technology enhances bit rate, channel capacity, and transmission speed in wireless communication by utilizing multiple antennas for both transmission and reception, effectively leveraging multipath propagation. Most *MIMO* antennas are designed using microstrip technology due to their lightweight, low-profile, and easy-to-fabricate nature. However, at higher frequencies, microstrip antennas face challenges such as increased losses and RF leakage between antenna elements. To ensure optimal *MIMO* performance, the correlation between antenna elements should be minimized. Various techniques have been explored to improve isolation between elements, including the integration of decoupling structures. However, achieving low correlation without additional external components remains a key design challenge. This thesis focuses on innovative design strategies to make *MIMO* antenna systems more isolated while eliminating the need for separate decoupling structures, ultimately improving the *Envelope Correlation Coefficient*. While wireless antenna design has evolved significantly from 2G monopoles to 4G MIMO arrays, this work focuses exclusively on 5G New Radio requirements, particularly in the mmWave spectrum (24–30 GHz), where propagation challenges and spatial multiplexing demands necessitate novel MIMO architectures. Antennas for legacy systems (2G–4G) or non-cellular applications (e.g., Wi-Fi, Bluetooth) operate under fundamentally different constraints and are outside the scope of this research.

Chapter–3

Comparative Analysis of various Planar MIMO Antennas operating in Millimeter Frequency range.

3.1 OVERVIEW

This chapter presents a thorough investigation of mmWave *MIMO* antennas, encompassing a range of technical considerations aimed at improving their overall performance. The conversation commences with a comprehensive analysis of mmWave *MIMO* antennas, encompassing methodologies aimed at enhancing isolation and mitigating surface wave current. The focus of this chapter is to provide a comprehensive analysis of efficient feeding methods and strategies for reducing their size. Main contribution of the chapter:

- It gives an overview of mmWave *MIMO* antennas as well as different ways for improving isolation and lowering surface wave current.
- The benefits of *Dielectric Resonator Antenna (DRA)*s are detailed in the manuscript, along with the most effective antenna feeding and size reduction approaches. Additionally, advanced design methods to improve individual *DRA* gains are examined. *Radio Frequency (RF)* front-end designers receive help on selecting antenna topologies to meet desired performance in frequency response, gain, and polarization.
- Different approaches of *MIMO* array are discussed to focus considerable improvement in data speeds and network efficiency that results from their capacity to transmit/receive many data streams simultaneously.
- Examining the structure of the metamaterials help to improve design performance.

- Along with their effect on the antenna's performance, it looks at the importance of slots/slits, stubs, patches, and *Defected Ground Structure* in antenna structure design.
- It examines the advantages of current designs and the difficulties in enhancing the antenna structure for improved *MIMO* antenna performance.

3.2 CLASSIFICATION OF PLANAR MIMO ANTENNAS FOR MMWAVE APPLICATIONS

Different types of designs have been specifically developed for *Millimeter Wave (mmWave)* applications that utilize *MIMO* technology. This section classifies *MIMO* designs according to their structural design, including slot/ patch/stub antennas, defected ground antennas, *MIMO* Antenna Array, *Dielectric Resonator Antenna (DRA)*, and Meta-surface/metamaterial-based antennas. The analysis of *MIMO* antennas is carried out in this chapter with an emphasis on several parameters including bandwidth, gain, efficiency, and isolation. This study goes beyond the assessment of the benefits offered by existing designs, and instead focuses on the inherent problems associated with upgrading antenna structures in order to achieve greater performance in *MIMO* antennas. Figure 3.1 shows the classification of *MIMO* antennas through design structure.

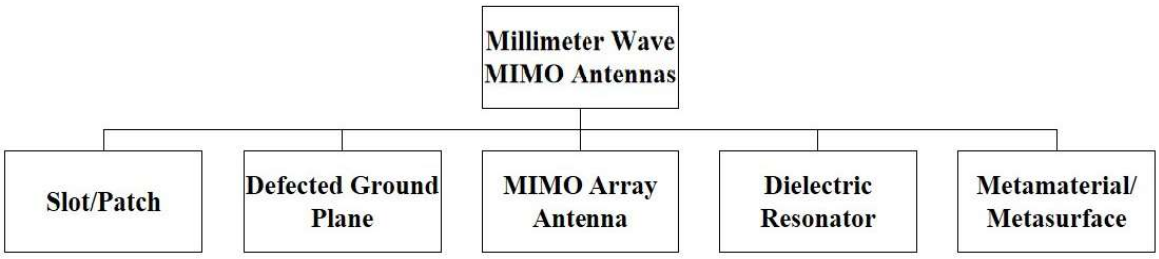

Fig. 3.1: Types of MIMO antenna for Millimeter Wave (mmWave)

3.3 MIMO ANTENNA PERFORMANCE METRICS FOR COMPARISON

This section provides an overview of key performance metrics used to evaluate antennas with many inputs and outputs, focusing on parameters that influence their efficiency, diversity, and channel capacity.

3.3.1 Envelope Correlation Coefficient (ECC)

A key metric in millimeter wave multiple-input multiple-output, the envelope correlation coefficient measures how similar or correlated the radiation patterns of various antenna elements are. In *MIMO* communication, achieving low *ECC* values is crucial for ensuring high diversity gain and minimizing signal interference between antennas. The diversity performance of antenna systems can be exactly represented using input parameters [60]. In an ideal *MIMO* system, antenna elements should have minimal correlation, allowing them to transmit independent data streams efficiently. The envelope correlation coefficient (ECC) for a multi-port antenna system, accounting for radiation efficiency, is given by [61]: *Envelope Correlation Coefficient* is used to measure this correlation and is expressed mathematically as Equation (3.1):

$$\rho_e(i,j,N) = \left| \frac{\sum_{n=1}^{N} S_{i,n}^{*} S_{n,j}}{\prod_{k=i,j} \left(1 - \sum_{n=1}^{N} S_{k,n}^{*} S_{n,k}\right) |^{1/2}} \right|^2 \frac{1}{\eta_{t;} \eta_j \eta_N} \tag{3.1}$$

where $S_{i,n}$ are the scattering parameters, and η_i, η_j, η_N represent the radiation efficiencies of the respective ports, also N represents total amount of antennas within the *MIMO* system. .

A low ECC (typically < 0.5) ensures better isolation between antennas, leading to improved system performance.

3.3.2 Diversity Gain (DG)

Diversity gain is a crucial metric in *Millimeter Wave (mmWave) MIMO* systems, which helps improve signal quality and reliability by leveraging multiple transmission paths. Since mmWave frequencies (e.g., 28 GHz, 38 GHz, and beyond) experience significant signal degradation because of air absorption and path loss, and blockages, achieving a high diversity gain is essential for maintaining stable wireless communication. It is closely related to the envelope correlation coefficient (ECC) [62, 63]. It calculates how much the signal-to-noise ratio improves with the use of numerous antennas as opposed to a single antenna system. It helps mitigate fading by ensuring that the strongest available signal is utilized. Mathematically, *Diversity Gain (DG)* is

expressed as Equation (3.2):

$$DG = 10e_\rho \tag{3.2}$$

where, *DG* represents *Diversity Gain*, measured in decibels (dB) and e_ρ is a correlation-based factor mathematically calculated as given in Equation (3.3);

$$e_\rho = \sqrt{(1 - |0.99\rho_e|^2)} \tag{3.3}$$

where, ρ_e is the *Envelope Correlation Coefficient (ECC)*, which indicates the similarity between antenna radiation patterns. *A lower ECC value suggests better antenna isolation and improved diversity gain.*

3.3.3 Total Active Reflection Coefficient (TARC)

For systems with several inputs and outputs, the *Total Active Reflection Coefficient (TARC)* is a crucial performance aspect which assesses the total reflected power from all antenna elements when excited simultaneously. Unlike traditional S-parameters, which evaluate isolation and mutual coupling individually, *TARC* considers the overall interaction among the elements, making it a more comprehensive measure for multi-port antennas as seen below in Equation (3.4) and defined as [61]:

$$\Gamma_a^t = \sqrt{\sum_{i=1}^{N} |b_i|^2} / \sqrt{\sum_{i=1}^{N} |a_i|^2} \tag{3.4}$$

where, Γ_a^t symbolizes *Total Active Reflection Coefficient (TARC)*, which stands for the ratio of a *MIMO* antenna system's entire reflected power divided by entire incident power. It facilitates the analysis of the amount of power reflected when several antenna elements are activated at once, N represents total quantity of antenna components in the *MIMO* system, b_i indicates the reflected signal wave amplitude at the i_{th} antenna port. This accounts for the amount of input signal that is returned around due to impedance mismatching or coupling effects and a_i represents the incident signal wave amplitude at the i_{th} antenna port. A TARC value below 0.33 (or –9.6 dB) is considered acceptable for practical MIMO systems. For a *MIMO* system, with

two elements *TARC* can be explicitly computed using S-parameters from the following Equation (3.5):

$$\begin{aligned}\Gamma_a^t &= \sqrt{(|a_1(S_{11}+S_{12}e^{j\theta})|^2+|a_1(S_{21}+S_{22}e^{j\theta})|^2)}/\sqrt{2|a_1|^2} \\ &= \sqrt{((S_{11}+S_{12}e^{j\theta})|^2+|(S_{21}+S_{22}e^{j\theta})|^2)}/\sqrt{2}\end{aligned} \tag{3.5}$$

where, phase difference between the input signals is θ and S-parameters S_{11}, S_{12}, S_{21}, S_{22} stand for the antenna elements' coupling and reflection properties. The Total Active Reflection Coefficient (TARC) provides a comprehensive measure of multi-port antenna performance [64, 65].

After obtaining the S-parameters of the *MIMO* antenna system, the phase of the input signal is varied between 0 and 180 degrees. This variation in phase gives us an insight to the antenna resonant behavior and results in corresponding plots for effective bandwidth evaluation.

3.3.4 Channel Capacity Loss (CCL)

Channel capacity is a measure of number of bits per Hz of bandwidth. In other words, Shannon's theorem, as it is often known, is the fastest possible pace of unhindered information flow over a communication connection. It is a key indicator of MIMO system degradation due to mutual coupling and correlation [66]. It is a tool for assessing MIMO systems' performance with a single antenna. Other diversity performance characteristics affect it, and it increases linearly as the quantity of *MIMO* system antenna elements increases. One may assess the system deterioration measure using *Channel Capacity Loss (CCL)*. It is computed using the subsequent Equations (3.6) to (3.9):

$$C(Loss) = -\log_2 \det(\eta) \tag{3.6}$$

where, $C(Loss)$ represents *Channel Capacity Loss*, representing the decrease in the possible data rate as a result of system impairments and $\det(\eta)$ represents the determinant of the correlation matrix η, which characterizes the coupling between antenna elements.

$$\eta = \begin{bmatrix} \sigma_1 & \sigma_1 \\ \sigma_2 & \sigma_2 \end{bmatrix} \tag{3.7}$$

where, η indicates the correlation matrix, capturing the interdependence between different *MIMO* antenna elements and σ_1, σ_2 represents parameters related to the mutual correlation and efficiency of the antenna elements.

The correlation matrix η for a 2-port MIMO system is constructed using the scattering parameters as follows [61]:

For diagonal elements:

$$\sigma_{ii} = 1 - |S_{ii}|^2 - |S_{ji}|^2 \tag{3.8}$$

For off-diagonal elements:

$$\sigma_{ij} = -\left(S_{ij}^* S_{jj} + S_{ji} S_{ii}^*\right) \tag{3.9}$$

This matrix quantifies the power distribution and coupling between ports, and is used to compute Channel Capacity Loss (CCL) for evaluating MIMO performance under correlated fading channels.

where, S_{ii} indicates reflectivity (S-parameter) of the ith antenna element, representing the amount of power reflected at that port, S_{ji} indicates mutual coupling coefficient between antenna elements i and j, indicating the interaction between the antennas and S_{ii}^* represents complex conjugate of S_{ii}, used in correlation calculations.

3.3.5 Radiation pattern

In millimeter wave (mmWave) *MIMO* antennas, the radiation pattern plays a key role in making sure signals are transmitted and received efficiently. Since mmWave frequencies (from 24-100 GHz) experience high path loss, antennas must be designed to maximize signal strength and minimize interference. The radiation pattern consists of different lobes, each influencing the

antenna's performance in unique ways. It is usually stated as a function of the directional coordinates and the radiation pattern is defined in the far-field region. The characteristics of radiation include directivity, phase, polarization, field strength, radiation intensity, power flux density, and radiation intensity. A 2-dimensional or 3-dimensional spatial distribution of radiated energy is referred to as an object's radiation property. The pattern of radiation can be represented using either a logarithmic scale or in decibels (dB). Figure 3.2 displays a traditional radiation pattern consisting of different lobes.

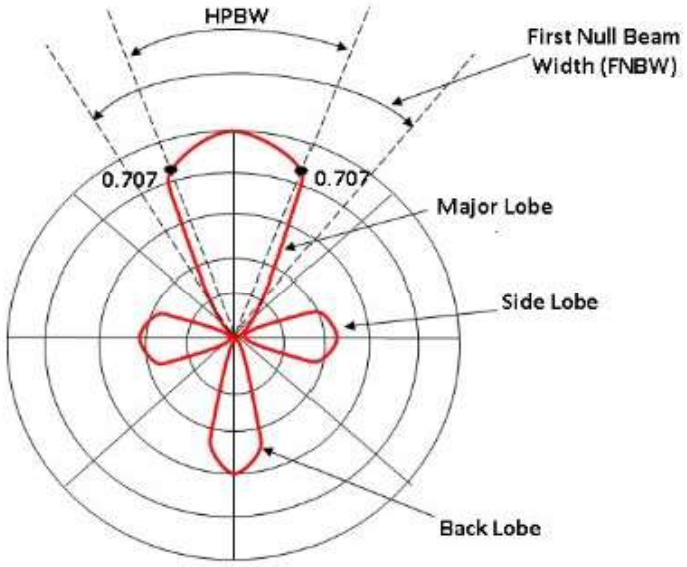

Fig. 3.2: Radiation characteristics of the MIMO antenna, depicting The direction of the power's radiation.

- **Major Lobe:** The main lobe is where most of the signal power is directed. This is the primary radiation beam and is essential for establishing strong communication links. In mmWave *MIMO* systems, having a narrow, high-gain main lobe helps compensate for signal attenuation and improves beamforming efficiency. The major lobe is depicted in the diagram above at θ=0 degree, vertically pointing upward.

- **Side Lobe:** Additional radiation lobes that emerge at angles to the primary lobe are known as side lobes. Because they can interfere with other signals and lessen the primary beam's efficacy, they are typically undesired.

- **Back Lobe:** The radiating lobe's direction forms an angle of 180 degrees with the major lobe's direction. It describes radiation emitted in the main beam's opposite direction. In mmWave *MIMO*, strong back lobes are problematic as they cause signal reflections and unwanted multipath propagation, especially in dense urban areas.

3.3.6 Bandwidth (BW)

The bandwidth of an antenna system that has multiple inputs and multiple outputs is the range of frequencies that the antenna can operates efficiently while maintaining acceptable *impedance matching*, *low reflection loss*, and *stable radiation characteristics*. The operational bandwidth of an antenna is commonly defined as the frequency range over which the return loss satisfies $S_{11} \leq -10$ dB [67].

Mathematically, the antenna's operational bandwidth is determined using **S-parameters**, specifically the S_{11} *parameter* (or return loss) and other scattering parameters as defined by Equation 3.10. The bandwidth is defined as the frequency range where the magnitude of the reflection coefficient ($|S_{11}|$) remains below -10 dB, ensuring that at least 90% of the power is transmitted rather than reflected:

$$BW = f_2 - f_1, \quad \text{where } S_{11} \leq -10 \text{ dB} \tag{3.10}$$

where BW represents the bandwidth, f_2 symbolizes the upper frequency range and f_1 symbolizes the lower frequency range.

Additionally, in *MIMO* systems, bandwidth can also be analyzed using the *Total Active Reflection Coefficient (TARC)* given in in Equation (3.4) as to account for the influence of multiple ports operating simultaneously [68]. The bandwidth is defined over the frequency range where *TARC remains below a certain threshold*, ensuring efficient multi-port operation:

Thus, the *MIMO* bandwidth analysis using S-parameters is crucial in evaluating the appropriateness of antenna for either narrowband or wideband applications, ensuring optimal performance in contemporary wireless communication technologies, including 5G, *LTE*, and *Wi-Fi*.

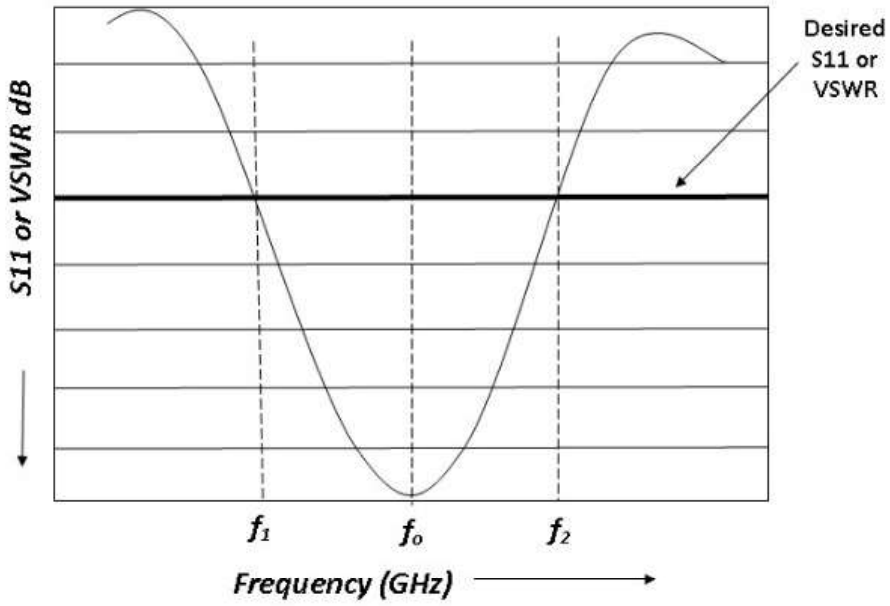

Fig. 3.3: Figure illustrates the process of determining the bandwidth of the MIMO antenna system based on the S-parameters.

3.3.7 S-Parameters

Scattering parameters, commonly referred to as S-parameters, are represented using the scattering matrix. The "S" in S-parameters represents scattering. Figure 3.4 illustrates the significance of S-parameters stated by [69]. S-parameters are employed in electrical systems to specify how input and output terminals are related. For example, S_{NM} denotes the power transferred from Port M to Port N in the case of two ports (Port M and Port N). The electricity transferred from port N to port M is denoted by S_{MN}.

Where a_1 is the incident signal at port1, b_1 is the reflected signal at port1, a_2 is the incident signal at port2, b_2 is the reflected signal at port2

The theory of S-parameters for N-port networks is detailed in Chapter 4 of [70]. The S-parameters of the network illustrated above are expressed in Equation (3.11) as:-

$$\begin{pmatrix} b_1 \\ b_2 \end{pmatrix} = \begin{pmatrix} S_{11} \\ S_{21} \end{pmatrix} S_{22} \begin{pmatrix} a_1 \\ a_2 \end{pmatrix} \tag{3.11}$$

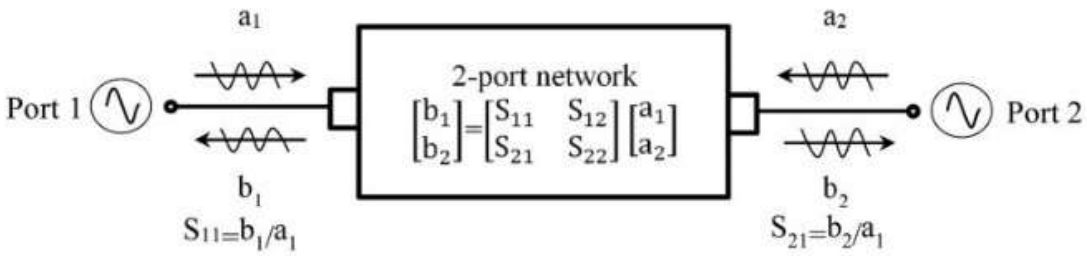

Fig. 3.4: Scattering parameter illustrations with a two-port network

3.3.8 Directivity (D)

Directivity refers to an antenna's capacity to focus its radiation in a particular direction, compared to an isotropic radiator (which radiates uniformly in all directions). The directivity of an antenna is defined as [67, Eq. 2-19]:

$$D = \frac{U}{U_0} = \frac{4\pi U}{P_{rad}} \tag{3.12}$$

Equation (3.12) gives the mathematical representation of directivity. Where, U represents intensity of radiation ($\frac{W}{Solidangle}$), U_0 indicates the isotropic source's radiation intensity., P_{rad} represents overall power radiated.

Directivity is a key performance parameter in *Multiple-Input Multiple-Output (MIMO)* antenna systems, as it determines how efficiently an antenna concentrates emitted energy in a certain direction. In *MIMO* communication, where multiple antennas work together to enhance signal quality, high directivity helps in beamforming, spatial diversity, and interference mitigation, improving overall system efficiency as shown by the main lobe in Figure 3.2.

3.3.9 Antenna Gain (G)

Gain is a critical parameter in mmWave *MIMO* antenna systems, as it determines how effectively an antenna radiates or receives energy in a specific direction. In *Millimeter Wave (mmWave)* communications, where signals suffer from high path loss, high-gain antennas are essential to ensure reliable and efficient transmission. In comparison to an isotropic radiator, antenna gain is a measurement of the amount of power radiated in a particular direction. The antenna gain is defined as the product of directivity and radiation efficiency [67, Eq. 2-21]. Equation (3.13)

define antenna gain as:

$$G = D \times \eta \tag{3.13}$$

Where G is the antenna gain, D denotes the directivity, η represents the efficiency which accounts for losses due to dielectric, conductor, and mismatch losses..
As the gain rises, the beam width will decrease. It is therefore important to keep a balance while building an antenna system.

3.3.10 Efficiency

Efficiency in mmWave *MIMO* antennas is a key performance factor influencing signal quality, power utilization, and system reliability. At high frequencies, multiple efficiency parameters need to be taken into account to maximize the antenna's performance. The main types of efficiency in mmWave *MIMO* are radiation efficiency, total efficiency, and system efficiency. Each of these aspects has a significant impact on determining how well the antenna transmits and receives signals in a multi-antenna environment.

1. **Radiation Efficiency** Radiation efficiency (η_r) measures how well an antenna generates electromagnetic waves from input powers, considering conductor and dielectric losses or in other words Radiation efficiency is defined as the ratio of radiated power to input power [67, Eq. 2-92], as given in Equation (3.14):

$$\eta = \frac{P_{radiated}}{P_{input}} \tag{3.14}$$

   where $P_{radiated}$ is the radiated power, and P_{input} is the total power delivered to the antenna.

   At mmWave frequencies, radiation efficiency is significantly impacted by increased metal and substrate losses, leading to a drop in overall performance. To enhance η_r, high-performance low-loss substrates (e.g., Rogers 5880) and metasurface designs are often used to minimize attenuation.

2. **Total Efficiency** Total efficiency (η_t) accounts for both radiation efficiency and impedance mismatch losses [71, p. 152]. It is defined as (3.15)

$$\eta_t = \eta_r \times (1 - |\Gamma|^2) \tag{3.15}$$

where, η_t represents total efficiency of the antenna system, considering both radiation efficiency and impedance matching, η_r indicates the radiation efficiency, which accounts for the power actually radiated by the antenna relative to the total accepted power and Γ represents the reflection coefficient, which represents the portion of the incident signal that is reflected due to impedance mismatch.

3. **Mean Effective Gain** In a *MIMO* system, efficiency is evaluated not only for individual antenna elements but also for the entire array. The overall efficiency is significantly influenced by mutual coupling effects between the elements, which can impact system performance. One of the key metrics used to assess *MIMO* system efficiency is the *Mean Effective Gain (MEG)*. It considers both radiation efficiency and mutual coupling, ensuring an accurate evaluation of the antenna's contribution to the communication system [72, 73]. The MEG for the *i*th antenna element in an *M*-element *MIMO* system is stated mathematically as Equation (3.16):

$$MEG_i = 0.5\eta_{i,r} \times \left[1 - \sum_{j=1}^{M} |S_{ij}|^2\right] \tag{3.16}$$

where, $\eta_{i,r}$ is radiation efficiency of the *i*th antenna element, In the *MIMO* system, M is the total number of antenna components, and S_{ij} is the scattering parameter (S-parameter), which indicates the coupling between antennas i and j. The factor of 0.5 accounts for averaging over two orthogonal polarizations in isotropic multipath environments. This metric quantifies the effective radiated power under real-world fading conditions and is critical for evaluating MIMO system performance.

3.4 COMPARATIVE ANALYSIS OF PLANAR MIMO ANTENNAS FOR MMWAVE RANGE

3.4.1 Slot/Patch MIMO Antennas

Many of the planar patch designs use one substrate, making them cheaper and simpler. For multi-band resonant frequency and bandwidth, the planar design uses the slots[74, 75]. Also, Rectangular slots [76], E-shape [77, 78, 79], U-shape [80, 81], fractal-shape [82, 83], annular slots [84], Dual-mode slotpatch [85], U-shaped patch-slotted (four-element) design [86], and

many more dominate the radiating plane of the design. To maximize radiation efficiency, match the port at input, of the radiating element, with the microstrip feed line of 50Ω, which depends on its width. This section compares slot *MIMO* antennas.

Circular design and *Substrate Integrated Waveguide (SIW)* transmission line technologies help reduce the device's footprint. The antenna operates effectively for 5G applications due to its high port isolation. Monostatic *STAR* antennas are compatible with this design. Since *In Band Full Duplex (IBFD)* allows *Simultaneous Transmit and Receive (STAR)* on the same frequency, it has the potential to increase system capacity and spectral efficiency in wireless communications. However, achieving separation of 90 to 120 dB between the *Transmitter (Tx)* and *Receiver (Rx)* signal channels is a significant challenge for *IBFD* systems. This level of isolation requires solutions beyond antenna design alone. Additional self-interference cancellation methods are recommended, as improving antenna isolation can reduce the need for extensive *RF* and digital *Successive Interference Cancellation (SIC)* techniques. The architecture in [84] permits any combination of the 3-ports for the *Tx* and *Rx* without physical changes. The single port excitation case has 4.71 dBi maximum gain, whereas the two port case has 8 dBi. Both have 88.78% radiation efficiency. From frequency range 27.5 GHz to 28.05 GHz, the lowest -10 dB bandwidth is 0.55 GHz. The *ECC* for this bandwidth is below 0.002. The author also says that the 3D simulated and comparable model results agree well. A novel two-mode slot-patch design for Ka-band frequencies is suggested [85].

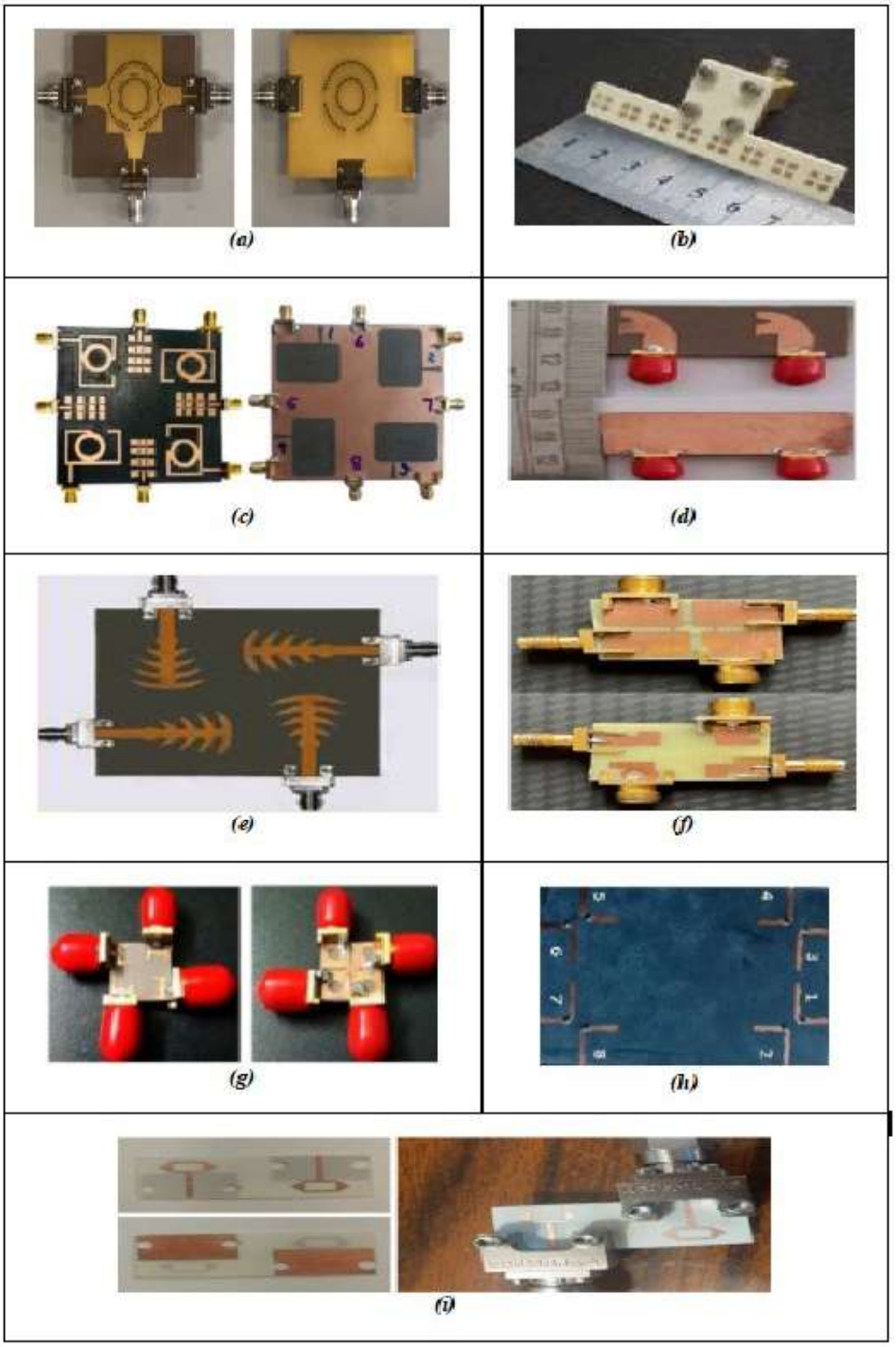

Fig. 3.5: Fabricated slot/patch MIMO design. Source: (a) Kobal et al. (2022), (b) Wang et al. (2022), (c) Jabeen & Khan (2022), (d) Usman et al. (2022), (e) Sehrai et al. (2020), (f) Patel et al. (2022), (g) Jetti et al. (2023), (h) El-Nady & Attiya (2022), (i) Ali et al. (2021), as reproduced in Design and Fabrication of Millimeter Wave Antenna for Future Wireless Applications (2024, p. 45).

An integrated *MIMO* system with high isolation for sub-6 GHz and mmWave frequencies is reported in [87]. The design features monopole antennas decoupled with 24 and 28 GHz (5G) The design isolates the lower band by -22 dB and exhibits 0.284 envelope correlation. The design operates at 4G *LTE*, 5G and *Wireless Local Area Network (WLAN)* with the bandwidth of 1.75 GHz and 1.08 GHz respectively. The simple and compact design, good gain, and large spectrum make it appropriate for *WLAN*, 5G, and 4G LTE. Sub-6 GHz decoupling is added to mmWave radiation in this patch antenna. External decoupling is no longer needed to detach monopole antennas. Isolation is achieved through the orthogonality of ground plane slots and antenna elements.

An asymmetric flare-shaped patch *MIMO* antenna with two inputs and two outputs is suggested for use in mWave communication systems in [39]. *MIMO* design achieves -10 dB return loss across 20-40 GHz with more than 20 dB isolation between the design components. Return loss, gain, effective coupling coefficient, and radiation pattern for the proposed *MIMO* design are realized by the authors. The design meets *MIMO* diversity performance with two antenna elements by isolating signals by more than 20 dB and amplifying them by 8.17 dB with an *ECC* value of < 0.0001. Single-element antennas have a peak gain of 8.14 dB and an impedance bandwidth of 10 dB at 20–40 GHz. To obtain higher than -20 dB isolation across the frequency spectrum, the best-optimized value is 11.2 mm between the two elements [39].

[88] presents a new compact tree-shaped planar quad element *MIMO* antenna. Maximum gains of 10.58 dB, 8.87 dB, and 11.45 dB were obtained at 28 GHz, 33 GHz, and 38 GHz radiation patterns, respectively. At *Millimeter Wave (mmWave)* frequencies, the *MIMO* antenna exhibits an efficiency of approximately 70%. In addition, *MIMO* systems meet the conditions of *MEG* being less than 3 dB and *ECC* being less than 0.5. The suggested arrangement arranges *MIMO* antenna elements orthogonally. To prevent mutual interference between *MIMO* antenna parts, diagonal components are built anti-parallel. Ground surfaces of the antenna elements are also coupled to ensure consistent voltage in the *MIMO* antenna setup that is being suggested.

An interconnected 3 and 4 element wideband *MIMO* design is used by the author for mmWave 5G applications in [89]. To generate *MIMO* antennas with three or four elements, the unit element is carefully created and positioned utilizing orthogonal rotation. An interconnected ground for both cases improves the resonator's practicality. Both designs have 43% impedance

bandwidth from 26 to 40 GHz. The three and four-element *MIMO* antennas also work well in millimeter wave 5G applications.

Single-element design optimization for wideband frequency resonance was the authors' initial emphasis in [89]. This single-element configuration allowed the development of 3 and 4 element *MIMO* designs. Both designs have a connected ground plane that meets real-world requirements. Using a connected ground plane design provides over 20 dB of isolation. This design has advantageous diversity metrics, with *ECC* below 0.02 and the value of *DG* above 9.9.

A compact-slotted four-element planar monopole *MIMO* design for 5G mmWave n257/n258 and n262 bands is presented [86]. To enhance *MIMO* antenna impedance, 1.3 mm × 0.2 mm, rectangular strip and two slots to each radiating element is added. The U-shaped slotted radiating components provide introductory operational band at a frequency of 27.1 GHz (25.9 - 27.8 GHz). Carving hexagonal grooves on the ground creates the 2^{nd} operating band at a frequency of 48.7 GHz (47.1 – 49.9 GHz). The antenna isolates at a level higher than -27 dB by positioning slots and radiating elements at 90 degrees on the ground. The design displays consistent radiation patterns, such as radiation efficiency > 90%, peak gain > 5.95 dBi, *Envelope Correlation Coefficient (ECC)* $<10^{-6}$, *Total Active Reflection Coefficient (TARC)* $\leq$-10 dB, and *Channel Capacity Loss (CCL)* < 0.03 bits/s/Hz.

The *MIMO* antenna system in [90] uses these antenna pieces on 4 corners of a substrate. The authors propose a wideband *Circularly Polarized (CP) MIMO* mmWave design for 5G applications with a range of frequency from 27.5 to 31 GHz. *Circularly Polarized* has been achieved with the help of phase difference and also, with the change in the location of feed point. The antenna is perfect for the millimeter wave n261 5G-band (27.5 - 28.35 GHz). The design is fed by a coaxial probe, eliminating complex feeding networks. To accomplish circular polarization, the microstrip line is L-shaped with the feeding network moved from the corner. The L-shaped microstrip line antenna has stubs (fishtail) on one side. Adjusting the stub spacing guides the center frequency wavelength. Fishtail stubs mitigate anti-phase magnetic currents, boosting microstrip line radiation.

In [91], two $26 \times 9 \times 11$ mm^3 monopole components enable dual-band operation at 27 and 39 GHz. Investigation and optimization of mutual coupling minimizes the effect of one element on the other. The first and second bands of the *MIMO* antenna have 5 dBi and 5.7 dBi gains,

respectively, and 99.5% and 98.6% radiation efficiency. Simulations of *MIMO* performance show a diversity increase of 10 dB over the two operational bands and an envelope correlation of $10^{\check{}}4$. Following are the design investigations:

- The study explores novel frequencies in the millimeter wave region using two wide bands.
- Thorough analysis of radiation and diversity performance.
- The design is planar and easy-to-fabricate.
- High element isolation.
- Achieved high efficiency of radiation with the RT Rogers 5880 dielectric substrate.

The degree of separation between antenna elements reduces interference and improves *MIMO* system performance. Figure 3.5 (a-i) shows antenna prototypes, revealing their physical designs. These extensive descriptions and performance measurements help researchers choose antennas for specific applications and strengthen mmWave *MIMO* communication systems.

Table 3.1 gives a detailed overview of millimeter wave antenna designs, including key technical criteria for assessing their appropriateness for *MIMO* applications in mmWave communication systems. Designs are categorized based on operating frequencies, bandwidths, gains, number of elements, efficiency, and other critical performance indicators. Additionally, the MIMO parameters as discussed in this chapter provide valuable insights into the system's effectiveness.

3.4.2 Defected Ground Plane MIMO Antennas

Millimeter Wave MIMO antennas benefit from defected ground structures. To reduce antenna port interaction, the ground plane was artificially designed. In millimeter wave *MIMO* systems with crucial antenna separation, *Defected Ground Structure (DGS)* minimizes interference, improving signal quality and network stability. By decreasing mutual coupling, *DGS* allows small antennas to be placed near together without affecting performance. For 5G networks to deliver quicker data transfer and greater connectivity in densely populated locations, this technology is essential.

Table 3.1: Comparison between the Performances of Slot and Patch MIMO antennas

Ref.	Antenna Design	Freq. (GHz)	BW (%)	Gain (dB)	No.of Ant.	Efficiency (%)	ECC	MEG (dB)	DG (dB)	TARC (dB)	Isolation (dB)
[84]	SIW triple-port annular slot antenna	27.5-28.05	0, 55	8 (two port)	—	88, 78%	—	—	—	—	5G mm-wave IBFD
[85]	Dual-mode slot/patch antenna	27	23	15.4 (array)	8	—	—	—	—	—	Ka-band
[87]	Integrated MIMO antenna system	2.5, 3.5, 5.2, 24, 28	—	11.4 (28 GHz)	4 (mm-wave)	—	0, 284	—	10 (over 2 bands)	—	-22
[39]	Asymmetric flare-shaped patch MIMO antenna	20-40	10	8, 17	2	—	< 0.0001	—	> -20 (over 20-40 GHz)	> 20	mmWave
[88]	Tree-shaped planar quad element MIMO antenna	23-40	—	11.45 (38 GHz)	4	> 70%	—	< 3 (dB)	—	—	> 20
[89]	Wideband interconnected 3 element and 4 element MIMO design	26-40	43	—	3 (case 1), 4 (case 2)	> 20 dB (connected ground)	—	> 9.9	—	—	> 20
[86]	Compact-slotted four-element MIMO planar monopole antenna	27.1, 48.7	—	> 5.95	4	> 90%	—	—	—	—	> -27
[90]	L-shaped microstrip line with fishtail stubs	27.5-31	—	—	4	—	—	—	—	—	—
[91]	Dual-band monopole components	27, 39	—	5.7 (39 GHz)	2	98.6% (39 GHz)	< 0.0001	10 (dB)	—	—	—

For 5G and *Internet of Things (IoT)* applications, a compact 2-band 2-element *MIMO* design is discussed in [92]. The antenna uses multiple frequencies between 26.5 and 27.1 GHz and 39.15 and 40.69 GHz in *Millimeter Wave (mmWave)* range. The antenna has dimensions of $10 \times 28 \times 0.787$ mm^3 and has a peak gain of 7.29 dBi at resonance frequencies of 26.8 GHz and 39.8 GHz, respectively. The antenna outperforms others due to its design compactness, low *ECC* (< 0.03), and isolation, superior gain, and efficiency.

A two-element arrangement actuated by a T-junction power combiner/divider feed network was proposed by author in [93]. Although various slot forms, such as rectangular, zigzag and circular, are used to intentionally alter the ground plane, the array uses rectangular slotted-patch antennas to improve antenna radiation. In [93], authors claim that structure can use 25.5 GHz – 29.6 GHz for millimeter wave 5G applications. In the stated frequency range, the maximum gain is 8.3 dBi. To isolate antenna elements, polarization diversity is used between adjoining radiators, thus reduces *ECC*. Further performance indicators of the suggested structure include *DG*, *CCL*, and *MEG*.

According to [94], *MIMO* antennas have a rectangular patch structure with a 1×2 layout. Each patch is placed in the center of a 20×20 mm^2 RO4350B substrate. Rectangular slots are added to the ground layer and radiating patches to downsize and improve performance. A center ground plane E-shaped slot is also appropriately placed. The antenna's operating impedance bandwidth covers the key mmWave frequency spectrum ranges from 26.4 to 30.9 GHz. *MIMO* antenna performance indicators include the *ECC*, which must be below 0.12 for each 2-element array to meet the standard of 0.5.

Sub-mmWave 5G *New Radio (NR)* bands were covered by a compressed *Co-Planar Waveguide (CPW)* fed linked ground *MIMO* antenna [48]. A compact structure with a wide working bandwidth, good gain & improved efficiency of radiation results from planar design. Arranging the single antenna arrangement rotationally orthogonally creates a 4-port design. For isolation levels > -20 dB over the frequency range, a circular ring connects the ground's bottom plane.

This antenna has two mushroom-shaped radiating units and a ground plane with two square ring-loaded flaws [95]. *MIMO* antennas show low mutual coupling ($|S_{21}|$, $|S_{12}| < -20$) dB with

DGS. The authors look at factors like efficiency, gain, radiation pattern, and return loss in antenna performance. For *Ultra Wide Band (UWB)* frequencies, diversity factors such as mutual coupling, $ECC < 0.002$, $DG > 9.995$, $CCL < 0.3$ bits/sec/Hz are achieved.

A 28 GHz circular microstrip patch antenna featuring a single element, an elliptical slot, and a defective ground structure is proposed in [96]. This *MIMO* antenna is $20 \times 20 \times 0.8$ mm^3. With a bandwidth of 2.1 GHz, simulations show returns at each port are less than -10 dB from 26.867 to 28.975 GHz. The antenna has 9.24 dB gain due to unidirectional emission and mutual coupling below -20 dB.

Small four-port uniplanar *MIMO* for n79/n46 mmWave applications is proposed by [97]. The quad *MIMO* design has dimensions of 30 x 30 x 0.8 mm^3. *MIMO* design employs four Z-shaped radiators that are identical to one another and shared ground on the same plane with no isolation barriers used. It has a bandwidth of 12 GHz and can cover frequencies between 18 and 30 GHz. The isolation for the mid-band was -11 dB, and the isolation for the mmWave was -24 dB. A uniplanar quad MIMO antenna can deliver strong diversity performance, demonstrated by a *Diversity Gain (DG)* of 10 dB, an *Envelope Correlation Coefficient* of 0.07, a *Total Active Reflection Coefficient (TARC)* of -3 dB, and a *Mean Effective Gain (MEG)* ranging from -5 dB to 1 dB.

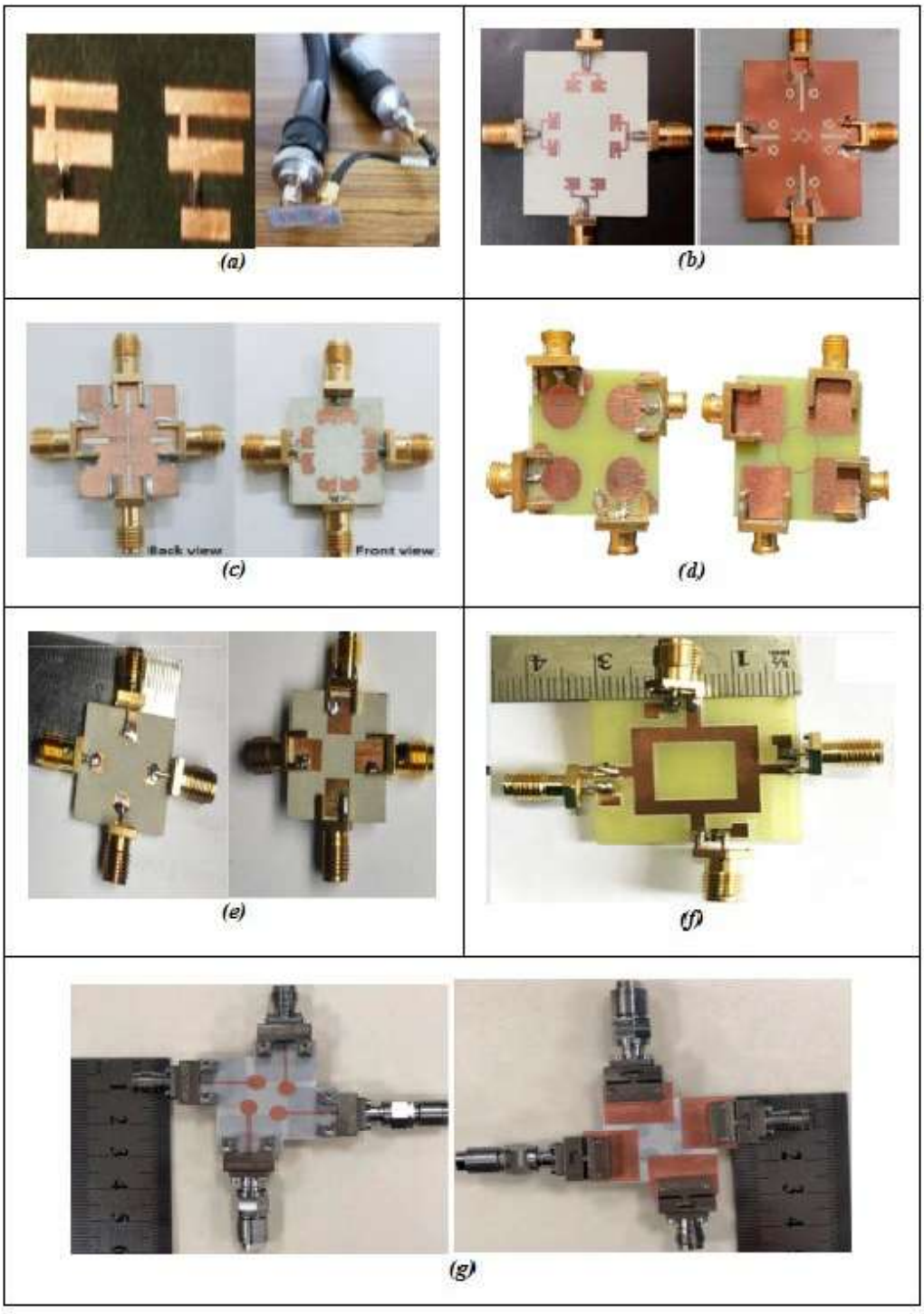

Fig. 3.6: Fabricated defected ground plane MIMO design. Source: (a) Farooq & Lokam (2023), (b) Khalid et al. (2020), (c) Abdullah et al. (2021), (d) Patel et al. (2022), (e) Sharma & Arora (2022), (f) Joseph et al. (2023), (g) Abbas et al. (2023), as reproduced in Design and Fabrication of Millimeter Wave Antenna for Future Wireless Applications (2024, p. 52).

Ultra Wide Band (UWB) antenna in [51] uses *Defected Ground Structure (DGS)* technology from 25 to 50 GHz. The prototype may integrate many telecommunication devices for different applications due to its small size. The antenna design has compact dimensions of 33 mm by 33 mm with a thickness of 0.233 mm. *MIMO* systems perform best in diversity due to orthogonally placed antenna elements. Also, align *DGS* and antenna elements for operating band separation. A *DGS* reduces mutual coupling and boosts gain to tune a reference antenna for bandwidth augmentation.

The Table 3.2 provides an in-depth look at cutting-edge millimeter wave antenna for a variety of uses. A variety of parameters, including *ECC*, *CCL*, *MEG*, *DG*, *TARC*, and isolation, are shown for each entry, each of which is designated by a reference number. The advances in size, variety, and performance of these antennas make them ideal for use with cutting-edge wireless standards like 5G *IoT*, mmWave 5G, and *UWB*. Also, the design fabrications are shown in Figure 3.6 (a–g), each unique layout, from winding grids to concentric rings to Z-shaped radiators, is tailored to meet a variety of communication requirements. To ensure optimal performance for diverse communication scenarios and developing technologies, this thorough description is a vital reference for engineers and academics.

3.4.3 MIMO Antenna Array

MIMO array antennas are at the forefront of advanced wireless communication technologies. They significantly increase data throughput and improve network efficiency by making it possible to send and receive many data streams at once. At *Millimeter Wave* frequencies, where data transmission is rapid but highly sensitive to environmental factors, *MIMO* arrays improve through spatial diversity. Leveraging multiple antennas, this technology ensures robust connectivity and increased network coverage, even in cities with high population density. These transformative capabilities make *MIMO* array antennas indispensable for achieving high-speed, low-latency communication in next-generation millimeter wave networks.

According to [98], the antenna array dimensions are $1.02\lambda \times 3.86\lambda \times 0.021\lambda$ (at 25.66 GHz). Experimental results show a bandwidth of 49.62% (25.30 GHz to 42.0 GHz) with a 12.02

Table 3.2: Comparison between the Performances of the Defected Ground Structure (DGS) MIMO antenna.

Ref.	Antenna Design	Freq. (GHz)	BW (%)	Gain (dB)	No. of Ant.	η (%)	ECC	CCL	MEG (dB)	DG (dB)	TARC (dB)	Isolation (dB)
[92]	Meandering patch with slots and ground modification	26.5-27.1, 39.15-40.69	—	7.29, 7.45	2	—	—	—	—	—	—	—
[93]	Slotted-patch antennas with modified ground	25.5-29.6	—	8, 3	2	—	< 0.03	—	—	> -20	—	—
[94]	Rectangular patch with slots (1 × 2 configuration)	26.4-30.9	—	—	2	85%	< 0.12	—	10	—	-19	—
[48]	Circular patch with CPW and circular structures	24.8-44.45	79, 35	8, 6	4	85%	—	—	—	—	> -20	—
[95]	Mushroom-shaped radiating units with DGS	31.6-48.8	43, 17	—	—	—	< 0.002	< 0.3	> 9.995	> -20	—	< -20
[96]	Circular microstrip patch with elliptical slot	26.867-28.975	2,1	9, 24	1	—	< -10	—	—	> -20	—	> -20
[97]	Z-shaped radiators with shared ground	4.4-6.3, 18-30	12	—	4	—	< 0.07	< -3	< -5, 1	10	—	-11 (mid-band), -24 (mmWave)
[51]	DGS technology with small form factor	25-50	UWB	—	—	—	—	—	—	—	—	—

dBi of peak gain. In addition, the *ECC* is < 0.0014, the isolation between the design components is greater than 24 dB for the mmWave *MIMO* antenna array across the full frequency range.

The antenna array contains four evenly spaced concentric pentagonal slots [99]. The antenna is excited in the sub-6 GHz range by a single open-end microstrip transmission line, and in the mmWave spectrum by a 1×8 *Power Divider (PD)* with a T-junction structure. On a 120 × 60 mm^2 substrate, the design was created with an edge-to-edge spacing of 49 mm. *MIMO* performance demonstrates that the suggested antenna design works effectively with a 0.113 maximum envelop correlation coefficient. Gain and efficiency peaked at 91% and 8.5 dBi across the complete operation band. The design supports 4G and future 5G wireless systems of communication, such as sub-6 GHz and 28 GHz bands.

For 5G-enabled access points, this study presents a 2-element *MIMO* antenna that uses the same components in millimeter wave and sub-6GHz bands with different feeding topologies. The work's contribution consists of:

- The antenna design emphasizes the utilization of millimeter wave antennas in conjunction with sub-6 GHz antennas that share the same radiating aperture/structure.
- The research presents a novel concept for a 5G access point that makes use of a shared aperture antenna architecture that operates at sub-6 GHz and millimeter wave frequencies and has pentagonal slots. Because of this, distinct antenna structures for millimeter wave frequencies and sub-6 GHz bands are no longer necessary.
- A design for a multi-band antenna that incorporates basic modes for each circular slot. Better gains and efficiency values in all major modes make the antenna an attractive option.
- The antenna that was recommended demonstrates outstanding *MIMO* performance in both the sub-6 GHz and the 28 GHz millimeter wave bands.

The suggested concept uses a co-shared radiating design for both sub-6 GHz and mmWave bands, despite their unique feeding mechanisms.

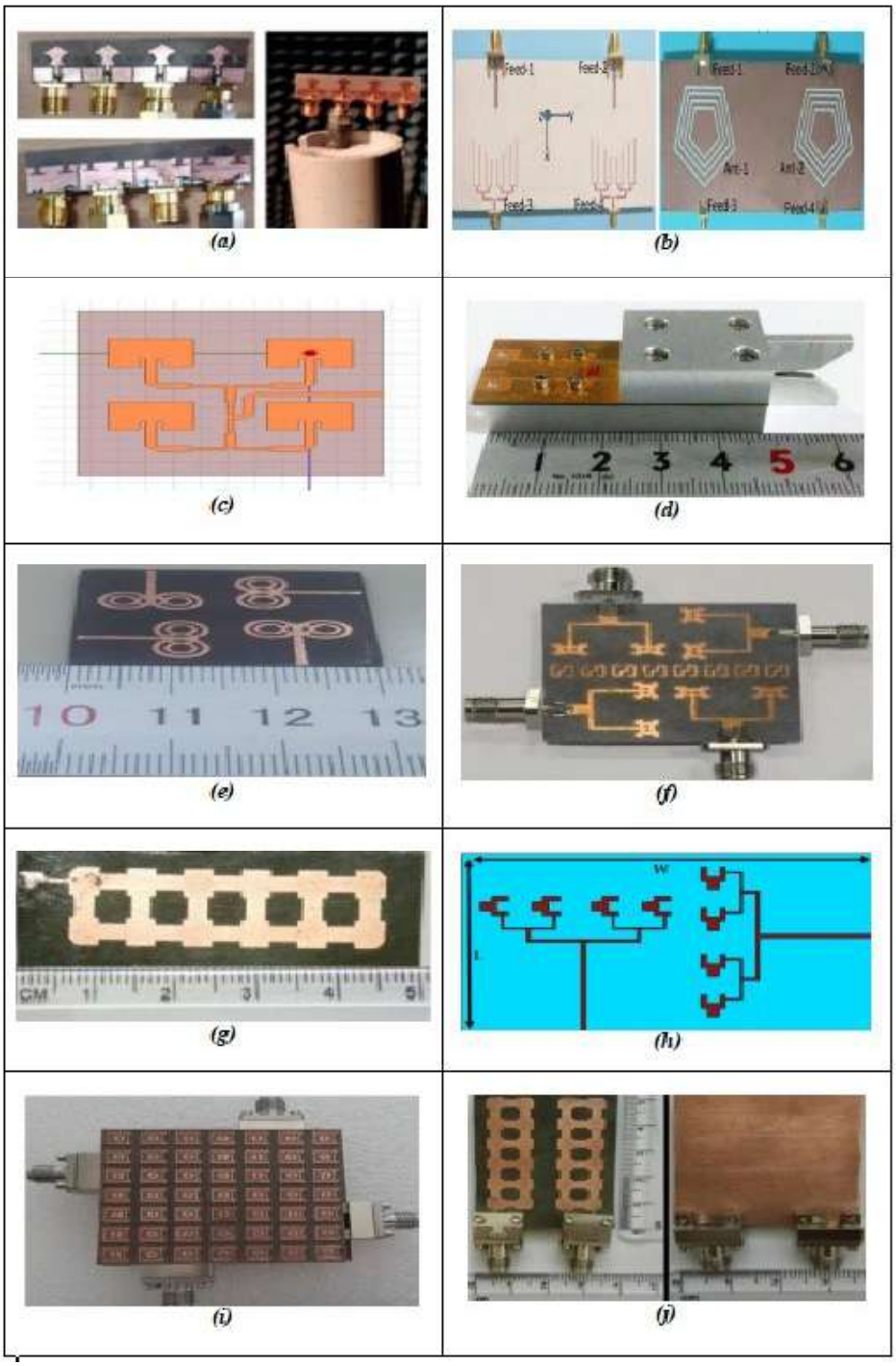

Fig. 3.7: Fabricated MIMO array design. Source: (a) Kumar & Kumar (2023), (b) Hussain et al. (2022), (c) Tahat et al. (2020), (d) Yang et al. (2017), (e) Kamal et al. (2021), (f) Bilal et al. (2022), (g) Malviya & Gupta (2023), (h) Khan et al. (2022), (i) Ud Din et al. (2023), (j) Mandloi et al. (2023), as reproduced in Design and Fabrication of Millimeter Wave Antenna for Future Wireless Applications (2024, p. 57).

A 2×2 microstrip antenna array of 11.9×15.3 mm^2 and operating at 38 GHz is described in [100]. Design achieves 14.58 dB gain, -17.7 dB return loss, and 500 MHz impedance bandwidth. Duplicating this antenna twelve times at 30° creates a dodecagon with low-profile. Each sector can cover 58° for 12 (360-degree beams). Author's antenna concept was smaller and had more gain than published antennas targeting compact size and low profile at 38 GHz.

The *Tapered Slot Antenna (TSA)* array has been designed for mmWave massive multi-beam communication [101]. The authors claim that element spacing that meets half-wavelength requirements in the H-plane allows the antenna array to perform well in beam-forming. *Millimeter Wave (mmWave)* electronics can directly integrate with the design element via a *SIW*. Reflection coefficient < -15 dB, *VSWR* < 1.45 was achieved in the frequency range 22.5 - 32 GHz while meeting *ITU* (24.25 - 27.5 GHz) and *FCC* (27.5 - 28.35 GHz) 5G requirements. The antenna element's 24 – 32 GHz gain is 8.2 – 9.6 dBi. Medium gain and big bandwidth make the *TSA* appropriate for mmWave communication systems. A *SIW*-fed metallic *TSA* with a distinctive tapered slot transition forms the antenna element. The design's impedance matching and emission patterns are excellent across many frequencies. The *SIW* feeding topology simplifies antenna array integration with planar circuitry.

[102] describes *MIMO* antenna array elements as triplet circular rings with an infinite shell. The design's simulated gain was 6.1 dBi, while the actual gain was 5.5. Additionally, actual and simulated antenna efficiency are 90% and 92%. *ECC* for *MIMO* is below 0.16 throughout the whole operational bandwidth. The antenna features 16 dB isolation, 80% efficiency, and 2.45 GHz and 28 GHz frequency response. The described multi-band antenna design becomes more complicated with a tapered slot. Studies show that mmWave resonating structures are complex and huge. Due to the congested sub-6 GHz spectrum, mmWave offers a wide bandwidth to use for 5G's faster data throughput and reduced latency than 4G. The unique mmWave antenna's circular ring-shaped radiating construction provides high isolation without *DGS*, tapered slot, or *EBG* structures.

MIMO antennas are 2-element arrays with corporate feeding networks, while the single patch antenna with bow-tie slots and slits is designed by [49]. Vertical and horizontal slots serve as *Defected Ground Structure (DGS)* to improve antenna performance. The top surface has a decoupling structure (slotted zig-zag) carved from edge to edge for isolation. Spatial

and polarization diversity isolate antenna elements (> -40 dB). The proposed antenna may provide 12.02 dBi gain in the 5G mmWave frequency with a -10 dB bandwidth from 27.6 to 28.6 GHz. A 2-element array with the *DGS* achieves high gain. A slotted construction reduces antenna interaction. The authors advised 5G connectivity research to focus on *Ultra Wide Band* operational frequency and mmWave channels. For wider coverage, add beam guiding. To span maximum 5G frequency ranges, shared aperture designs may include sub-6 GHz channels with mmWave bands.

A single-element with 2:1 *VSWR* array antenna using RT Duroid 5880 substrate, is built for 5G applications in the 27.06 – 28.35 GHz frequency range [103]. The substrate measures 51.44 × 18.34 mm^2. Each patch is approximately 3.8 × 4.5 mm^2. The recommended array has a gain of 16.07 dBi, radiation efficiency of 93.5%.

The proposed *MIMO* system [104] has two antennas. Four elements are uniformly distributed in each antenna array, whereas two have a 90-degree tilt. The 37 GHz *MIMO* antenna array addresses 5G millimeter wave communication. A four-element array can boost the antenna element's 6.84 dB gain to 12.8 dB. *ECC* and *DG* are below the standard for antenna array performance. The suggested *MIMO* antenna array has over 85% radiation efficiency in the defined operating frequency range.

An article [105] describes a redesigned circular patch radiating element for 2 × 2 5G *MIMO* arrays. Orthogonal radiating elements limit mutual interaction and boost system performance in the array. *MIMO* arrays provide 7.2 dBi gain and approximately 26 dB isolation at a frequency of 28 GHz. Each antenna has a measured 1.6 GHz bandwidth ranging from the 27.25-28.85 GHz. Also, the *Frequency Selective Surface (FSS)* boosts the 28 GHz *MIMO* design gain to 8.6 dBi. The radiation from MIMO arrays is orthogonal to their plain. 5G operational frequency (28 GHz, 26.5 GHz to 29.5 GHz) has an *ECC* < 0.002 and a *DG* of better than 9.99 dB due to low coupling in the *MIMO* design between radiating parts.

A *MIMO*-array beamforming antenna with a 2:1 *VSWR* is designed for the band of 28.0 GHz in [106]. This antenna covers the frequency range of 27.04-28.35 GHz, allowing it to be utilized in the mmWave n261 5G band. A beamforming *MIMO* antenna typically has between one hundred and two hundred main lobe directions. Less than 28.0 dB of mutual coupling can be found between the *MIMO*-array ports. Both the band's gain and radiation efficiency that

Table 3.3: Comparison of the performance of MIMO design

Ref.	Antenna Design	Freq. (GHz)	BW (%)	Gain (dBi)	No. of Ant.	η(%)	ECC	CCL	DG (dB)	TARC (dB)	Isolation (dB)
[98]	DGS-Loaded MIMO Array	25.3-42	49, 62	12, 2	2	—	< 0.0014	< 0.29	—	—	> 24
[99]	Concentric Pentagonal Slots	1.4-4.5, 28	4-4.5, 3.1-3.8, 2.48-2.9, 1.82-2.14, 1.4-1.58	8, 5	1x8	—	Sub-6 GHz 28 GHz MIMO	< 0.113	8, 5	> 9.99	—
[100]	12-Element Dodecagon Array	38	500 MHz	14, 58	2x2	—	—	—	—	—	—
[101]	Metallic Tapered Slot Array	22.5- 32	ITU 24.25-27.5 GHz, FCC 27.5-28.35 GHz	8.2-9.6	—	8.2-9.6	mm-wave	—	—	—	—
[102]	Triplet Circular Rings	2.45, 28	Dual-Band	5, 5	—	90-92%	< 0.16	—	—	—	16
[49]	Patch with Bow-Tie Slot and Slits	27.6-28.6	-10 dB BW	12, 2	2	—	—	—	> 9.99	—	> -40
[103]	Circular Patch Radiating Element	27.06-28.35	—	16, 7	2	93, 50%	—	—	—	—	—
[104]	Orthogonal Radiating Elements	27.25-28.85	1.6 GHz	7.2-8.6	2x2	> 26 dB	< 0.002	> 9.99	—	—	—
[105]	MIMO- Array Beamforming Antenna	27.04-28.35	1.31 GHz	13, 99	2x12	—	$\leq 10^{-4}$	—	—	> 93%	> -28
[106]	2x2 MIMO Array	27.5-28.35	4, 73%	> 13.99	2x2	—	$\leq 10^{-4}$	—	—	> 93%	> -28

was displayed are higher than 13.99 dBi and 93.0% respectively. The proposed architecture benefits from a $\leq 10^{-4}$ *ECC* in the stated frequency spectrum. With 1.31 GHz of *TARC* active bandwidth, it is capable of supporting Gaussian applications both indoors and outdoors. It has a simulated and measured fractional bandwidth of 4.65% and 4.73% respectively. In order to minimize return loss, port radiators are parallel and have 450 degree cutting at the patch corners.

The Table 3.3 summarizes various *MIMO* antenna array. These antenna array are tuned to certain frequency ranges, making them ideal for use with 5G networks. Their gains are substantial, their correlation coefficients are low, and their radiation patterns are effective. The designs incorporate cutting-edge features like circular rings, bow-tie holes, and orthogonal parts to guarantee top performance and compatibility with 5G technology requirements. Also, the design fabrications are shown in Figure 3.7 (a–j).

3.4.4 Dielectric Resonator Antennas (DRAs)

The effective methods for manipulating the circuit and radiation properties of *DRA*s are discussed [107]. In this section, the benefits of *DRA*s are detailed, along with the most effective antenna feeding and size reduction approaches. Additionally, advanced design methods to improve individual *DRA* gains are examined. *Radio Frequency (RF)* front-end designers receive help on selecting antenna topologies to meet desired performance in frequency response, gain, and polarization. This section focuses on analyzing the development in applying *DRA* technology at millimeter wave frequencies. Here are the primary benefits of *DRA*s:

- The size of the *Dielectric Resonator Antenna (DRA)* is proportional to $\frac{\lambda_0}{\sqrt{\varepsilon_r}}$, (where $\lambda_0 = \frac{c}{f_0}$ is the wavelength in free space at the (f_0) resonant frequency and ε_r is the relative permittivity). *DRA*s have a smaller form factor compared to typical metallic antennas, particularly when they are constructed out of materials that have a high dielectric constant (ε_r).

- Due to the absence of any substance that conducts electricity, *DRA*s that make use of low-loss dielectric materials demonstrate a high degree of radiation efficiency. Due to these properties, they are ideally suited for use in applications involving high frequencies,

ranging from 30 GHz to 300 GHz. Also, conductor losses in common metallic antennas are increased when operating at these frequencies.

- A large impedance bandwidth for *DRA*s may be achieved by carefully selecting the size of the resonator and also the material's dielectric constant.
- *DRA*s can be excited using a range of different methods, which is beneficial for a variety of applications as well as integration of the array.

3.4.4.1 Millimeter-wave DRAs

Inherently, *DRA*s have no conduction losses that makes *DRA*s useful for the applications of high frequency. Technology of *DRA* at millimeter wave frequencies has advanced recently. *Millimeter Wave (mmWave)* frequencies and beyond require small *DRA*, making *DRA* manufacturing problematic without expensive fabrication. Electrically larger *DRA*s with higher-order modes can overcome this limitation and boost antenna gain. For better antenna gain and broadband performance the combination circular patch and ring-shaped *DRA* are used in [108]. Radiating structures have a 12% impedance matching bandwidth (57 GHz - 64 GHz) according to numerical predictions. Simulated antenna gain is 16.5 dBi, the highest for a single-element *DRA*. [109] describes *Substrate Integrated Waveguide*-fed cylindrical *DRA*s with linear and circular polarization. The *DRA*s are 60 GHz resonance-oriented. Linearly and circularly polarized *DRA*s have 24% and 4.5% impedance bandwidths, respectively.

Bond-wiring is reduced by direct antenna integration on chip, enabling downsizing and lower manufacturing costs. The 60 GHz (rectangular) and 27 GHz (Circular) *DRA* on the substrate of silicon is described in [110, 111]. Setting the *Dielectric Resonator*'s relative permittivity higher than the silicon substrate's (ε_r = 11.9) decreases fringing field effect and substrate losses by concentrating *RF* power on it. When DR permittivity is $40 < \varepsilon_r < 70$, antenna gain and efficiency peak, according to research. A 45% efficiency and 1 dBi gain of cylindrical *DRA* on silicon substrate is given in [112], while a rectangular *DRA* is presented in [113]. Isolating the *DR* from the lossy substrate & directing the radiation beam broadside gives the antenna with *CPW* feeding mechanism 3.2 dBi gain at 60GHz.

[114] presents a three-layer mmWave hemispherical *DRA* with 35.8% impedance bandwidth, 9.5 dBi maximum gain, and 90% radiation efficiency. Assembling the three dielectric layers is difficult and expensive with this technology. Antenna air gaps boost multilayer *DRA* gain [115]. For mmWave applications, this study used a *DRA* (low-profile hybrid multi-permittivity) with perforated construction. Drilling the *DRA* increases bandwidth by creating air holes. Small *DRA*s make it hard to maintain air hole size and distance. Authors made 21 identical cylindrical holes in the dielectric resonator. While retaining 5.65 dBi gain, operational bandwidth increased 27.4% from 48.4% to 75.8%. An similar mmWave approach utilizes a *DRA* with a conical horn (plastic-based) to boost gain [116]. A slot-coupled microstrip line drove the antenna, which had 16.6% bandwidth, 94% radiation efficiency, and 11.3 dBi gain. *DRA* gain is 8 dBi without the plastic conical horn. However, antenna placement is tricky. *Substrate Integrated Waveguide (SIW)* technique maximizes *DRA* gain and efficiency [117].

Table 3.4: Comparison of Performance for Millimeter Wave DRAs

Ref.	**Type of DRA**	**Frequency (GHz)**	**BW (%)**	**Gain (dB)**	**Gain Enhancement Method**	**Efficiency (%)**	**Mode**
[107]	Rectangular	35	12.0	5.5	Substrate-Integrated DRA	94	TE_{10}
[114]	Hemispherical	25	35.8	9.5	3-Layer DRA	90	TE_{711}
[115]	Cylindrical	20	75.8	5.65	Hybrid Multi-Permittivity DRA	92	HE_{11}
[116]	Cylindrical	30	16.6	11.3	Conical Horn (Truncated Plastic-Based)	94	HE_{11}

The Table 3.4 references three distinct resonant modes in millimeter-wave Dielectric Resonator Antennas (DRAs), each tailored to a specific geometry and application. The TE_{711} mode in a hemispherical DRA (25 GHz) is a high-order transverse electric mode with complex azimuthal field variations, suited for wideband designs using layered structures. The HE_{11}

mode in cylindrical DRAs (20 GHz and 30 GHz) is a fundamental hybrid electromagnetic mode common in cylindrical geometries offering efficient radiation and broader bandwidth, often excited via conical horn feeds. The TE_{10} mode in a rectangular DRA (35 GHz) is the fundamental transverse electric mode, featuring a simple field distribution uniform along one transverse dimension, providing predictable broadside radiation and ease of integration, especially in substrate-integrated configurations. Each mode directly influences the antenna's gain, bandwidth, and radiation characteristics, reflecting deliberate design choices aligned with target performance metrics. For *Millimeter Wave* applications, [118] discusses *DRA* properties including feeding, reduction of size, and gain improvement to help designers of *RF* front-end to choose antenna designs for gain, optimal response of frequency and polarization.

3.4.4.2 Dielectric Resonator Antennas Array

Many factors have been used to improve *DRA* array gain in various studies. Specific references [119, 120, 121, 122] used *SIW* feed networks. Abdel-Wahab et al. [119] used N-element array of linear elements and 2-feeding slot configurations to improve radiation efficiency. A study by the same author as [119, 123] employed a *SIW* feeding network at a frequency of 33.9 GHz to build a four-*DRA* array with 11.70 dBi gain, 4.7% bandwidth, and 90% efficiency. Absence of matching circuit to promote coupling in *SIW* longitudinal slot situation is a drawback of [119].

DRA elements of four connected rectangular ring at a frequency of 28 GHz are proposed in [124], employing glue to shrink air gaps between the ground plane and *DRA*s. To improve alignment, dielectric structure contains arms. However, dielectric arm positions greatly affect *DRA* mutual coupling, radiation efficiency, and gain.

The modes in Table 3.5 correspond to dominant resonant field distributions in rectangular or grid based millimeter wave DRA arrays. The TE_{10} mode [119, 122] is the fundamental transverse electric mode offering broadside radiation and predictable performance ideal for arrays. The TE_{111} mode [120] is a higher order mode with one half wavelength variation in all three dimensions enhancing gain in large 64 element arrays. The $TE_{11\delta}$ mode [121] likely denotes a perturbed TE_{111} variant where δ signifies design modifications such as slots or parasitic elements to improve bandwidth or mutual coupling in substrate integrated waveguide SIW arrays. Lastly the $TE_{3\delta1}$ mode [124] is a higher order transverse electric mode with three half wavelengths

Table 3.5: Comparison of Performance for DRA Arrays

Ref.	Type of DRA	Frequency (GHz)	BW (%)	Gain (dB)	No. of Elements	Efficiency (%)	Mode
[119]	Rectangular	34	4.7	11.7	4	90	TE_{10}
[120]	Rectangular	35	6.4	21.5	64	85	TE_{111}
[121]	Rectangular	38	2.5	13.0	12	91	$TE_{11\delta}$
[122]	Grid	32	18.4	12.0	8	76	TE_{10}
[124]	Rectangular	28	31.6	8.0	4	86	$TE_{3\delta1}$

along the x direction, one along the height, and δ representing a deliberate structural or feeding perturbation introduced to enable wide bandwidth (31.6%) through controlled multi resonance behavior while maintaining radiation pattern stability in its 4 element connected ring array.

Mutual coupling between *MIMO* elements can substantially reduce *MIMO* system performance and antenna characteristics. Thus, metamaterial walls have been used to reduce *MIMO* element mutual coupling [125, 126], which greatly reduced mutual coupling.

In [127], metallic vias are used to decouple millimeter wave *MIMO Dielectric Resonator Antenna* units for better isolation. At appropriate locations, *DRA* pieces have vertical vias. Vias interact with electromagnetic fields to affect field distributions and lower linked fields. *DRA* of *MIMO* elements can be better isolated. The vias in the *DRA* components make the antenna system small and straightforward. The feasibility and universality of this technology were demonstrated by developing, constructing, and measuring two examples: an H-plane and an E-plane connected 1×2 *MIMO DRA* arrays. Using vias efficiently can isolate the H-plane connected *MIMO DRA* array and the E-plane array are from 15.2 to 34.2 dB and from 13.1 to 43 dB respectively at 26 GHz. For the first time in [127], advocates employing simple metallic vias to isolate mmWave *MIMO DRA* parts. Research shows that vertically placing vias inside *DRA* elements reduces mutual coupling without increasing antenna footprint or height. Although the decoupling vias change the excited antenna's field distributions, the emission patterns are essentially identical to the single *DRA*. Since the DRs are the principal radiator and the vias do not resonate in the operational band, their loss is negligible.

In [128], rectangular microstrip-fed slots activate the substrate using *Dielectric Resonator (DR)*. To isolate antenna elements, each *DR* includes an upper metal strip that redirects the strongest coupling field from the exciting slot. The design having a frequency spans of 27.5 - 28.35 GHz at the 28 GHz and gives the isolation of 12 dB. For the boosting of isolation, a metal strip on the upper side of each *DR* is placed. The proposed *MIMO DRA* with metal strips has no *DRA* impedance matching difficulties and a reflection coefficient of less than -10 dB at 27.25 - 28.59 GHz.

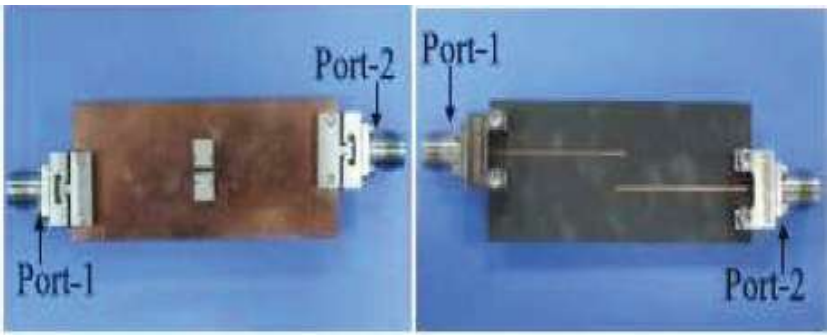

(a)

(b)

Fig. 3.8: Fabricated DRA array antennas. (a) Source: Pan et al. (2019), (b) Source: Zhang et al. (2019), as reproduced in Design and Fabrication of Millimeter Wave Antenna for Future Wireless Applications (2024, p. 66).

In [129], a rectangular*DRA* with four elements is proposed for 5G applications, having slot-coupled microstrip feeds for each element. The size is of the design 20 mm × 40 mm. Four *DRA* are placed above the slot with precision. Metamaterial is printed on top of *DRA* to improve the isolation by removing solid coupling fields. Interaction between metamaterial structure

and electromagnetic fields disrupts field distributions, reducing coupled fields. The structure operates at 2.23 GHz, covering the 28 GHz, ranging from 27.5 GHz - 28.35 GHz, FCC-allocated spectrum for 5G applications. It operates from 26.71 GHz to 28.91 GHz. The suggested structure exhibits broadside radiation with gain exceeding 7 dBi across all working bands with all four-port stimulation. Also, the fabricated prototype is given in Figure 3.8.

3.4.4.3 Circularly Polarized Dielectric Resonator Antenna

Different dielectric materials are used for feed structure and *DRA*. *DRA* installation errors on the feed network can severely damage antenna performance. This is especially true for millimeter-wave operations. The integrated *DRA* substrate idea uses the same material and production technique for the 4-*Dielectric Resonator* elements and feed network, eliminating errors. This design had 1.6% bandwidth and 13.6 dBi linear polarization gain. Moreover, the axial ratio bandwidth of 1.1%, the *CP* antenna offers 16.48% bandwidth and 12.7 dBi gain. The element's profile, which limits [130], was ignored.

5G mmWave applications use a unique single-fed *Dielectric Resonator Antenna (DRA)* [131]. In 5G channels, the *DRA* achieves dual bandwidth and circular polarization. This two band antenna resonates at 22.06, 24.5, and 29.84 GHz. The bandwidth ranges from 19.52 – 26.36 GHz and 7.69% at 28.26 – 30.26 GHz. Both obtained bands are 5G Band 30 GHz. A 50Ω microstrip line feeds a trapezoidal *DRA* instead of a rectangular one. The *DRA* has electrical dimensions of $0.25\lambda_0 \times 0.29\lambda_0 \times 0.22\lambda_0$ and a resonating frequency of 26 GHz. *DRA* is mounted on a RT duroid substrate ($0.5\lambda_0 \times 0.5\lambda_0 \times 0.1\lambda_0$) with a permittivity of 2.2. *DRA* is circularly polarized and has 5.23% axial ratio bandwidth of 3 dB. *DRA* gain 3.28 dB. Circular polarized wideband antenna with enhanced *Signal-to-Noise Ratio* is reported in [131]. The design is *Circularly Polarized* using the microstrip line (edge feed) to the *DRA*. Various feeding sites are evaluated for circular polarization using edge feeding.

At 26 GHz, a trapezoid *DRA* achieved 26.3% bandwidth and 5.2% axial ratio [132]. However, angular cutting of the rectangular *DRA* framework into a trapezoid may have caused production errors. In [133], a coaxial probe stimulated and drilled a cylindrical *DRA* at 26 GHz. This method is difficult and rarely used in investigations. High tolerance is needed for fabrication. Metasurface converts linear polarization to circular polarization. The metasurface boosts gain and

axial ratio. *Circularly Polarized (CP)* bandwidth of 26.3% and axial ratio of 1.35% are achieved. In [134], a *SIW*-stimulated *DRA* (stacked rectangular structure) has been used at 20 GHz and 30 GHz. Two rectangular *DRA*s are stacked with a metal strip on top to get circular polarization in both frequency bands. However, its many steps and components make this procedure complicated and expensive. At 20 GHz and 30 GHz,circular polarized bandwidths of 6.4% and 12.8%, with axial ratios of 5.2% and 4.1% is achieved. Despite its complexity, this study did not address alignment.

Table 3.6: Comparison performances of Circularly Polarized DRAs.

Ref.	**Type of DRA**	**Frequency (GHz)**	**Bandwidth (%)**	**Gain (dB)**	**Axial Ratio (%)**	**Mode**
[130]	Rectangular	30	16,48	12, 7	1,1	$TE_{11\delta}$
[131]	—	28.26– 30.26 GHz	—	—	—	—
[128]	Trapezoidal	26	26,3	3, 28	5,28	TE_{x21}
[133]	Cylindrical	26	26	6, 6	1,35	TE_{412}
[134]	Rectangular	30/30	6.4/12.8	6.6/8.2	5.2/4.1	TE_{111}

The modes in Table 3.6 enable circular polarization in dielectric resonator antennas. The $TE_{11\delta}$ mode [130] is a perturbed TE_{111} mode where δ introduces asymmetry for circular polarization in a rectangular DRA. The TE_{x21} mode [128] in a trapezoidal DRA supports dual band circular polarization via its asymmetric shape. The TE_{412} mode [133] is a high order cylindrical mode with four azimuthal, one radial, and two axial variations, enabling wideband circular polarization through multi resonance. The TE_{111} mode [134] is inherently linear but achieves circular polarization in a stacked rectangular DRA through dual feed or asymmetric stacking.

Antenna designers can modify *DRA* circuital properties and radiation patterns at mmWave frequencies [135]. Many feeding systems and their benefits and cons are covered in [135]. Resonance at specific frequencies increases *DRA* gain. For higher-order modes, use larger antennas or horns. *Circularly Polarized DRA*s can solve attenuation difficulties, however there are few investigations on their application in the mmWave range. Numerous studies

have examined *MIMO* methods. *MIMO* channel capacity, data throughput, compact size, and connection reliability can be improved by moving *DRA*s. Advanced *DRA* technology will make these antennas practical for real-world applications, surpassing popular ones.

3.4.5 Metamaterial/Metasurface Structures

A "metasurface" is a man-made structure with extraordinary electromagnetic properties including -ve permittivity and permeability. In recent years, metamaterials and metasurfaces have garnered interest for their unique properties. These two materials appear to be capable technologies for enhancing microwave component performance and overcoming restrictions, particularly in antennas [136]. Figure 3.9 (a-f) shows the Metamaterial Inspired antenna.

A new $30 \times 30 \times 1.52\ mm^3$ two band 28/38 GHz, 2×2 PCB-based, *MIMO* design with *Complementary Split Ring Resonator (CSRR)* construction is shown in [137]. The antenna's gain and directivity are improved by placing *CSRR* metamaterial unit cells on top and ground. Comparison of actual and calculated results showed that the enhanced *MIMO* antenna array had a 28.29 GHz resonance frequency and -20.54 dB effective reflection coefficient at 38.78 GHz. They have 15.30% and 13.97% bandwidth and -24 dB and -38.71 dB isolation in their resonant bands. The realized gain is 8.65 dBi at 28 GHz and 8.24 at 38 GHz. *ECC* between *MIMO* antenna elements is 0.0041.

A 14 mm × 14 mm planar four-port microstrip line-fed *MIMO* antenna is introduced in [138]. The antenna operates at 28 GHz/38 GHz, possible 5G millimeter wave frequencies. Rectangular patch antennas are used as primary radiators to achieve the resonant frequency of 28 GHz. Etching a *Split Ring Resonator (SRR)* (single element) metamaterial unit cell formed from the fundamental patch radiator creates a 38 GHz resonance band. Port isolation between antenna elements exceeds 25 dB throughout both frequency bands without complex decoupling methods. Lumped components of the antenna's equivalent circuit diagram characterize its electrical responses. The diversity performance metrics studied were $ECC < 0.005$, DG of 10 dB, and $CCL < 0.35$ bits per second per hertz. The antenna described has numerous important qualities that makes a good candidate for the 5G *RF* antenna system. Additionally, the equivalent circuit model evaluates a system's electrical characteristics in relation to an *RF* signal input.

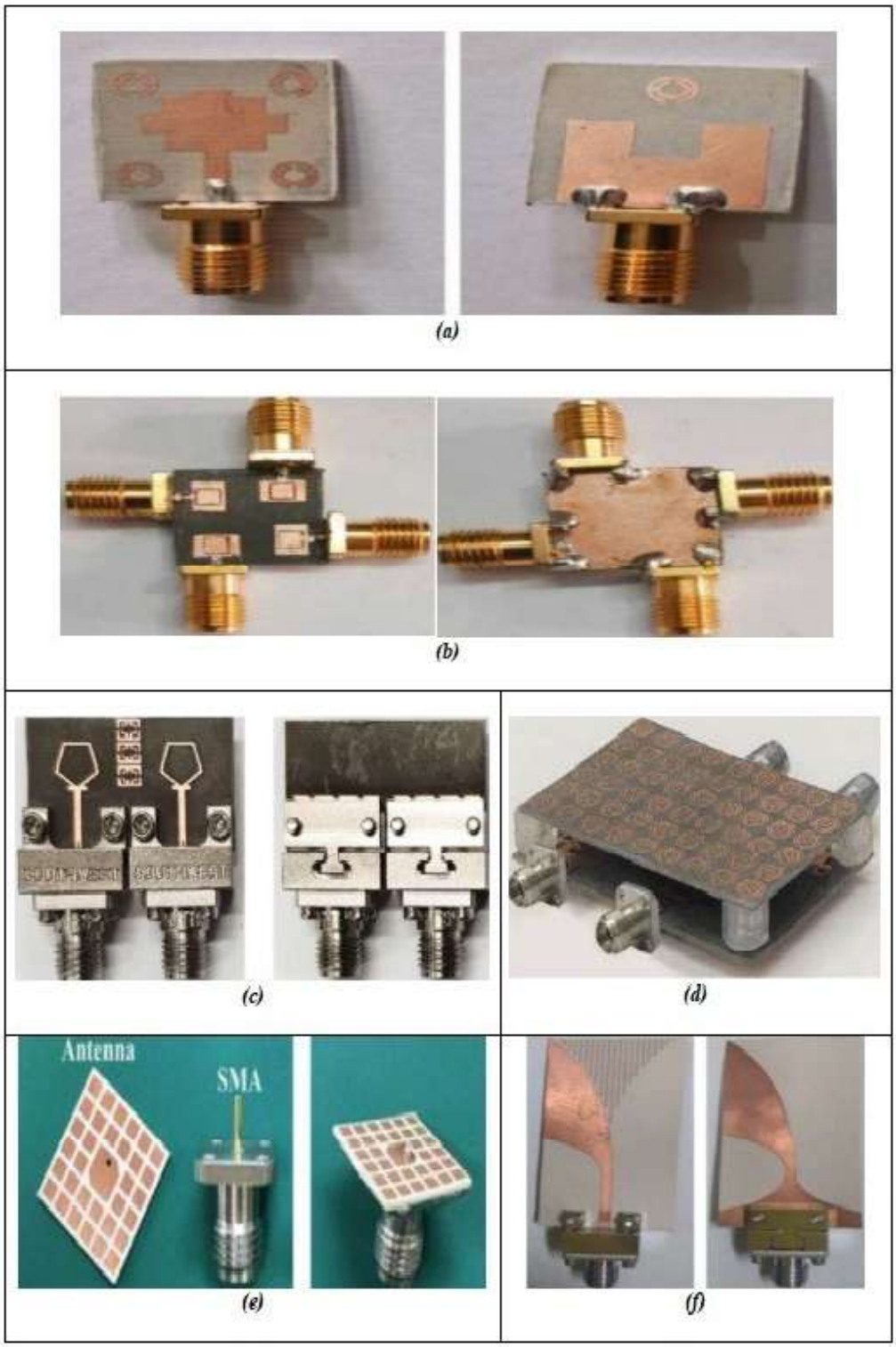

Fig. 3.9: Fabricated Metamaterial Inspired antennas. Source: (a) Singh et al. (2022), (b) Tadesse et al. (2022), (c) Esmail & Koziel (2023), (d) Tariq et al. (2021), (e) Hussain et al. (2020), (f) Kumar & Dixit (2021), as reproduced in Design and Fabrication of Millimeter Wave Antenna for Future Wireless Applications (2024, p. 70).

- The utilization of planar geometry, a straightforward design, and a convenient fabrication process are desirable attributes.
- The incorporation of a compact form factor is advantageous for seamless integration within 5G devices.
- Achieving high isolation between antenna elements without the need for elaborate decoupling structures.
- The practice of printing on a common ground plane is often exploited in [68].

In [139], a metamaterial-based two-band *MIMO* antenna ($5.5 \times 5.4 \times 0.508$ mm^3) is reported for the 5G mmWave communication networks with high isolation. Two-band response and wide operating bandwidth are offered by the 5G 28/28 band pentagon-shaped monopole antenna. Two nearby symmetric radiating elements constitute the V system, which has -18.5 dB mutual coupling at both of the frequency. Two radiators are separated by a dual-band metamaterial to reduce interaction. Isolation is improved to -39 dB at 28 GHz and -38 dB at 38 GHz by adding a 3×1 metamaterial antenna array. The system's wide bandwidth, low profile, strong gain (> 5 dB), improved isolation (-38 dB), low *ECC* (<0.0001), *CCL* (< 0.05), and *DG* (> 9.99 dB) are all impressive features, it works on all 28/28 5G bands and has excellent diversity performance, says author.

Metamaterial-based *MIMO* was highly diverse. The 5G millimeter wave communications system is stable with appropriate *ECC* (< 0.0001), *TARC* ($\leq$ 10 dB), *CCL* (< 0.05), and *DG* ($\approx$ 10 dB) values at 28/38 GHz dual-band.

For 5G mmWave communication systems, [140] introduces a 4-element *MIMO* antenna with a 1×2 metasurface design and corporate feed parallel network. Furthermore, a 9×6 *Circular Split Ring (CSR)* metasurface array improves *MIMO* antenna gain and isolation. In mmWave frequency, the antenna operates from 24.55 to 26.5 GHz. After adding the metasurface layer, peak gain was 10.27 dBi. Metasurface boosts isolation by 5dB. *MIMO* performance measures including *ECC*, *DG*, *CCL*, and *MEG* demonstrate good antenna characteristics. The metasurface of 9×6 *Circular Split Ring (CSR)* cells on *MIMO* antennas enhances gain and reduces coupling effects.

In [141], the design has a patch with truncated corner and a 2×2 periodic square metallic plate metasurface. The antenna's low profile, low cost, high gain, and wideband features are obtained by printing all radiating parts (radiator and MS) on the dielectric substrate's single layer. Wideband *CP* radiations from the MS's surface-waves are detailed. Stable radiation patterns, > 95% radiation efficiency, and 11 dBic flat gain characterize the antenna. Mainly, the antenna operates in the 5G mmWave range from 25–29.5 GHz. In [141], the author presents a single-layer planar antenna with *CP* and *MIMO* capabilities for the 25-29.5 GHz 5G band with a low height profile (0.51 mm) and few assembly elements, making it cost-effective and mass-manufacturing.

A wideband *Antipodal Vivaldi Antenna (AVA)* with a *Negative Index Metamaterial (NIM)* was designed in [142]. The antenna is linearly tapered. *Negative Index Metamaterial* improve antenna performance. The top surface between two *Antipodal Vivaldi Antenna* radiators has 'V'-shaped metamaterial unit cells that increase the end-fire electric field. The antenna is having a size ($50 \times 24 \times 0.51\ mm^3$) is small compared to other *Antipodal Vivaldi Antenna* antennas. The gain is relatively stable, ranging from 9.25 ± 1.75 dBi at 15-40 GHz. No high-gain millimeter wave antenna is available, according to the authors. But also, various techniques are found in the literature to improve the performance of the antennas at millimeter wave [143, 144].

Table 3.7 lists 5G *MIMO* antennas' frequency bands, diameters, bandwidths, gains, isolations, and performance metrics like *ECC*, *CCL*, *MEG*, and *DG*.

Table 3.7: Comparison of the performances of Metamaterial/Metasurface structures.

Ref.	Antenna Design	Freq. Bands (GHz)	Antenna Size (mm)	BW (%)	Peak Gain (dBi)	Isolation (dB)	ECC	CCL (bits/s /Hz)	MEG (dB)	DG (dB)	TARC (dB)
[137]	CSRR- Enhanced MIMO Array	28, 38	30 × 30 × 1.52	15.30, 13.97	8.65, 8.24	-24, -38.71	0	—	—	—	—
[138]	Planar Microstrip MIMO	28, 38	14 × 14	—	—	> 25	< 0.005	< 0.35	—	> 10	—
[139]	Metamaterial- Based Dual-Band MIMO	28, 38	5.5 × 5.4 × 0.508	—	> 5	-18.5, -38	< 0.0001	< 0.05	> 10	> 9.99	< -10
[140]	Metasurface- Based MIMO	24.55–26.5	—	—	10,27	—	—	—	—	—	—
[141]	Single-Layer CP MIMO Antenna	25–29.5	$1.0\lambda_0 \times 1.0\lambda_0 \times 0.04\lambda_0$	23,4	11	—	—	—	—	—	—
[142]	Wideband Antipodal Vivaldi Antenna	15–41.3	50 × 24 × 0.51	9.25–15.26	—	—	—	—	—	—	—

3.5 CHAPTER SUMMARY

This chapter presents a detailed comparative analysis of different planar *MIMO* antennas designed for *Millimeter Wave (mmWave)* frequency bands, focusing on their classification, performance parameters, and suitability for next-generation wireless communication systems. The primary goal is to evaluate various antenna designs and understand their strengths and limitations in 5G and beyond applications. The discussion begins with classification of planar *MIMO* antennas, where different designs are categorized based on radiation mechanisms, substrate materials, and isolation techniques, all of which play a crucial role in mmWave communication.

The discussion covers slot/patch antennas, known for their compact size and ease of fabrication, and *MIMO* array antennas, which enhance capacity and reliability while addressing mutual coupling. *Dielectric Resonator Antenna (DRA)* are highlighted for their high efficiency and wide bandwidth, whereas *Defected Ground Structure (DGS)* improve isolation and bandwidth by modifying the ground plane. Additionally, metamaterial/metasurface antennas are examined for their potential in miniaturization, beam steering, and gain enhancement. The chapter also identifies key research challenges, including antenna miniaturization, fabrication complexity, and seamless integration with 5G/6G networks, paving the way for future advancements in the field.

Chapter–4

Design of a Planar Antenna for Millimeter Wave (mmWave) band

In this chapter design of a single planar antenna is presented for millimeter wave range that can be utilized for 5G applications. The design of efficient and compact antennas is crucial for modern wireless communication systems, especially in mmWave and 5G applications. This chapter focuses on the design and optimization of a single-element antenna incorporating *Defected Ground Structure (DGS)* to enhance performance. *DGS* is essential for increasing bandwidth, isolation, and impedance matching by altering the current distribution on the ground plane.

4.1 INTRODUCTION

With the rapid advancements in wireless communication, the demand for compact, high-performance antennas has significantly increased, especially for mmWave and 5G applications. Conventional antenna designs often face challenges such as large size, limited bandwidth, high mutual coupling in *MIMO* systems, and impedance mismatches, which can degrade overall system performance. To overcome these limitations, this chapter focuses on design process of single planar antenna.

4.2 DESIGN CONFIGURATION OF A PROPOSED SINGLE ANTENNA

The development of a suggested single-element antenna is presented in this section, focusing on its structural composition and performance enhancements. To support high frequency operation with minimal dielectric loss, the antenna is fabricated on a Rogers RT Duroid 5880 substrate, which has a thickness of 0.254 mm. This material is well-known for its low dielectric constant

(ε_r= 2.2) and low loss tangent, making it an ideal choice for millimeter wave frequencies. A key aspect of the design is the incorporation of a *Defected Ground Structure (DGS)*, which plays a crucial role in enhancing antenna characteristics. The *DGS* is strategically implemented on the ground plane to suppress unwanted side lobes, enhance main beam stability, and improve overall radiation efficiency, which are considered to be the critical factors in high frequency wireless methods for communication..

The proposed antenna features a compact, symmetrical, and straightforward design, making it suitable for millimeter wave applications. However, achieving optimal performance requires precise alignment between the feed plane and ground plane, ensuring proper impedance matching and minimal signal interference. In the following sections, the design evolution is presented in a step-by-step manner, detailing the modifications and optimizations that lead to the final antenna structure. The design is structured into two primary components:

- **Feed Plane:** This includes the patch geometry, feedline configuration, and slot incorporation to control impedance and resonant frequency. The suggested antenna, as shown in Figure 4.1(a), is structured around a compact rectangular patch measuring 6 mm × 5.5 mm. This patch acts as the main source of radiation and is excited using a microstrip feedline that is 0.8 mm in width. In order to minimize signal reflection and maximize power transfer to the radiating structure, the feedline is meticulously built to guarantee appropriate impedance matching.

  For the purpose of improving the antenna's impedance bandwidth, resonance properties, and radiation efficiency, three distinct types of slots are incorporated into the patch:

  1. **Circular Slot:** At the patch's upper-middle area, a 2 mm radius circular slot is engraved. This slot plays a crucial role in altering the current distribution, thereby influencing the resonant frequency and improving impedance matching.
  2. **Diamond-Shaped Slots:** Below the circular slot, two diamond-shaped slots are symmetrically positioned, each with dimensions of 1.27 mm × 1.27 mm. These slots contribute to enhancing the antenna's impedance characteristics. Additionally, two smaller diamond-shaped slots with dimensions of 0.85 mm × 0.85 mm are placed above the circular slot. The combination of these slots helps in fine-tuning the resonant frequencies and improving radiation characteristics.

3. **Side Slots Near the Feedline:** To further enhance impedance matching and radiation efficiency, two symmetrical slots measuring 2.2 mm by 0.4 mm are placed on the sidewalls of the feedline. These slots help control surface current distribution, thereby optimizing the antenna's reflection coefficient and minimizing unwanted losses.

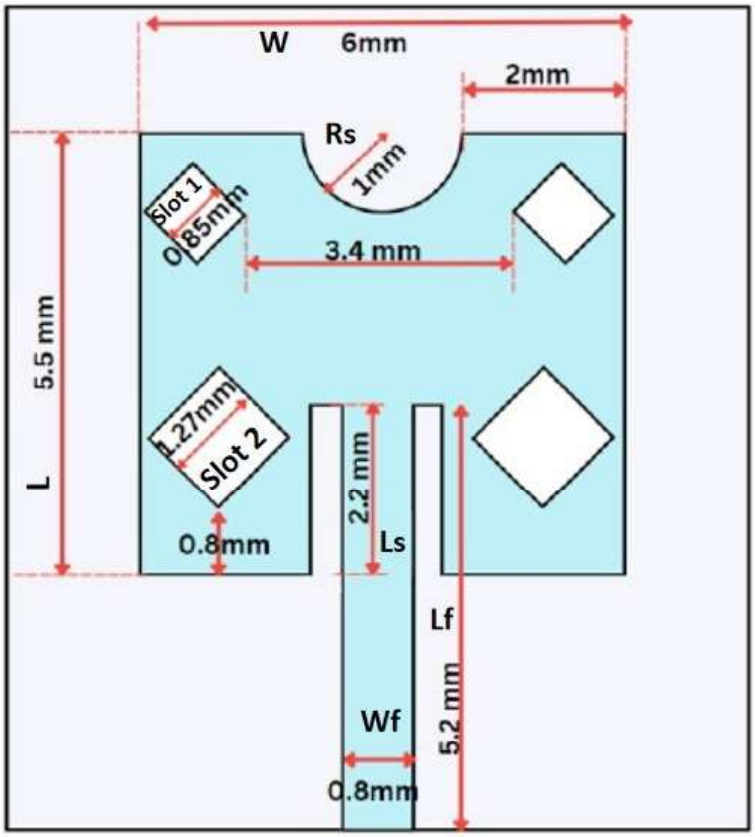

Fig. 4.1: Top view of the feed plane of the proposed single-element antenna, showing the inset-fed rectangular patch with integrated circular and diamond-shaped slots for impedance tuning and bandwidth enhancement.

The final measurements of the suggested planar antenna are provided in Table 4.1.

Table 4.1: Dimensional Specifications of the Feed Plane for a Single Antenna

Parameter	Symbol	Dimension (mm)
Patch Width	W	6.0
Patch Length	L	5.5
Circular Slot Radius	Rs	1.0
Diamond Slot - Top	Slot 1	0.85 × 0.85
Diamond Slot - Bottom	Slot 2	1.27 × 1.27
Feedline Width	Wf	0.8
Feedline Length	Lf	5.2
Slit Length	Ls	2.2

- **Ground Plane:** The ground plane, as shown in Figure 4.2(b), is designed to enhance the performance of the proposed *MIMO* antenna. It features two circular slots (a dumbbell-shaped Defected Ground Structure (DGS) is etched into the ground plane to tailor the current distribution and enhance impedance matching.), each with a radius of 0.75 mm, connected by a rectangular slot measuring 2.5 mm × 0.5 mm. This setup was selected with care to enhance impedance matching and isolation, both of which are critical for optimal antenna performance in millimeter wave 5G applications.

  - To adjust the response of antenna, the centers of circular slots are slightly shifted upward by 0.6 mm from the center line of the rectangular slot. This adjustment helps in achieving better resonance and impedance characteristics by impacting the ground plane's current distribution. The overall structure forms a "dumbbell" shape, which is a well-known technique for decreasing mutual interaction and improving isolation in antenna arrays.
  - Furthermore, to further improve impedance matching and minimize reflection losses, an additional round patch whose radius is 0.74 mm is placed within each circular

slot. This modification contributes to better return loss, increased bandwidth, and improved radiation performance.

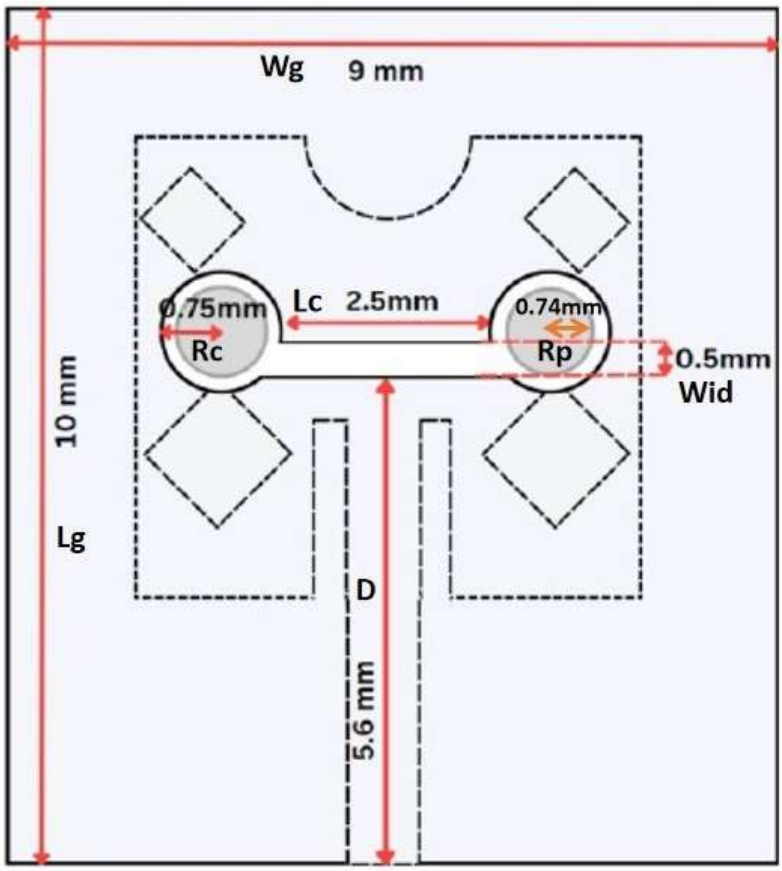

Fig. 4.2: Top view of the ground plane featuring a dumbbell-shaped Defected Ground Structure (DGS) composed of two circular slots connected by a rectangular slot, with embedded circular patches to improve impedance matching and radiation efficiency.

The incorporation of these slots is a strategic approach to achieving a compact, high-performance millimeter wave antenna, ensuring improved impedance bandwidth, reduced mutual coupling, and enhanced overall efficiency. The combination of these design elements ensures that the proposed *MIMO* antenna meets the stringent requirements of millimeter wave 5G communication. The suggested planar antenna's final measurements are shown in Table 4.2.

Table 4.2: Dimensional Specifications of the Ground Plane for a Single Antenna

Parameter	**Symbol**	**Dimension (mm)**
Ground Plane Width	Wg	9.0
Ground Plane Height	Lg	10.0
Circular Slot Radius	Rc	0.75
Circular Patch Radius	Rp	0.74
Center Line	Lc	2.5
Connecting Slot Width	Wid	0.5
Vertical Slot Length	D	5.6

4.3 EVOLUTION OF PROPOSED ANTENNA DESIGN

The design of a millimeter wave antenna follows a systematic approach to ensure optimal performance characteristics. Through this procedure, changes are made to improve important performance metrics like isolation and impedance matching. This section presents the detailed design procedure for a single antenna element. The antenna is made especially to function in the n261 frequency band (27.5–28.35 GHz), essential for applications involving 5G millimeter waves. The design incorporates slot structures and methods of optimization to attain the intended level of performance.

The final antenna design is the result of multiple refinements, each aimed at enhancing key performance parameters such as resonance frequency, bandwidth, and return loss. Although various adjustments were made throughout the development process, the key design evolution can be outlined in four fundamental stages. Each phase involved systematic modifications to the size and shape of structural components, gradually improving the antenna's performance to meet the target specifications. The step-by-step progression is detailed below:

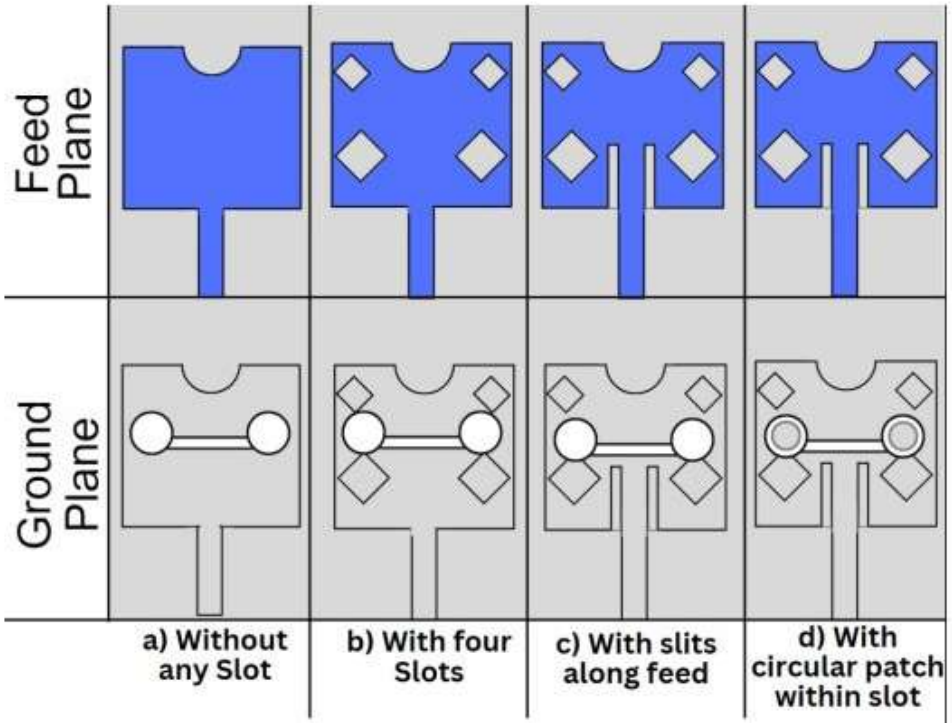

Fig. 4.3: Progressive evolution of single element antenna design showing systematic modifications to feed and ground planes across four design iterations (a-d) for performance enhancement.

- **Step 1: Initial Design with Basic Patch and Ground Plane Etching**

  At the outset, as illustrated in Figure 4.3(a), a basic rectangular patch was created and fed through a microstrip feedline. The initial dimensions of the rectangular patch are calculated using standard microstrip design formulas [67, Sec. 14.3.1]. First, the patch width W is estimated using the dominant-mode resonance condition as given in Equation(4.1).

$$W = \frac{c}{2f_r}\sqrt{\frac{2}{\varepsilon_r + 1}}, \tag{4.1}$$

  Subsequently, the effective dielectric constant $\varepsilon_{\text{reff}}$, which accounts for the inhomogeneous nature of the microstrip medium, is computed using Equation (4.2) [67, Eq.14-10]:

$$\varepsilon_{\text{reff}} = \frac{\varepsilon_r + 1}{2} + \frac{\varepsilon_r - 1}{2}\left(1 + 12\frac{h}{W}\right)^{-1/2}. \tag{4.2}$$

The electrical length extension due to fringing fields at the radiating edges is then evaluated using the Hammerstad–Jensen empirical model, expressed in Equation(4.3) [67, Eq.14-16]:

$$\Delta L = \frac{0.412h\left(\varepsilon_{\text{reff}}+0.3\right)\left(\frac{W}{h}+0.264\right)}{\left(\varepsilon_{\text{reff}}-0.258\right)\left(\frac{W}{h}+0.8\right)}. \tag{4.3}$$

where h is the height of the substrate.

Finally, the physical patch length L is obtained by subtracting twice the fringing length correction from the half-guided-wavelength length, as defined in Equation(4.4) [67, Eq. 14-17]:

$$L = \frac{c}{2f_r\sqrt{\varepsilon_{\text{reff}}}} - 2\Delta L. \tag{4.4}$$

Subsequently, the ground plane featured two circular slots, linked by a horizontal bar. This preliminary configuration exhibited weak resonance at approximately 29.43 GHz, with limited bandwidth and poor return loss, indicating the need for further refinement.

- **Step 2: Incorporation of Diamond-Shaped Slots**

  To enhance impedance characteristics, four diamond-shaped slots were introduced into the feed plane, as shown in Figure 4.3(b). This modification significantly altered the current distribution and resonance behavior, shifting the resonant frequency to 27.64 GHz. While the bandwidth demonstrated noticeable improvement, the resonance frequency remained outside the required n261 band (27.5–28.35 GHz). Therefore, additional adjustments were required to fine-tune the operating frequency.

- **Step 3: Performance Enhancement by Removing Feedline Stubs**

  In the next stage, two stubs located on either side of the feedline were removed, as shown in Figure 4.3(c). This structural adjustment led to a substantial improvement in return loss, optimizing impedance matching and reducing signal reflection. To ensure consistent functioning within the specified frequency range and improve the antenna's bandwidth, more modifications were required..

- **Step 4: Final Tuning with Circular Patch in the Ground Plane**

  In the last stage, an additional circular patch was embedded within the previously etched circular slots in the plane of the ground, as seen in Figure 4.3(d). This adjustment played a crucial role in further improving impedance matching and minimizing losses. As a result,

the antenna precisely resonated within the required 27.5–28.35 GHz band, achieving an optimized bandwidth and significantly enhanced return loss. The final performance characteristics are graphically represented in Figure 4.4.

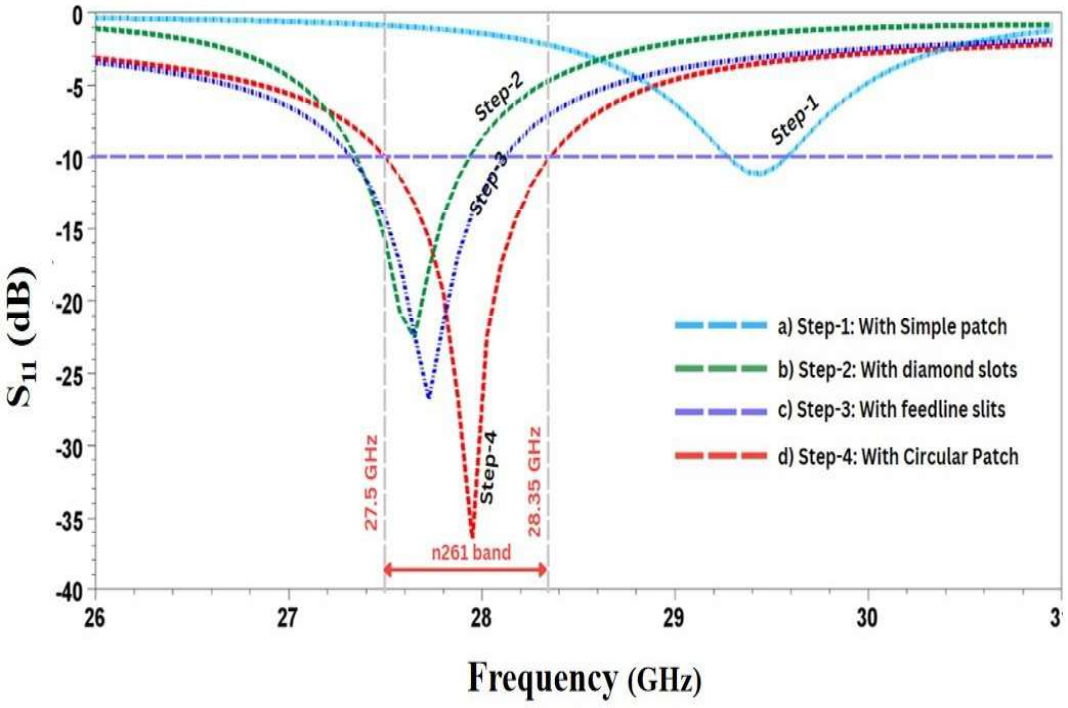

Fig. 4.4: Return loss (S_{11}) comparison across four design iterations for the n261 band (27.5–28.35 GHz).

This structured, step-by-step progression demonstrates the significance of methodical design improvements in reaching the intended antenna performance for millimeter wave 5G applications. Each modification is carefully evaluated to improve resonance characteristics, ensuring that the antenna works well in the n261 frequency range. As can be observed from Figure 4.4, the antenna design begins with Step-1, where a simple patch structure is implemented (represented by the sky-blue curve). At this stage, the return loss is relatively shallow and fails to meet the standard -10 dB threshold, which reflects poor impedance matching and inadequate radiation performance at the target frequency. No significant resonance is observed within the desired frequency range, indicating the need for further enhancement.

In Step-2, diamond-shaped slots are introduced on the radiating patch (green curve). This modification leads to a noticeable improvement in impedance matching, and a return loss dip

emerges near 27.5 GHz. However, while some resonance is observed, the return loss remains insufficient for optimal operation, indicating only partial enhancement.

Step-3 involves the incorporation of slits along the feedline (purple curve), which serve to fine-tune the current distribution and further improve the impedance characteristics. As a result, a much sharper dip in the S_{11} parameter appears around 28.1 GHz. This indicates a significant enhancement in antenna performance, with the return loss now falling below the -10 dB threshold, demonstrating effective operation over a portion of the n261 mmWave band (27.5–28.35 GHz).

Finally, in Step-4, a circular patch is added within the slot region (red curve), completing the hybrid antenna structure. This step marks a major improvement in design, with the return loss reaching values below -30 dB. The antenna now demonstrates strong and broad resonance across the entire n261 band, providing excellent impedance matching and optimized radiation performance.

4.3.1 Antenna Feeding Techniques and Rationale for Microstrip Line Feed Selection

The performance of a microstrip patch antenna is significantly influenced by its feeding mechanism, which governs impedance matching, bandwidth, radiation efficiency, fabrication complexity, and compatibility with integrated RF front-ends. Several feeding techniques have been developed, each with distinct trade-offs. The four primary methods: microstrip line feed, coaxial probe feed, aperture-coupled feed, and proximity-coupled feed are described below.

- **Coaxial Probe Feed**

  In this method, the inner conductor of a coaxial connector is soldered to the radiating patch through a via in the ground plane, while the outer conductor connects to the ground. It provides good isolation and minimal spurious radiation but suffers from non-planarity and parasitic inductance at high frequencies [67]. The mechanical complexity of probe alignment and substrate drilling makes it less suitable for mmWave MIMO arrays [70].

- **Aperture-Coupled Feed**

  First introduced by Pozar and co-workers [145], this technique uses a slot in the ground plane to electromagnetically couple energy from a microstrip line on a lower substrate layer to the patch. It offers excellent isolation and reduced feed radiation [67]. However, it requires precise multilayer fabrication, increasing cost and sensitivity to alignment errors particularly problematic at 28 GHz [146].

- **Proximity-Coupled Feed**

  Also known as electromagnetic coupling, this method places the feedline beneath the patch on a separate dielectric layer, enabling broadband operation [70]. While it avoids direct metallic contact, it still demands multilayer substrates and tight control over inter-layer spacing, limiting its practicality for compact, single-layer mmWave systems [67].

- **Microstrip Line Feed**

  This planar technique connects a microstrip transmission line directly to the patch edge. The inset-fed variant where the feedline is recessed into the patch by a distance Linset enables precise impedance tuning by adjusting the inset depth [67]. It is fully compatible with standard PCB processes, supports easy integration into MIMO arrays, and avoids vias or connectors, making it ideal for scalable mmWave designs [70].

  Thus, the inset microstrip feed offers the optimal balance of performance, simplicity, and manufacturability for the proposed mmWave MIMO antenna.

Defected Ground Structures (DGS) are widely employed in millimeter-wave antenna design to enhance performance by introducing controlled perturbations in the ground plane current distribution. These perturbations suppress surface waves, reduce mutual coupling, improve impedance bandwidth, and increase radiation efficiency key requirements for 5G mmWave systems [136]. In the proposed antenna, a dumbbell-shaped DGS is etched into the ground plane, comprising two circular slots interconnected by a narrow rectangular slot. A systematic parametric study of the DGS geometry specifically the circular slot radius (R_c) and the rectangular slot width (W_{id}) is conducted to optimize the resonant frequency and bandwidth for operation within the n261 band (27.5–28.35 GHz).

4.4 PARAMETRIC ANALYSIS

Selection of different size of circular or rectangular slots is carried out by modifying the size of antenna design's structures. The radiation properties are affected to varying degrees by different dimensional parameters. In this section, we will discuss those dimensional parameters of the design which have significant impact on the properties of antenna. The main focus of this study is to achieve the desired bandwidth for n261 band operation i.e., 27.50-28.35 GHz.

- **Effect of Feed-plane circle radius (Rs):** The variation in the circular slot's radius placed on upper position of rectangular patch changes the radiating frequency. As shown in Figure 4.5, the frequency shifts downward as the radius increases because the effective length increases as well. The graph in Figure 4.6 shows how different Rs values, ranging from 0.8 mm to 1.6 mm, impact the resonant frequency and impedance matching. As Rs increases, the resonance shifts, influencing the antenna's performance. This study helps in selecting the optimal Rs value to achieve better return loss and resonance for 5G millimeter-wave applications. However, the return loss needs to be enhanced by other structural changes. For n261 band, optimum results are generated at Rs = 1 mm.

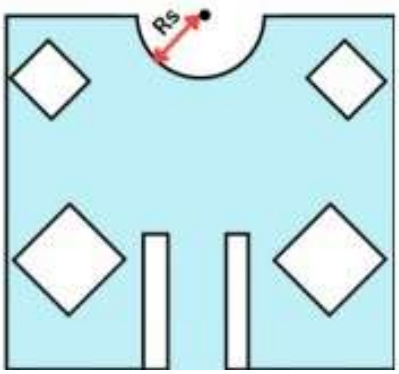

Fig. 4.5: Parametric analysis of the circular slot radius (R_s) on the feed plane, showing its influence on the resonant frequency and impedance matching of the antenna.

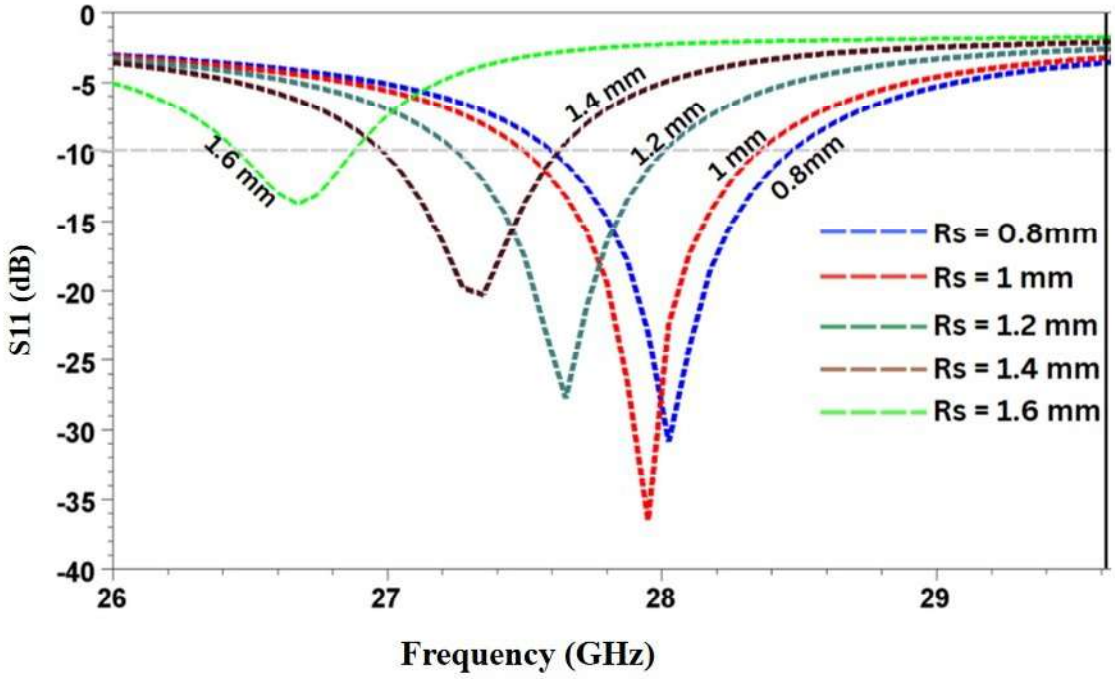

Fig. 4.6: Effect of varying the feed-plane circular slot radius (Rs) on the Return Loss (S_{11}) of the designed antenna.

Table 4.3: Resonant Frequency and Bandwidth for Different Values of Rs

Rs (mm)	**Upper Frequency f_h (GHz)**	**Lower Frequency f_l (GHz)**	**Bandwidth $(f_h - f_l)$ (GHz)**	**Resonant Frequency (GHz)**	**Fractional Bandwidth (FBW)**
0.8	28.6	27.5	1.1	28.1	3.91%
1.0	28.4	27.5	0.9	27.9	3.23%
1.2	28.1	27.3	0.8	27.65	2.89%
1.4	27.8	26.9	0.9	27.35	3.29%
1.6	27.6	26.8	0.8	26.7	2.99%

The Table 4.3 provides a detailed comparison of resonant frequencies, bandwidth and fractional bandwidth for different values of the feed-plane circle radius (Rs). As Rs increases, the resonant frequency gradually decreases, shifting from 28.1 GHz at Rs =

0.8 mm to 26.7 GHz at Rs = 1.6 mm. This indicates that a smaller Rs results in a higher resonance, while a larger Rs causes a downward shift in frequency. The bandwidth also decreases with increasing Rs, with the widest bandwidth of 1.1 GHz observed at Rs = 0.8 mm, which narrows to 0.8 GHz at Rs = 1.6 mm, improving frequency selectivity. The upper frequency (f_h) remains within the 27.6 GHz – 28.6 GHz range, while the lower frequency (f_l) shifts significantly downward as Rs increases. The widest absolute bandwidth of 1.1 GHz and the highest fractional bandwidth (FBW) of 3.91% is observed at $R_s = 0.8$ mm. However, the design with $R_s = 1.0$ mm provides an FBW of 3.23%, which adequately covers the entire 5G n261 frequency band from 27.5 to 28.35 GHz with a bandwidth of 0.85 GHz. This corresponds to a required FBW of approximately 3.05% relative to the band center frequency of 27.925 GHz, confirming that the $R_s = 1.0$ mm configuration meets the operational requirements for 5G mmWave applications. Among all values, Rs = 1.0 mm emerges as the most suitable for 5G n261 band applications, as it resonates at 27.9 GHz, close to 28 GHz, while maintaining a balanced bandwidth of 0.9 GHz. This suggests that optimizing Rs is essential for achieving the desired frequency response, where smaller values enhance bandwidth, and larger values improve selectivity.

- **Effect of Length of slit along the feed-line (Ls):** The return loss is improved significantly with the change of length of the slit placed on both sides of feed-line. As can be seen from Figure 4.7 and 4.8, the return loss is better for Ls = 2.2 mm.

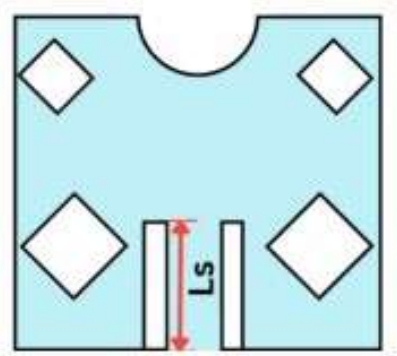

Fig. 4.7: Effect of Length of slit along the Feed-line (Ls) on antenna frequency tuning.

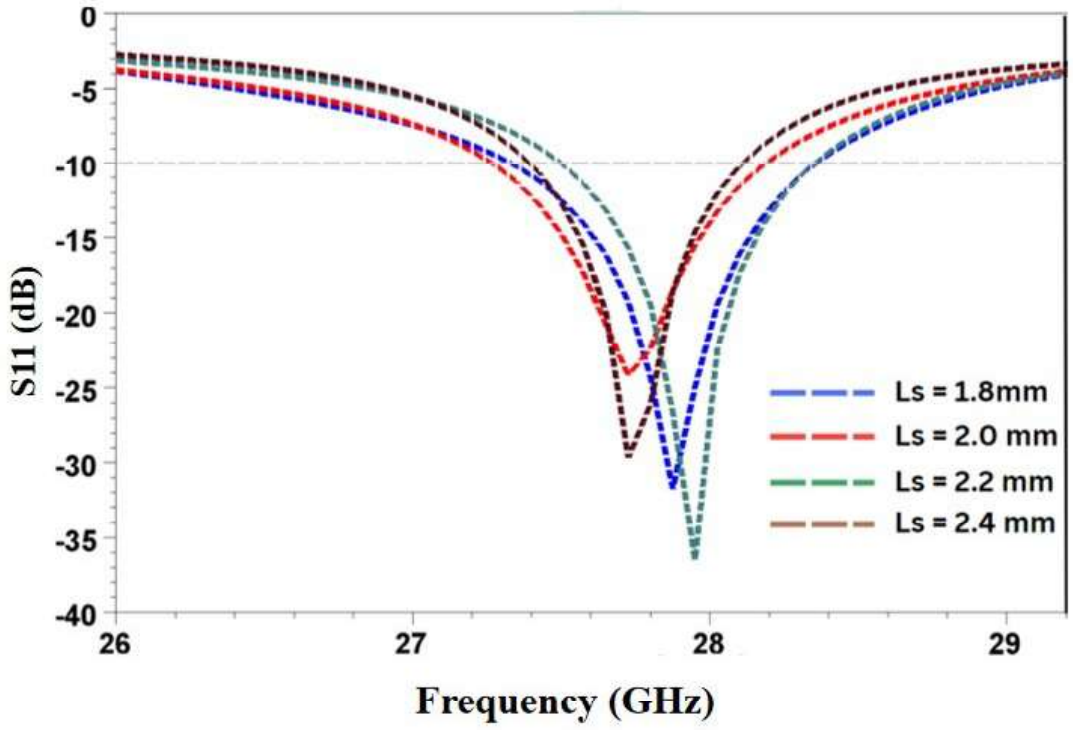

Fig. 4.8: Effect of varying the Length of slit along the Feed-line (Ls) on the return loss (S_{11}) ***of the designed antenna***

Table 4.4: Resonant Frequency and Bandwidth for Different Values of Ls

Ls (mm)	**Upper Frequency f_h (GHz)**	**Lower Frequency f_l (GHz)**	**Bandwidth $(f_h - f_l)$ (GHz)**	**Resonant Frequency (GHz)**	**Fractional Bandwidth (FBW)**
1.8	28.4	27.3	1.1	27.8	3.96%
2.0	28.3	27.4	0.9	27.85	3.23%
2.2	28.2	27.5	0.7	27.9	2.51%
2.4	28.1	27.6	0.5	27.7	1.81%

The Table 4.4 provides a detailed comparison of resonant frequencies, bandwidth and fractional bandwidth for different values of Ls. Although the configuration with $L_s =$ 1.8 mm yields the widest absolute bandwidth of 1.1 GHz and the highest fractional bandwidth of 3.96%, its resonant frequency of 27.8 GHz lies slightly below the target

28 GHz. In contrast, the design with $L_s = 2.2$ mm provides a more favorable trade-off, exhibiting a resonant frequency of 27.9 GHz closest to the desired 28 GHz and a 0.7 GHz bandwidth that adequately covers the majority of the 5G n261 band (27.5–28.35 GHz). This balance between resonance accuracy and bandwidth sufficiency makes $L_s = 2.2$ mm the preferred choice for the final antenna configuration. The key observation is that for Ls = 1.8 mm, the antenna resonates at 27.8 GHz, which is slightly lower than 28 GHz, and exhibits a wider bandwidth of 1.1 GHz. As Ls increases, the resonant frequency initially rises, reaching 27.9 GHz at Ls = 2.2 mm, before slightly dropping to 27.7 GHz at Ls = 2.4 mm. Additionally, the bandwidth decreases with increasing Ls, enhancing frequency selectivity. Among these values, Ls = 2.2 mm is the closest match to the n261 band (28 GHz).

- **Effect of Radius of Circular Slots in Ground Plane (Rc):** By variation of radius of two circular slots placed in ground plane, resonant frequency can be altered as shown in Figure 4.9. Since Our areas of interest in this work are n261 band, our requirement is satisfied by using Rc = 0.75 mm as indicated by Figure 4.10

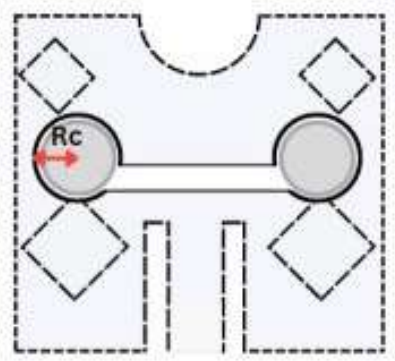

Fig. 4.9: Parametric analysis of the circular slot radius (R_c) in the ground-plane Defected Ground Structure (DGS), demonstrating its role in tuning the resonant frequency and bandwidth of the antenna.

The Table 4.5 shows how changing the ground plane's circular slots' radius (Rc) affects the antenna's resonance frequency and bandwidth. The resonance frequency decreases from 28.35 GHz to 27.6 GHz as Rc rises from 0.69 mm to 0.81 mm. The bandwidth also exhibits a fluctuating trend, with the widest bandwidth of 0.90 GHz observed at Rc

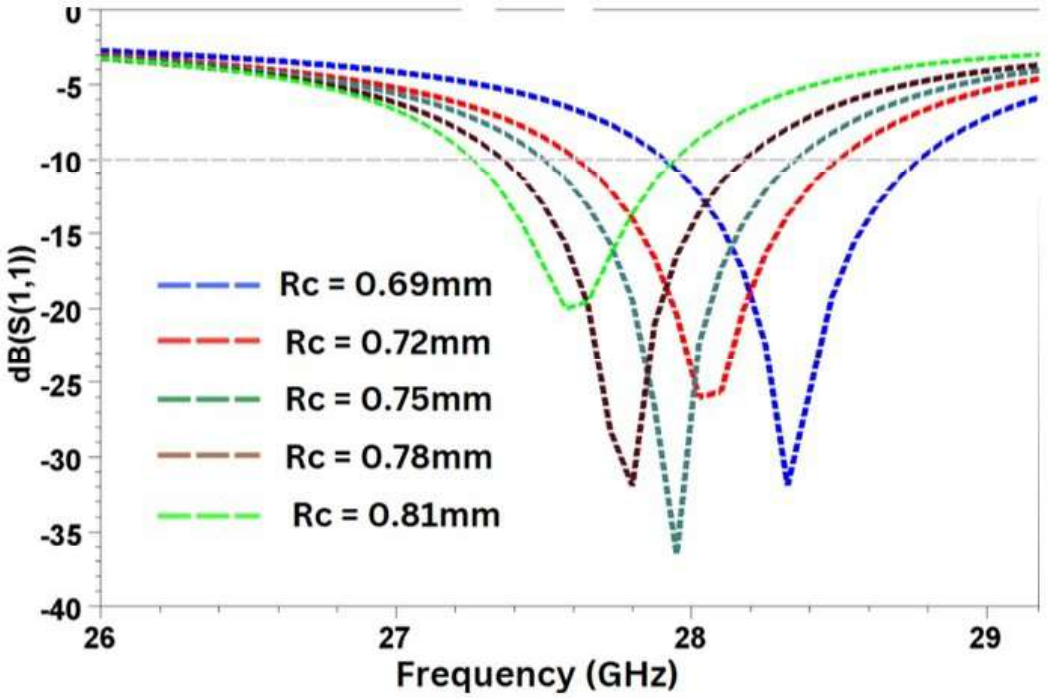

Fig. 4.10: Simulated S_{11} response for varying circular slot radii (R_c) in the DGS, illustrating frequency tuning and impedance matching improvement within the 5G n261 band.

= 0.75 mm, making it the most suitable choice for wideband applications. The upper frequency decreases from 28.75 GHz to 28.00 GHz, while the lower frequency decreases from 28.00 GHz to 27.30 GHz, indicating that a larger Rc shifts the entire operating band to a lower frequency range. The maximum fractional bandwidth of 3.23% is achieved at $R_c = 0.75$ mm, where the antenna resonates at 27.9 GHz and exhibits a 0.9 GHz bandwidth. This operating band fully encompasses the 5G n261 frequency range (27.5–28.35 GHz), thereby satisfying the spectral requirements for mmWave 5G applications. Consequently, $R_c = 0.75$ mm is identified as the optimal ground plane slot radius for the proposed design. Notably, Rc = 0.75 mm is the closest to the n261 band (28 GHz) with a resonant frequency of 27.9 GHz and an optimal bandwidth of 0.90 GHz, making it a favorable design parameter for 5G millimeter wave applications.

Table 4.5: Parametric analysis of the circular slot radius (R_c) in the ground-plane Defected Ground Structure (DGS): resonant frequency, bandwidth, and fractional bandwidth for 5G n261 band optimization.

Rc (mm)	**Upper Frequency f_h (GHz)**	**Lower Frequency f_l (GHz)**	**Bandwidth ($f_h - f_l$) (GHz)**	**Resonant Frequency (GHz)**	**Fractional Bandwidth (FBW)**
0.69	28.75	28.00	0.75	28.35	2.65%
0.72	28.40	27.70	0.70	28.10	2.49%
0.75	28.40	27.50	0.90	27.90	3.23%
0.78	28.20	27.40	0.80	27.80	2.88%
0.81	28.00	27.30	0.70	27.60	2.54%

- **Width of rectangular slot in Ground Plane (Wid):** By altering the width of the rectangular, there is a sharp change in the resonating frequency. In addition, the return loss is also good for resonating frequencies as shown in Figure 4.11 and 4.12. In this structure, the resonant cavity is formed by combined slot formed by both the circular slots and their inter-connecting rectangular slot making a shape of dumbbell. The resonant frequency is determined by the effective length created by the combined slot dimensions in ground plane. Consequently, any change in radius (Rc) and width (Wid) causes change in the effective length which leads to sharp change in the frequency. From the above discussion, it is clear that by making minor changes to the dimensional parameters, the suggested structure may be made to resonate throughout a wide frequency range.

  The Table 4.6 illustrates the impact of varying the width of the rectangular slot in the ground plane (Wid) on the resonant frequency and bandwidth of the antenna. As the width increases from 0.4 mm to 0.7 mm, there is a noticeable shift in both the upper and lower frequency limits, influencing the overall bandwidth and resonance. Although the highest fractional bandwidth (3.47%) occurs at $W_{\text{id}} = 0.7$ mm, the resonance at 28.8 GHz falls outside the 5G n261 band (27.5–28.35 GHz). The configuration with $W_{\text{id}} = 0.5$ mm

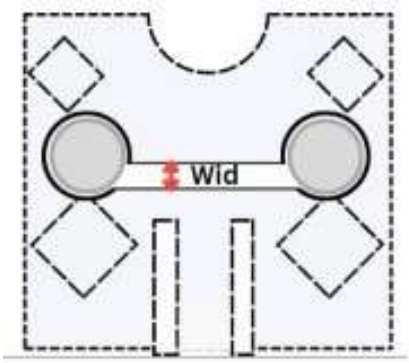

Fig. 4.11: Parametric study of the interconnecting rectangular slot width (W_{id}) in the dumbbell-shaped Defected Ground Structure (DGS), showing its impact on the antenna's resonant frequency.

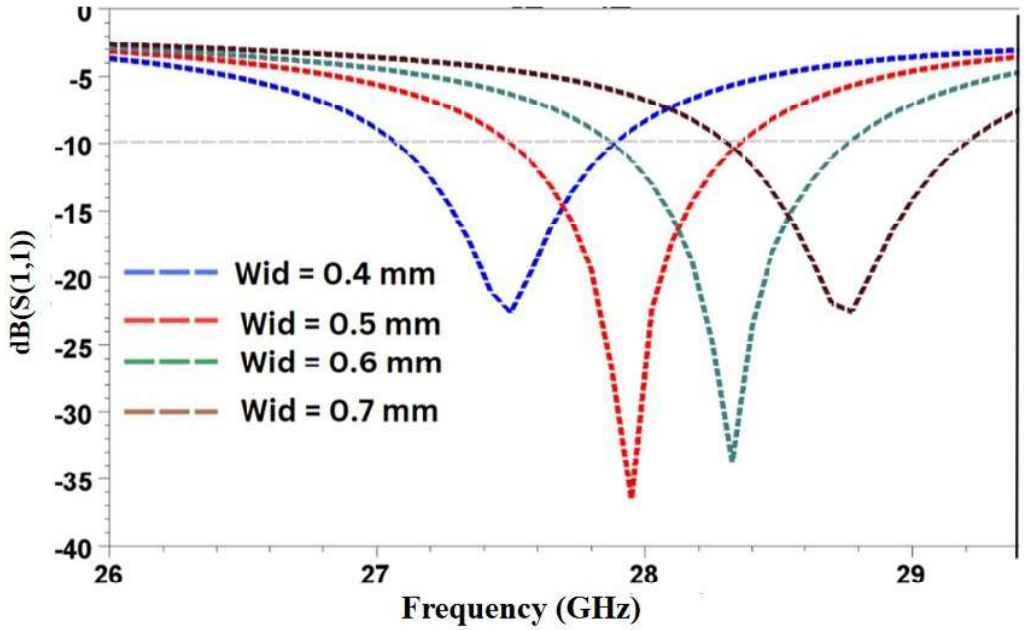

Fig. 4.12: (S_{11}) characteristics for different widths (W_{id}) of the rectangular slot in the DGS, highlighting bandwidth control and resonance alignment with the n261 band.

offers a fractional bandwidth of 3.22%, resonates at 27.95 GHz, and provides a 0.9 GHz bandwidth (27.5–28.4 GHz), fully covering the n261 band. Hence, $W_{\text{id}} = 0.5$ mm is chosen as the optimal design. This trend demonstrates that by carefully adjusting the width of the rectangular slot, the resonant frequency can be effectively tuned within the millimeter wave spectrum.

Table 4.6: Impact of rectangular slot width (W_{id}) in the Defected Ground Structure (DGS) on resonant frequency, bandwidth, and fractional bandwidth, demonstrating precise tuning for mmWave 5G operation.

Wid (mm)	**Upper Frequency f_h (GHz)**	**Lower Frequency f_l (GHz)**	**Bandwidth ($f_h - f_l$) (GHz)**	**Resonant Frequency (GHz)**	**Fractional Bandwidth (FBW)**
0.4	27.9	27.1	0.8	27.5	2.91%
0.5	28.4	27.5	0.9	27.95	3.22%
0.6	28.77	28.0	0.77	28.35	2.72%
0.7	29.3	28.3	1.0	28.8	3.47%

4.5 RESULTS AND DISCUSSION

4.5.1 Return Loss Performance of Single Planar Antenna at 28 GHz

Figure 4.13 presents the simulated return loss (S_{11}) for the designed single-element planar antenna. According to the graph, the antenna demonstrates effective impedance matching, within the frequency range of 27.5 GHz to 28.35 GHz, where the reflection level stays well below the -10 dB threshold. This corresponds to an impedance bandwidth of approximately 850 MHz, which completely covers the n261 frequency band in the FR2 spectrum. Such performance makes the antenna a strong candidate for fifth generation millimeter wave communication systems.

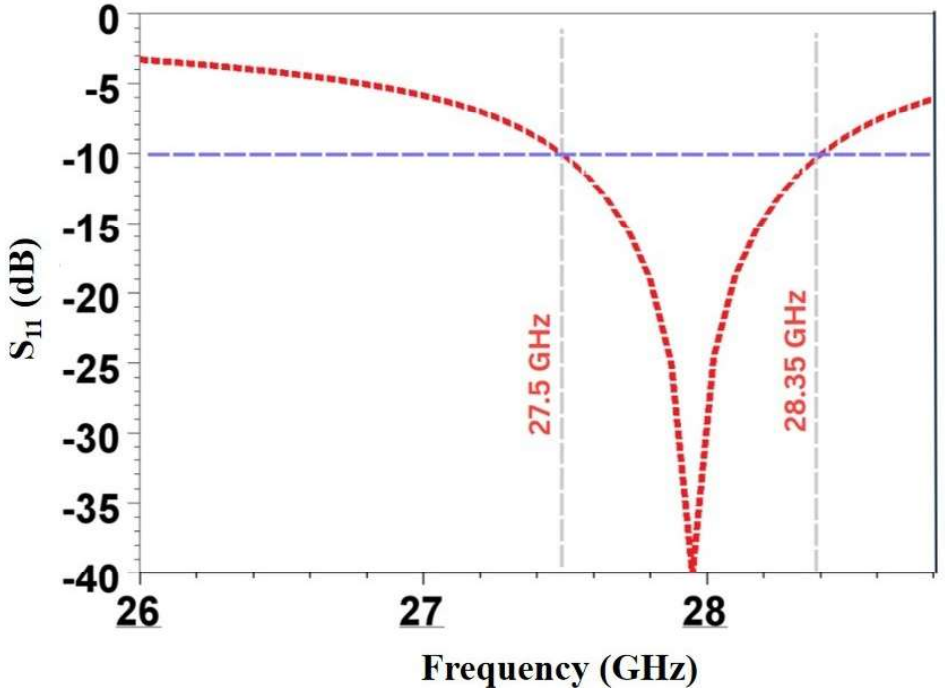

Fig. 4.13: Simulated Return Loss (S_{11}) of single planar antenna vs. Frequency.

4.5.2 Radiation and Total Efficiency

Figure 4.14 shows the radiation and total efficiency over the frequency span from 26-29 GHz. The radiation efficiency, represented by the blue dashed line, remains consistently high above 85% and reaches close to 100% near 28 GHz. The achieved response of radiation efficiency is > 0.93 for the wanted frequency range. The value for total efficiency varies within the range of 0.85 – 0.98. This indicates that the antenna effectively radiates the input power with minimal structural or material losses. The total efficiency, shown by the brown dashed line, begins at around 55% at 26 GHz and increases progressively, peaking near 28 GHz. This rising trend reflects improved impedance matching and reduced power loss due to better transmission. The efficiency values observed in this frequency range confirm the antenna's suitability for high frequency applications such as modern wireless communication systems.

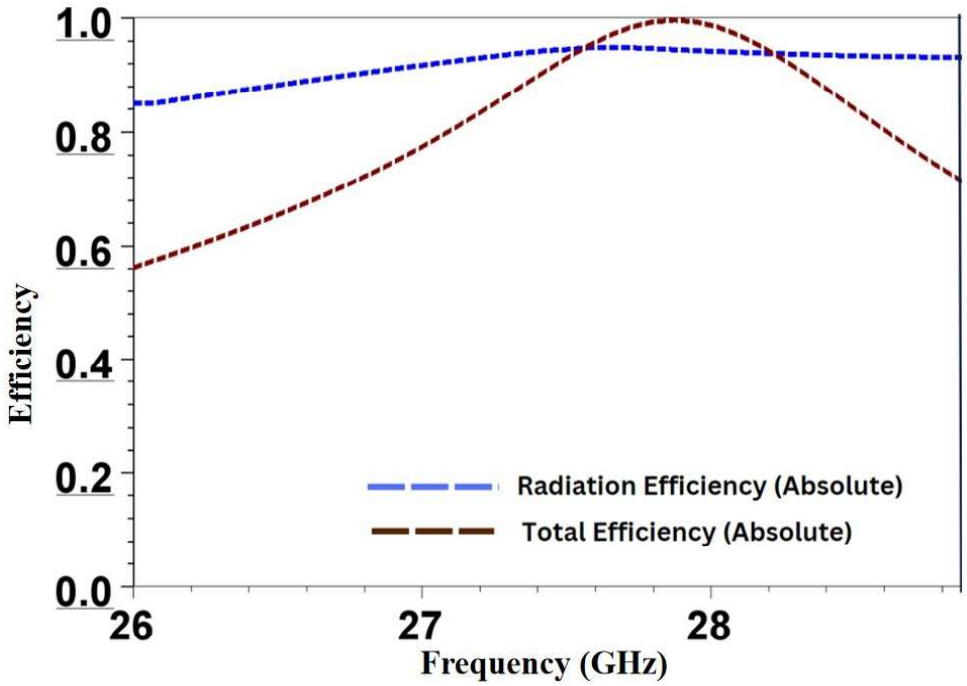

Fig. 4.14: Simulated results of single planar antenna in terms of Radiation and Total Efficiency vs. Frequency

4.5.3 Directivity

Figure 4.15 shows the suggested single planar antenna's computed directivity performance over a 26 GHz to 31 GHz frequency range. The plot highlights how effectively the antenna directs energy at different frequencies.

At 27.5 GHz, the antenna shows a directivity of approximately 3 dB, indicating moderate directional behavior. As the frequency increases, the directivity improves noticeably, reaching a maximum of around 7.01 dB at 28.35 GHz almost near the intended resonance frequency of the antenna. This peak signifies that the antenna radiates more effectively in a preferred direction at this point, which is ideal for targeted wireless communication.

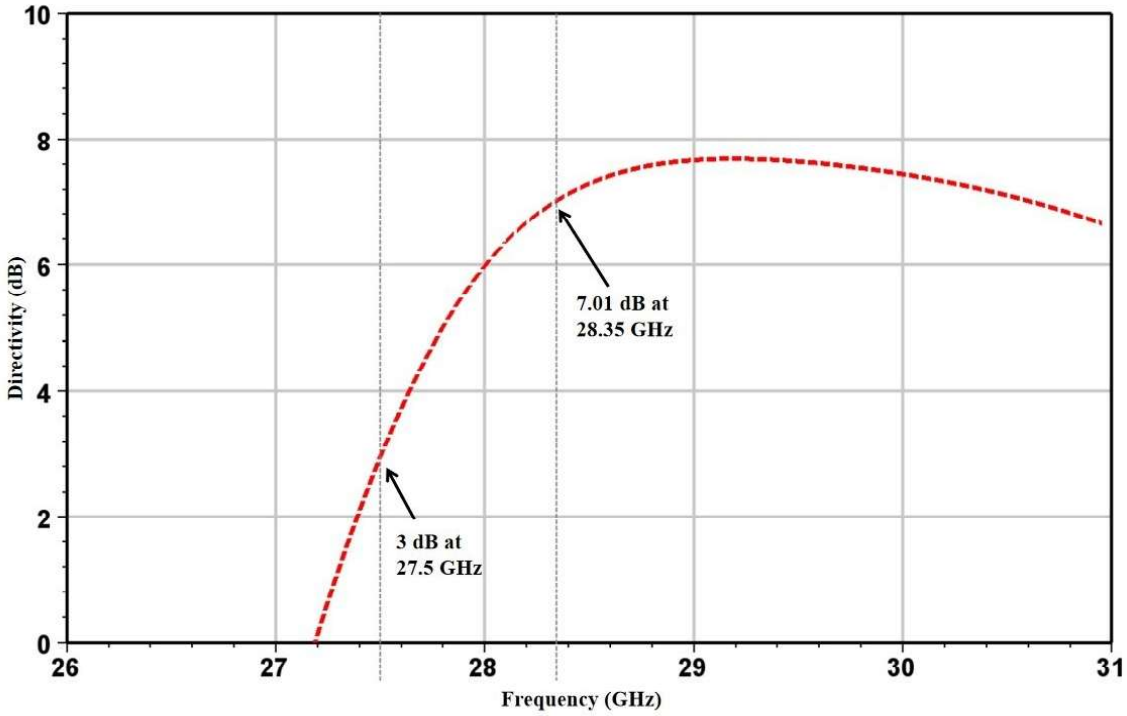

Fig. 4.15: Simulated results of single planar antenna in terms of Directivity vs. Frequency

After 28.35 GHz, a slight decrease in directivity is observed, yet the antenna continues to maintain reasonably good directional performance. This behavior indicates that the antenna is well-optimized for operation around 28 GHz, a key band for millimeter wave 5G systems where focused signal transmission is essential for better coverage and reduced interference.

Overall, the directivity response confirms that the antenna is well-suited for high-frequency applications, delivering efficient and directional radiation around its intended frequency band.

4.5.4 Gain

From the Figure 4.16, it is evident that the antenna's gain increases progressively as the frequency rises. At 27.5 GHz, the antenna delivers a gain of about 2.59 dB. As the frequency approaches the antenna's resonant point, the gain continues to improve, reaching a peak value of approximately 6.65 dB at 28.35 GHz. This peak gain near resonance highlights the antenna's optimal performance in terms of radiated power.

In millimeter wave communication systems like 5G, where signal strength and directivity are critical, the continuous improvement in gain is a reflection of the antenna's improved ability to concentrate energy in a particular direction. After reaching its maximum gain, there's a slight decrease beyond 28.35 GHz, indicating the frequency range where the antenna performs best.

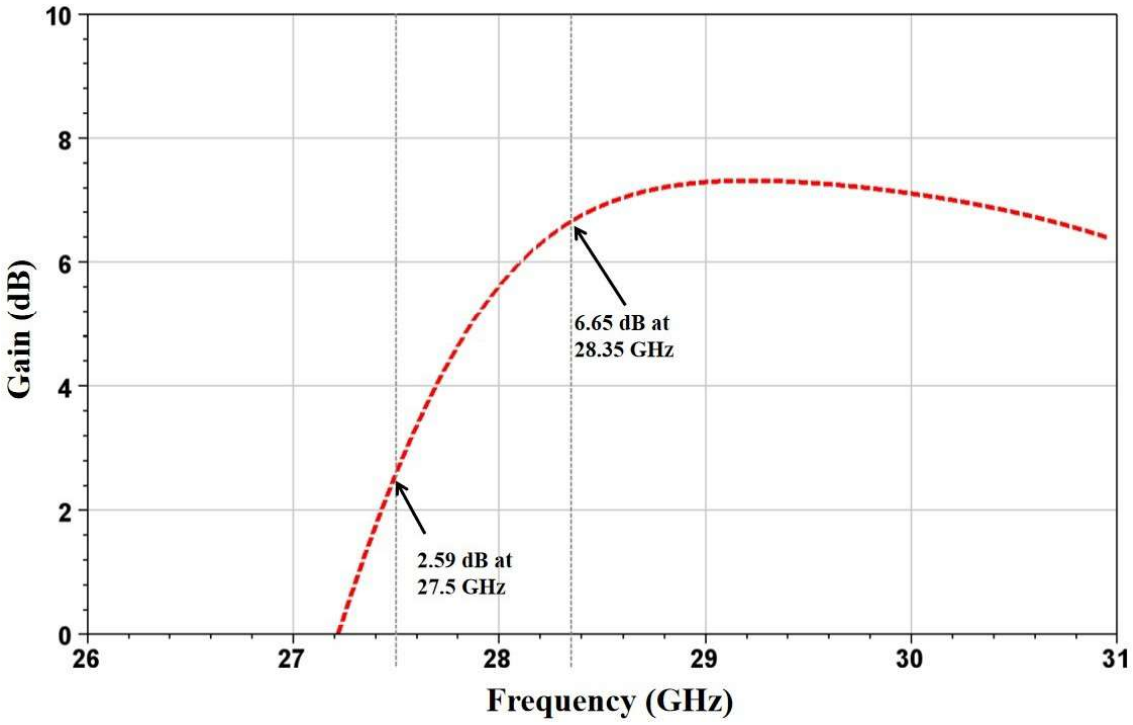

Fig. 4.16: Simulated results of single planar antenna in terms of Gain vs.Frequency

4.5.5 Effect of Gain with and without DGS

Figure 4.17 presents an antenna's gain performance comparison with and without the use of a *Defected Ground Structure (DGS)* across a 26–31 GHz frequency range. The blue dashed line represents the gain without *DGS*, showing a steady rise and reaching just over 6 dB around 30 GHz. However, in the target n261 frequency band (27.5–28.35 GHz), the gain remains moderate. On the other hand, the red dashed line, indicating the gain with *DGS*, demonstrates a noticeable improvement starting from approximately 27 GHz. The gain increases rapidly and peaks near 8 dB, with significantly better performance across the entire n261 band. This enhancement is primarily due to the role of the *DGS* in altering current distribution and minimizing surface wave

losses, which leads to better radiation efficiency. Overall, integrating *DGS* results in a more efficient antenna design, especially suited for 5G millimeter wave applications.

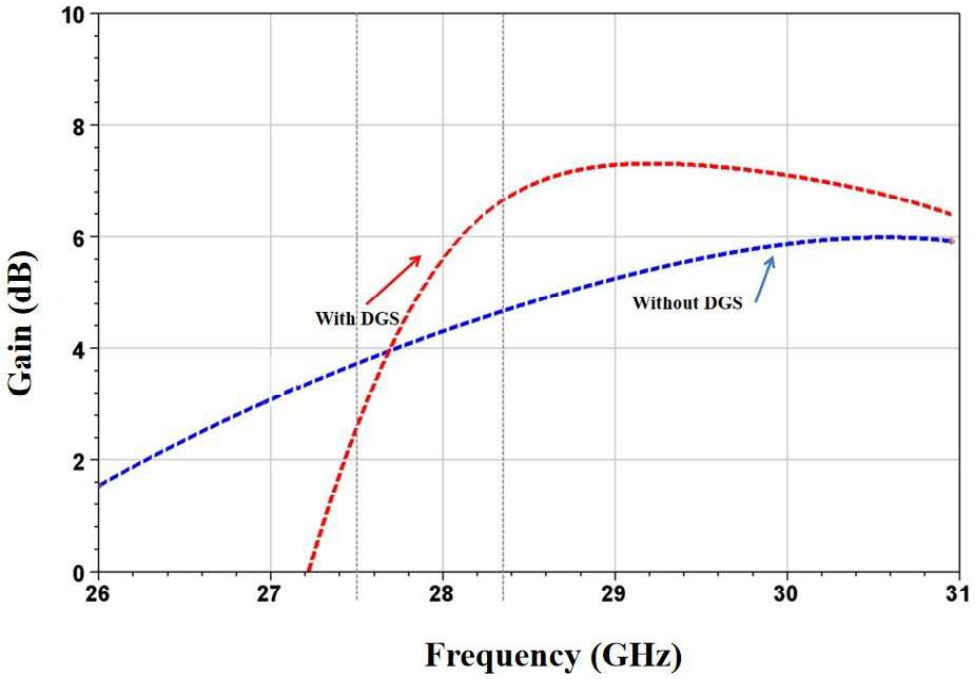

Fig. 4.17: Simulated results representing the effect of Gain with and without DGS vs.Frequency

4.5.6 Effect of Return Loss with and without DGS

Figure 4.18 illustrates the impact of incorporating a *Defected Ground Structure (DGS)* on the return loss (S_{11}) of the antenna across the frequency range of 26 to 31 GHz. The blue dashed curve represents the return loss without *DGS*, which remains above -10 dB throughout the band, indicating sub-optimal impedance matching and poor energy transfer between the antenna and the feedline.

In contrast, the red dashed curve shows the performance with *DGS* applied. A significant improvement in return loss is observed, with a deep resonance dip occurring around 28 GHz well below -30 dB. This indicates excellent impedance matching and minimal signal reflection at the feed point. The *DGS* structure effectively modifies the current distribution and enhances the

capacitive and inductive behavior of the ground plane, resulting in better coupling and resonance at the desired frequency.

Overall, the use of *DGS* significantly boosts antenna performance within the n261 mmWave band, making it a highly effective design choice for modern 5G communication systems.

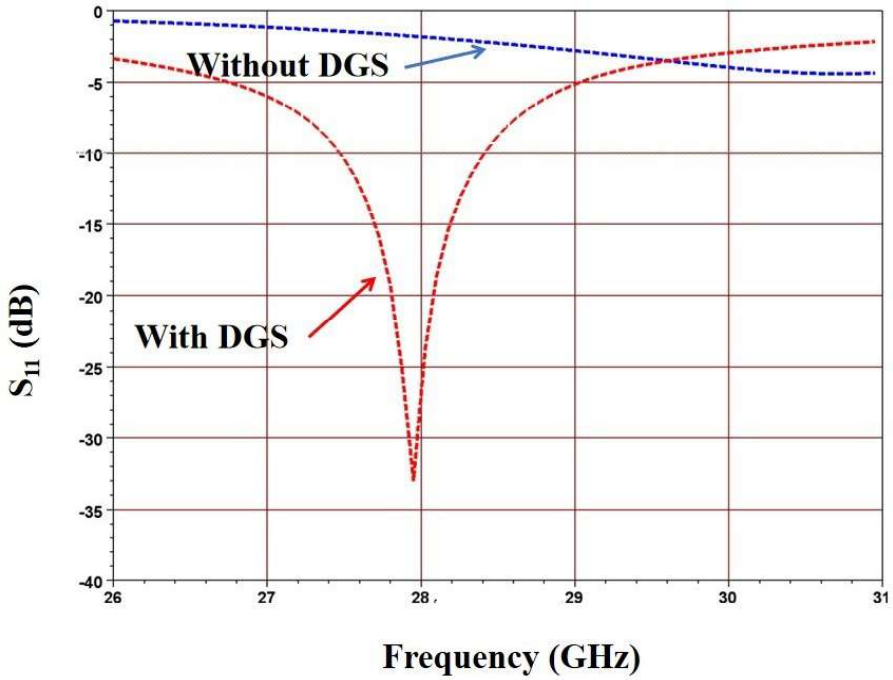

Fig. 4.18: Simulated results representing the effect of Return loss (S_{11}) with and without DGS vs.Frequency

4.5.7 Radiation Pattern

Figure 4.19 depicts the suggested polar radiation pattern that is simulated by single planar antenna, analyzed at two principal angular cuts: $\phi = 0^\circ$ (depicted by the red dashed line) and $\phi = 90^\circ$ (depicted by the blue dashed line). These cuts represent the electric field plane (E-plane) and magnetic field plane (H-plane), respectively.

In the E-plane ($\phi = 0^\circ$), the radiation pattern exhibits a narrower and more lobed structure, indicating moderate directivity with a bidirectional radiation profile. Although radiation is

directed in two opposite directions, the presence of side lobes and slight asymmetry indicates some variation in power distribution.

On the other hand, the H-plane ($\phi = 90°$) shows a broader, more symmetric pattern with enhanced gain at its peak lobes. This reflects a more focused and stronger radiation profile, which is advantageous for communication applications requiring efficient signal transmission.

Overall, the antenna demonstrates consistent and directional radiation characteristics in both principal planes. The improved performance in the H-plane, along with reduced back radiation due to the lobed structure, confirms its suitability for millimeter wave applications such as 5G communication systems.

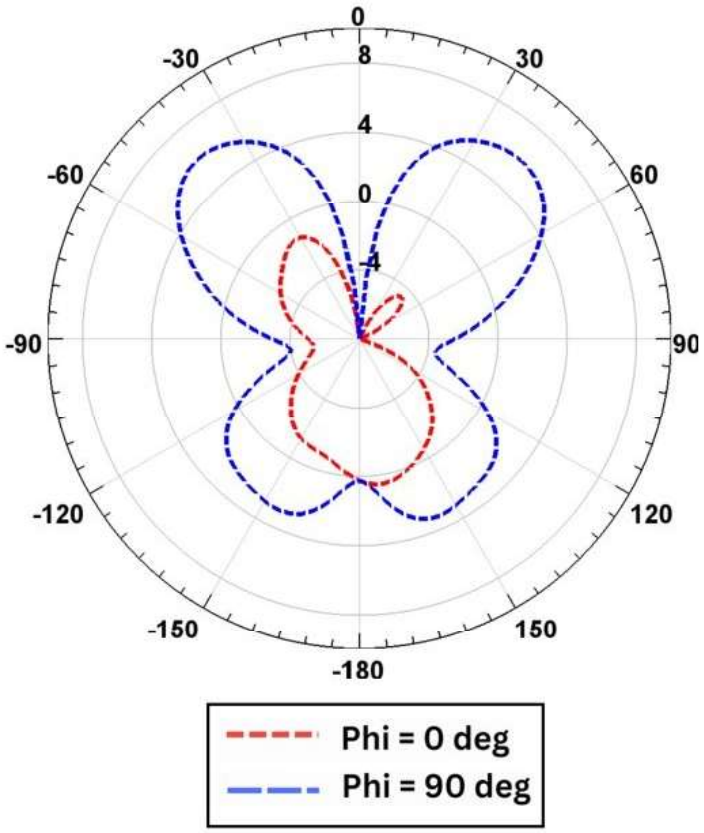

Fig. 4.19: Simulated results of Radiation pattern for single planar antenna.

The simulated radiation pattern of the single-element antenna, shown in Figure 4.19, reveals that the peak gain is achieved at an elevation angle $\theta = 0°$ in the azimuthal plane $\phi = 90°$. This corresponds to the broadside direction relative to the patch surface, but perpendicular to

the microstrip feedline orientation. In contrast, the E-plane ($\phi = 0°$) exhibits a null at $\theta = 0°$, indicating suppressed radiation along the feedline axis due to asymmetric current distribution caused by the inset feed and slot geometry.

This directional characteristic implies that the antenna delivers maximum radiation in the H-plane, making it suitable for applications where the antenna can be oriented such that its H-plane aligns with the desired propagation path; a common practice in mmWave MIMO systems employing beamforming. The peak gain of 6.8 dBi is observed at $\theta = 0°$, $\phi = 90°$, confirming that while the pattern is not omnidirectional, it provides sufficient directivity for targeted communication links.

The inset feed location, combined with the diamond-shaped and circular slots etched into the patch, perturbs the surface current paths, leading to a non-uniform field distribution that suppresses radiation along the boresight direction in the E-plane. While this configuration enhances impedance bandwidth and isolation as intended for MIMO applications, it compromises the ideal broadside radiation pattern typically desired for single-element antennas.

To mitigate this effect, future design iterations could consider:

- Symmetrically placing slots relative to the feed point to balance current flow.
- Using a centered feed instead of inset feed (though this may compromise matching).
- Adding parasitic elements or reflectors to reshape the pattern.
- Employing a multi-layer structure with a superstrate to enhance broadside gain.

Despite this pattern asymmetry, the antenna still delivers sufficient directivity and gain (6.8 dBi) in the H-plane, which remains suitable for directional beamforming in mmWave systems where the antenna array can be oriented to align with the dominant propagation path.

4.5.8 Surface Current

Figure 4.20 presents the simulated surface current distribution of the designed single planar antenna at its resonant frequency. The color scale indicates the magnitude of current density

in A/m, ranging from approximately 0.95 A/m (shown in deep blue) to a maximum of about 212 A/m (represented in red), effectively mapping areas of low to high current flow.

The left part of the figure displays the top view of the antenna structure. It is evident that the maximum current is concentrated around the feedline and near the edges of the radiating patch, particularly around the introduced slots and notches. These regions are critical for efficient radiation and impedance tuning. The diamond-shaped slots show strong current activity, suggesting their active role in shaping the antenna's resonant properties.

On the right side of the figure, the current distribution on the ground plane is shown, specifically focusing on the *Defected Ground Structure (DGS)*. The circular structures of the *DGS* exhibit intensified current flow along their periphery, highlighting their influence on the electromagnetic field distribution. This behavior confirms the effectiveness of the *DGS* in modifying current paths, which leads to improved impedance characteristics, better gain, and enhanced isolation requirements for high-performance millimeter wave antennas.

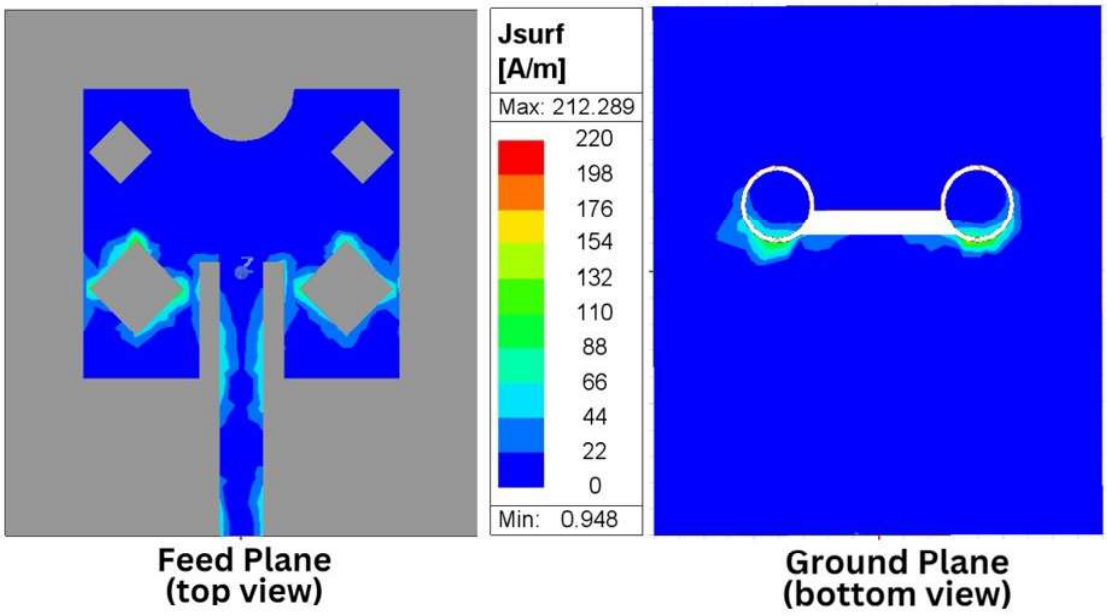

Fig. 4.20: Surface current distribution for single planar antenna

4.6 SUMMARY

This chapter focused on the development and performance assessment of a standalone antenna element designed for *Extremely High Frequency (EHF)* band applications, specifically targeting the 5G frequency band. The Rogers RT/Duroid 5880 substrate served as the foundation for the antenna, selected for its advantageous characteristics, including a low dielectric constant and thin profile, which help ensure efficient performance with minimal signal loss at high frequencies. The patch and feedline dimensions were carefully selected to achieve efficient signal transmission. To enhance bandwidth, impedance matching, and isolation, the ground plane had a *Dumbbell Shaped Defected Ground Structure (DB-DGS)* integrated into it. This structural feature played a key role in modifying the surface current distribution, leading to improved antenna behavior.

A thorough analysis was conducted using a number of performance parameters, including the distribution of surface current, efficiency, directivity, gain, and reflection coefficient. With an impedance bandwidth of 850 MHz, which ran from 27.5 GHz to 28.35 GHz, the antenna was able to cover the FR2 spectrum's n261 band. Peak gain and directivity were observed at 28.35 GHz, reaching 6.65 dB and 7.01 dB respectively, indicating focused and efficient radiation. The efficiency analysis further validated the antenna's high-performance characteristics, with radiation efficiency exceeding 93% and total efficiency ranging between 85% and 98% across the desired frequency band. Additionally, the surface current plots illustrated the influence of design features such as the feedline, slots, and *DGS* on improving radiation and reducing mutual coupling.

Chapter–5

Design of a Planar MIMO Antenna for Millimeter Wave (mmWave) band

The growing need for dependable, fast, and low-latency communication in 5G networks has made *MIMO* antenna technology essential, especially in the mmWave spectrum. However, challenges such as mutual coupling, impedance matching, and compact design need to be addressed for efficient performance. In this chapter, a 4-port *MIMO* antenna operating in the n261 band is developed and optimized. Because of the near arrangement of antenna elements, mutual coupling is a crucial consideration. Unlike many existing *MIMO* designs that rely on additional decoupling structures to reduce coupling, the suggested antenna has no additional decoupling devices to achieve great isolation. Instead, a *DGS* is incorporated, specifically a *DB-DGS*, which effectively modifies the distribution of current in the ground plane. This enhances impedance matching, reduces mutual coupling, and increases isolation while keeping the antenna's overall size same..

5.1 INTRODUCTION

With the rapid evolution of wireless communication, 5G mmWave technology has become essential for achieving higher data rates, ultra-low latency, and massive device connectivity. Traditional sub-6 GHz networks struggle to meet these demands, making mmWave frequencies, particularly the n261 band (27.5–28.35 GHz), a promising solution for next-generation networks. However, designing antennas for mmWave *MIMO* systems introduces challenges such as high path loss, increased mutual coupling between antenna elements, and the need for compact, high-gain structures.

The antenna is particularly suited for mmWave applications since it is built on Rogers RT/Duroid 5880, a low-loss substrate with 0.254 mm in thickness and 2.2 dielectric constant.

Measuring 5.2 mm in length and 0.8 mm in line width, a microstrip feed line is utilized to provide effective signal transmission while preserving compactness. The patch dimensions (5.5 mm × 6 mm) are optimized to achieve the desired resonant frequency while maintaining good radiation performance.

To validate the effectiveness of the proposed design, key performance metrics such as S-parameters (S_{11}, S_{21}), *Envelope Correlation Coefficient (ECC)*, *Diversity Gain (DG)*, and radiation characteristics are analyzed. The findings verify that the antenna provides dependable radiation performance, high impedance matching, and good isolation (without decoupling structures), making it a promising candidate for 5G mmWave applications. With its compact footprint, high efficiency, and optimized *MIMO* performance, this design contributes to the advancement of next-generation wireless networks, addressing critical challenges in mmWave *MIMO* technology.

5.2 MIMO ANTENNA DESIGN

The four-port *MIMO* antenna presented in Figure 5.1(a) is an extension of the single-element design introduced in Chapter 4, configured to support millimeter wave applications in a compact 20 mm × 19 mm layout. This structure comprises four identical antenna elements (Ant-1 to Ant-4), each excited by an individual microstrip feed line and strategically arranged to enable polarization diversity. To ensure minimal signal interference and enhanced isolation among elements, the design incorporates specific edge-to-edge spacings. A separation of 3.5 mm (d1) is maintained between Ant-1 and Ant-4, as well as between Ant-2 and Ant-3, while a lateral edge gap of 3 mm (d2) is maintained between Ants 1 and 2, as well as between Ants 4 and 3. These carefully selected spacings help suppress mutual coupling between adjacent antennas, which is essential for achieving reliable performance in *MIMO* systems. The overall layout not only supports high channel capacity and data rates but also maintains a compact footprint, making it ideal for next-generation 5G communication devices. Table 5.1 lists the dimensional parameters of proposed MIMO antenna.

The plane on the other side in Figure 5.1(b) shows the ground plane's top view for the suggested four-port *MIMO* antenna setup, has a common ground plane having separate dumbbell shaped slots corresponding to each element. Each antenna element (Ant-1 through Ant-4) is

strategically positioned to support both polarization and spatial diversity. Unlike the feed plane, which focuses on the excitation of signals, the ground plane incorporates uniquely shaped dumbbell slots aligned beneath each radiating element. These slots form a *Defected Ground Structure (DGS)*, which is instrumental in suppressing surface current propagation. This design helps reduce mutual coupling and electromagnetic interference among the antenna elements, thereby improving isolation and enhancing the overall system performance. The symmetrical layout of these slots ensures that each antenna functions independently, which is necessary to reach the high data rates required in millimeter wave 5G communication systems. The integration of the *DGS* with precise slot placement reflects a balance between electrical performance and compact structural design, all within a footprint of 20 mm × 19 mm.

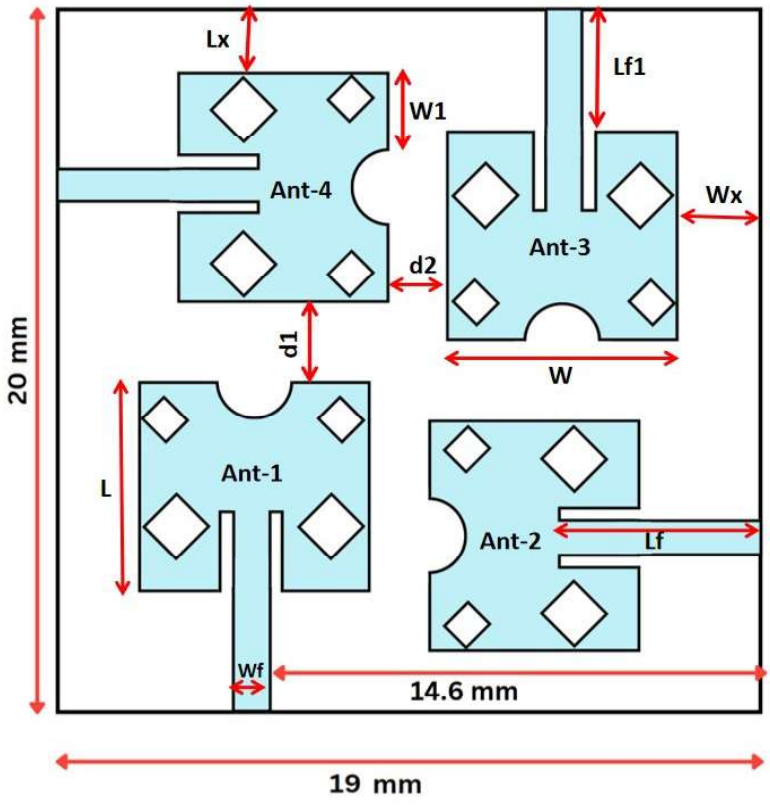

(a)

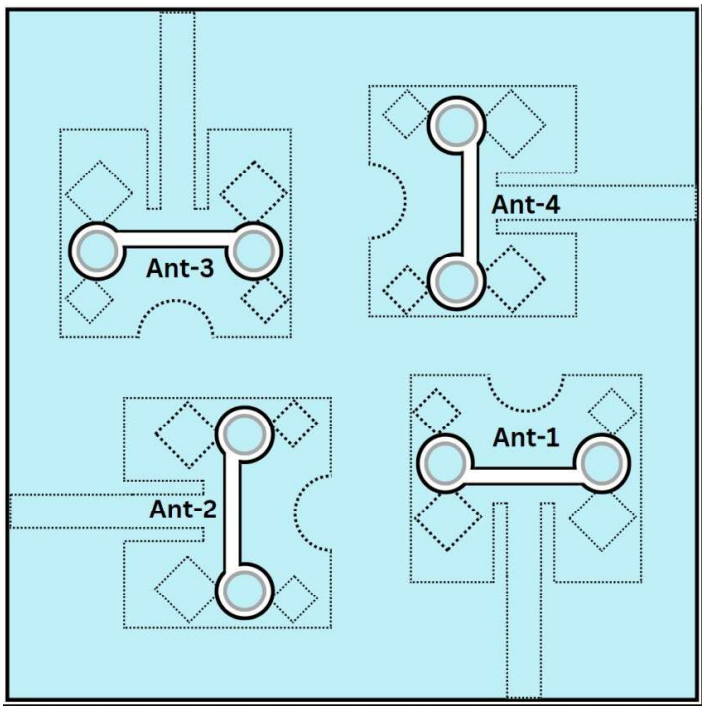

(b)

Fig. 5.1: Structural design of a proposed MIMO Antenna (a) Feed Plane (Top view) (b) Ground Plane (Top View)

Table 5.1: Dimensions of proposed MIMO antenna parameters in mm

Parameter	**Value (mm)**	**Parameter**	**Value (mm)**
L	5.5	Lx	2.0
Lf	5.2	Lf1	3.0
W	6.0	Wx	1.5
Wf	0.8	W1	2.2
d1	3.5	d2	3.0

5.3 FABRICATION AND PROTOTYPING OF THE PROPOSED MIMO ANTENNA

The fabrication and testing of the suggested 4-port *MIMO* antenna to verify its performance is the final objective of the study, and it is covered in this section. Following the comparative analysis of various planar *MIMO* antennas presented in Chapter 3, a new *mmWave MIMO* antenna design was developed, with its parameters carefully adjusted for enhanced performance. To assess its real-world behavior, the fabricated antenna was tested using a *Vector Network Analyzer (VNA)* to measure S-parameters, isolation, and impedance matching. Additional key performance indicators such as gain, radiation patterns, and MIMO parameters were evaluated further and compared to the outcomes of simulations. The findings confirm the effectiveness of the DGS-based design, establishing it as a promising option for upcoming 5G millimeter wave applications.

A substrate recognized for its low dielectric loss ($\varepsilon_r = 2.2$) and its ability to support efficient signal transmission , Rogers RT/Duroid 5880, is used to manufacture the antenna prototype, which has a compact design of 20 mm × 19 mm × 0.254 mm at millimeter wave frequencies. The design integrates a *Dumbbell Shaped Defected Ground Structure (DB-DGS)*, which naturally enhances isolation between antenna elements, eliminating the need for additional decoupling structures. Furthermore, the elements are arranged in a cross-polarized configuration, contributing to both the compactness of the layout and the reduction of mutual interference.

The constructed prototype of the suggested 4-port *MIMO* antenna is shown in the figures below. Figure 5.6(a) shows the feed plane with four cross-polarized radiating elements arranged in a compact 2×2 configuration. Figure 5.6(b) illustrates the ground plane, where *Dumbbell Shaped Defected Ground Structure (DB-DGS)* are etched beneath every element to enhance isolation by suppressing surface currents. The *SMA* connectors are soldered to each port for testing and measurement.

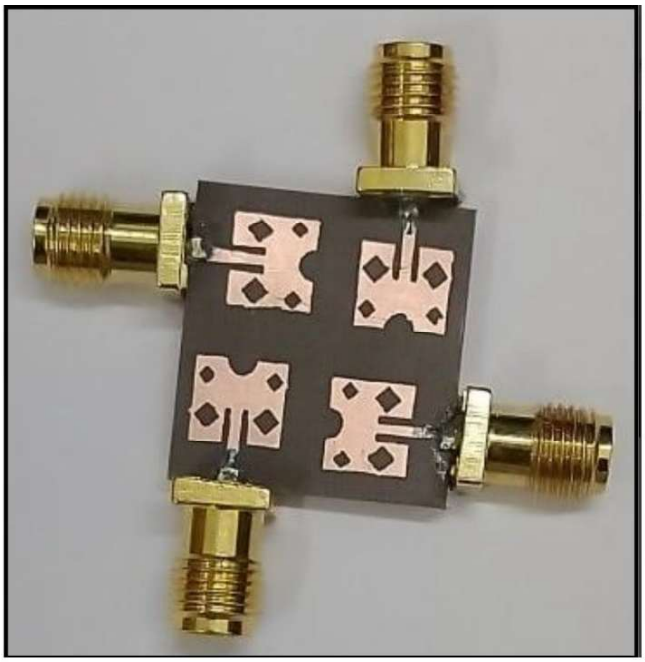

(a)

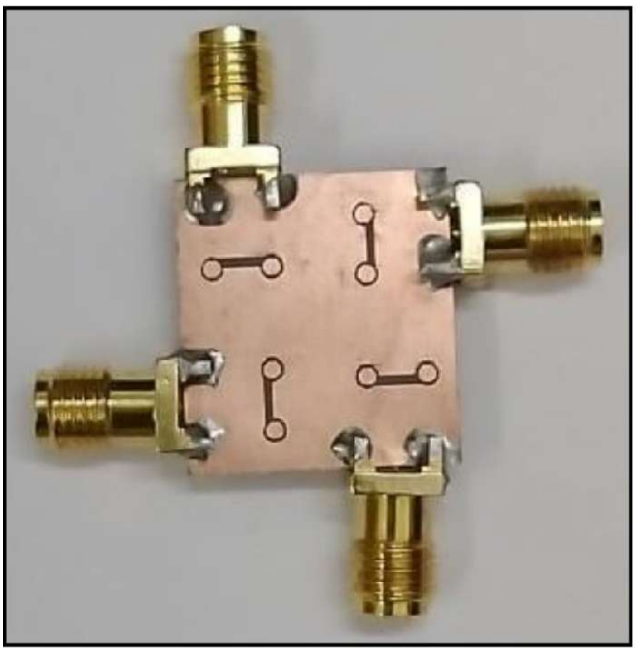

(b)

Fig. 5.2: Fabricated prototype of proposed MIMO antenna a) Feed Plane (Top view) b) Ground Plane (Bottom View)

5.3.1 Measurement Setup

The performance of fabricated *MIMO* antenna prototype was confirmed by experimental testing. Figure 5.7(a) shows the antenna placed inside an anechoic chamber, a controlled environment designed to eliminate external electromagnetic interference and reflections. The anechoic chamber supports frequency measurements up to 40 GHz. This setup helps accurately evaluate radiation attributes including radiation pattern and gain. Figure 5.7(b) displays the prototype connected to a *Vector Network Analyzer (VNA)* with a range of upto 40 GHz, which is used to measure important S-parameters, including return loss and isolation between ports. The outcomes of simulation and measurement show good agreement as depicted in Section 5.5.1 and 5.5.2.

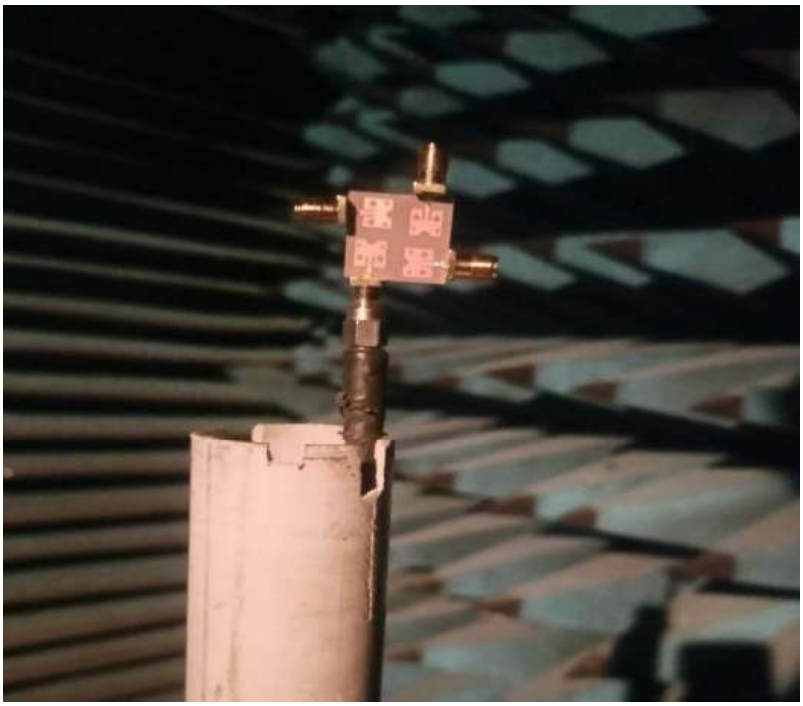

(a)

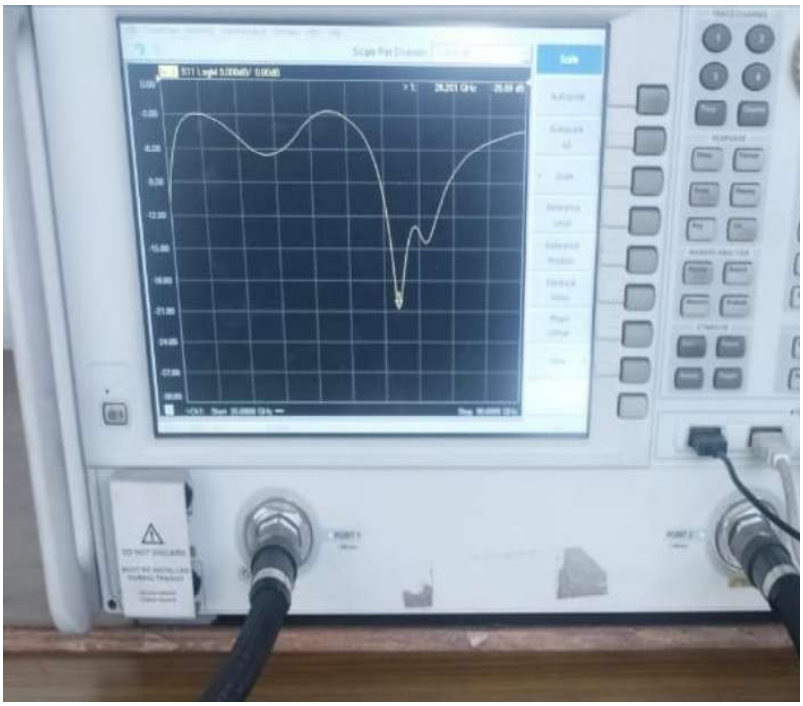

(b)

Fig. 5.3: Measurement setup (a) Prototype Testing under Anechoic chamber (b) Prototype Testing under Vector Network Analyzer (VNA)

5.4 RESULTS AND DISCUSSION

5.4.1 S-Parameters

- **Analysis of Reflection Coefficient through Simulated and Measured Results:** The fabricated prototype of the proposed *MIMO* antenna is as shown in Figure 5.6. Figure 5.8 displays the results of simulations and measurements using all four radiating *MIMO* antennas. Figure 5.8(b) illustrates a little change in the frequency of operation in contrast to the results of the simulation displayed in Figure 5.8(a). Antenna-1 radiates between 27.49–28.39 GHz, antenna-2 between 27.50 – 28.36 GHz, antenna-3 between 27.50–28.37 GHz, and antenna-4 between 27.50–28.42 GHz.

  Secondly,there is slight shift in resonant frequency range for all four antennas. Antenna-1 now has a bandwidth of -10 dB between 27.46 and 28.44 GHz., Antenna-2 ranging from 27.48 to 28.39 GHz, Antenna-3 ranging from 27.46 to 28.42 GHz, and Antenna-4 ranging

from 27.46 to 28.44 GHz as can be seen from Table 5.2. Although we can clearly see that in all four cases, the n261 range (27.5 to 28.35 GHz) gets completely covered.

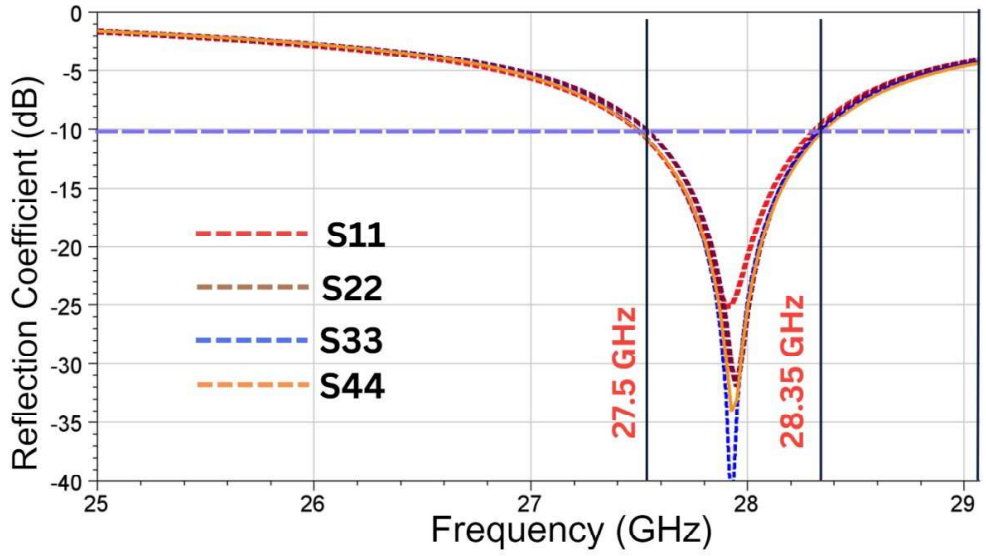

(a)

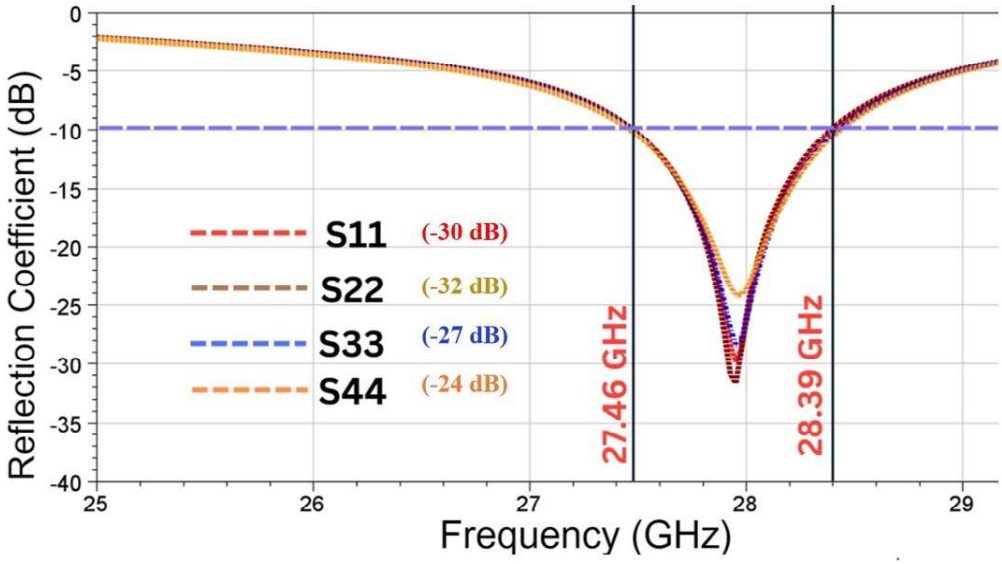

(b)

Fig. 5.4: Calculated Reflection Co-efficient for different elements of a proposed MIMO antenna (a) Represents Simulated values (b) Represents Measured values

Table 5.2: Comparing Measured Radiating Frequency Ranges with Simulated Ranges and Fractional Bandwidth

Antenna	**Simulated Range (GHz)**	**Simulated FBW (%)**	**Measured Range (GHz)**	**Measured FBW (%)**
Antenna-1	27.49 – 28.39	3.22%	27.46 – 28.44	3.51%
Antenna-2	27.50 – 28.36	3.08%	27.48 – 28.39	3.26%
Antenna-3	27.50 – 28.37	3.11%	27.46 – 28.42	3.44%
Antenna-4	27.50 – 28.42	3.29%	27.46 – 28.44	3.51%

The measured values show a slight shift in resonant frequencies compared to the simulated results as shown in Table 5.2. All four antennas operate within or very close to the 5G n261 band (27.5–28.35 GHz), and their fractional bandwidths range from 3.08% to 3.51%, which comfortably exceeds the required value of approximately 3.05% (based on a 0.85 GHz bandwidth relative to the center frequency of 27.925 GHz).

Table 5.3: Comparison of Simulated and Measured Reflection Coefficient S_{11} (dB)

Antenna	**Simulated S_{11} (dB)**	**Measured S_{11} (dB)**
Antenna 1	-25	-30
Antenna 2	-32	-32
Antenna 3	-40	-27
Antenna 4	-34	-24

The measured results of the reflection coefficient, shown in Figure 5.8(b) and Table 5.3, exhibit a minor deviation from the simulated results. For instance, the magnitude of S_{33} has increased from –40 dB to –27 dB, indicating a slight degradation in impedance matching. Similarly, the reflection coefficients for S_{11}, S_{22}, and S_{44} have also increased (i.e., become less negative), though all remain below –20 dB; an acceptable level for practical mmWave applications.

- **Analysis of Isolation through Simulated and Measured Results:** Simulated and measured results with all four radiating *MIMO* antennas are as shown in Figures 5.9. As seen from Figure 5.9(b), adjacent antennas isolation for the desired bandwidth is achieved to be less than −20 dB when compared to that in Figure 5.9(a). In this design, the mutual isolation is achieved without the use of any additional decoupling structure. Another method which is generally used in increasing the mutual isolation is by increasing the separation between the elements, but this method increases the overall dimensions of the antenna. In our design, the distance between the adjacent elements has been optimally placed to achieve adequate mutual decoupling. Moreover, the *MIMO* antennas are placed at orthogonal position with each other so as to achieve low coupling between neighboring elements, as seen in Figure 5.9(b).

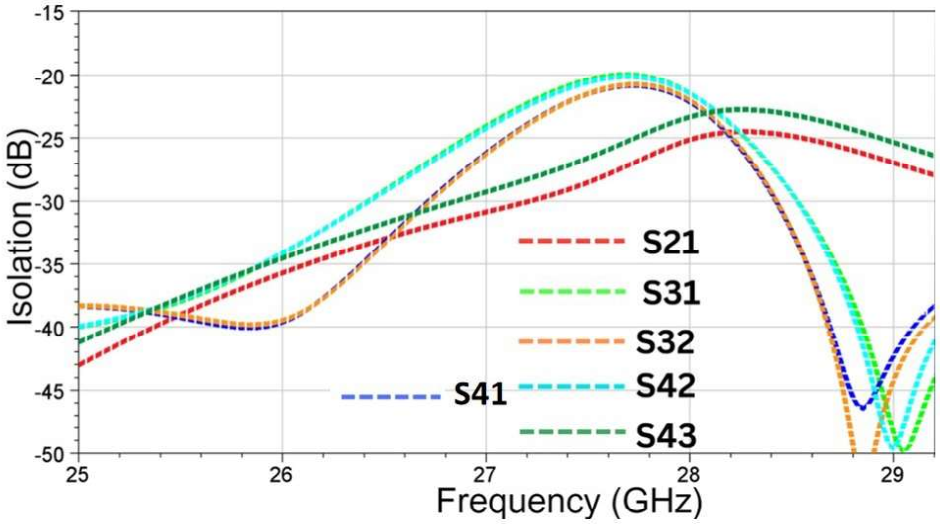

(a)

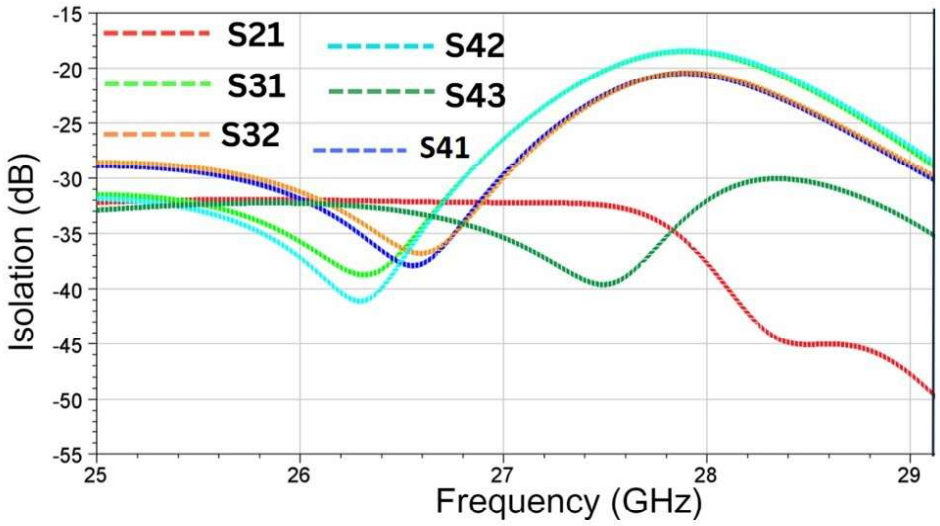

(b)

Fig. 5.5: Calculated Isolation among different elements of a proposed MIMO antenna (a) Represents Simulated values (b) Represents Measured values

Table 5.4: Comparing Measured and Simulated Isolation (dB)

Isolation Parameter	**Simulated Isolation (dB)**	**Measured Isolation (dB)**
S_{21}	-25	-32.5
S_{31}	-20	-18.5
S_{32}	-21	-20.5
S_{42}	-20	-18.5
S_{43}	-23	-30
S_{41}	-21	-21

The measured results for mutual coupling also show slight deviation as shown in Table 5.4. The mutual isolation which was less than -20 dB in simulated results is now measured to be less than -18.5 dB. The deviation in the measured and simulated results can be due to the addition of connectors and cables losses and measuring environment errors. Since the dimensions of the structure are very small, slight variation can cause deviation

in characteristics. Additionally, the design required precise alignment of the feed plane and ground plane. However, the measured results of the prototype are still well within the acceptable values. However, in all cases, the antennas successfully cover the n261 mmWave band (27.5–28.35 GHz), confirming their practical viability for 5G applications.

5.4.2 Radiation Characteristics

The four-element MIMO antenna's radiation patterns displayed in Figure 5.10(a)–(d), include both measured and simulated results at 28 GHz for $\phi = 0^\circ$ and $\phi = 90^\circ$. The patterns of Ant-1 and Ant-3, as well as Ant-2 and Ant-4, appear as mirror images with their main lobes pointing in opposite directions. This occurs due to the orthogonal alignment of antenna elements, allowing better polarization diversity. Each antenna element maintains a directional radiation pattern, and the overall structure supports balanced gain and isolation. The minor differences between simulation and measurement is attributable to measurement errors or manufacture tolerances, but the measured results closely follow the simulated ones, confirming proper antenna performance with consistent directional radiation across all elements.

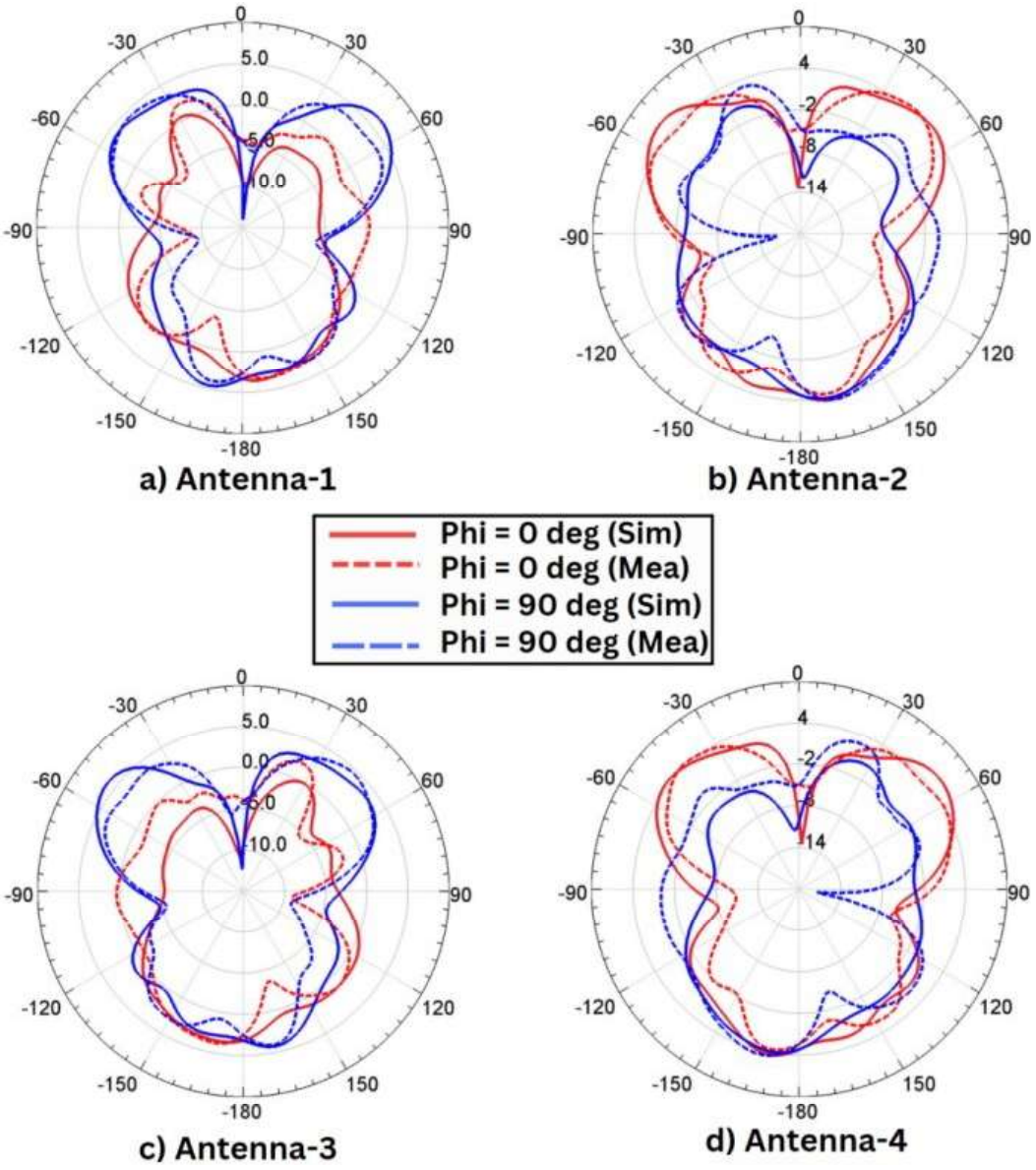

Fig. 5.6: Radiation Characteristics (dB)

Analysis of Polarization (Co and Cross) through Simulated and Measured Results: In addition, the radiation patterns of co-polarizations and cross-polarizations are shown in Figures 5.11, 5.12, 5.13, and 5.14. The radiation patterns have been taken at three frequencies for all four antennas, respectively. One observation is taken approximately at the middle of the bandwidth range, which is 28 GHz. Other two observations are taken at the edge of the frequency range, which are 27.7 GHz and 28.25 GHz.

- **Radaition Patterns of Antenna-1**

  The radiation patterns of Ant-1 have been examined at three frequencies: 27.7 GHz, 28 GHz, and 28.25 GHz to evaluate its performance across the operational bandwidth. These patterns are presented for both cross and co-polarization components in the $\phi = 0^\circ$ (E-Plane) and $\phi = 90^\circ$ (H-Plane) planes. The central frequency of 28 GHz represents the middle of the bandwidth, while 27.7 GHz and 28.25 GHz correspond to its lower and upper edges, respectively as shown in Figure 5.11(a), (b), (c). At all frequencies, the co-polarized fields are stronger than the cross-polarized ones, indicating stable radiation behavior and acceptable polarization purity. The measured results follow the simulated trends closely, with slight deviations due to fabrication and measurement conditions. The radiation characteristics remain consistent across the frequency range, confirming reliable performance of Antenna 1.

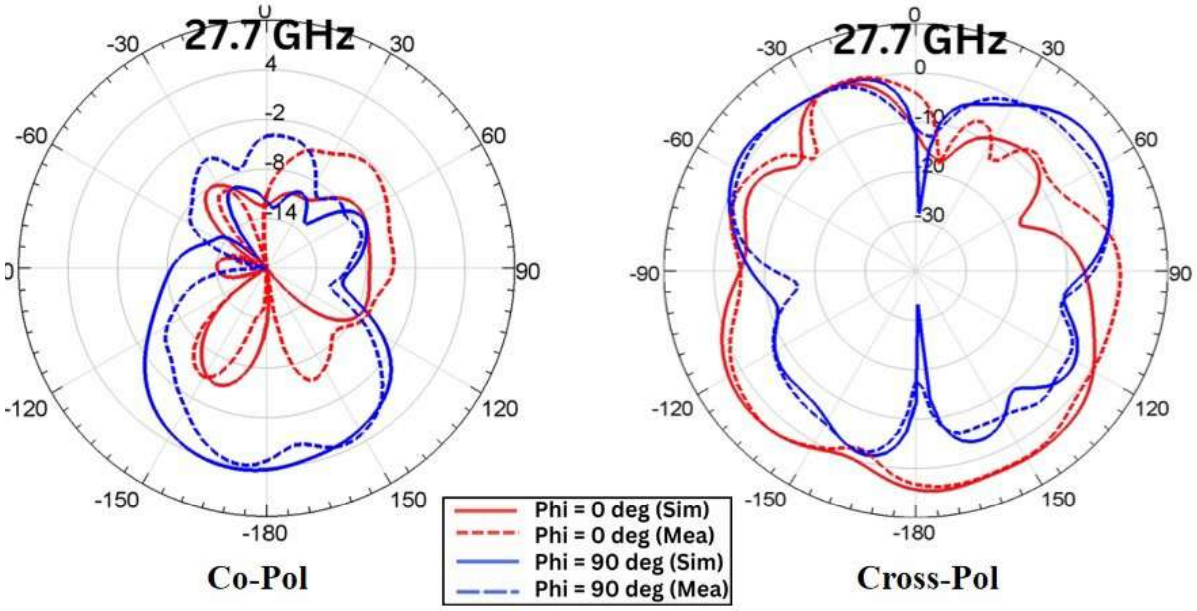

(a)

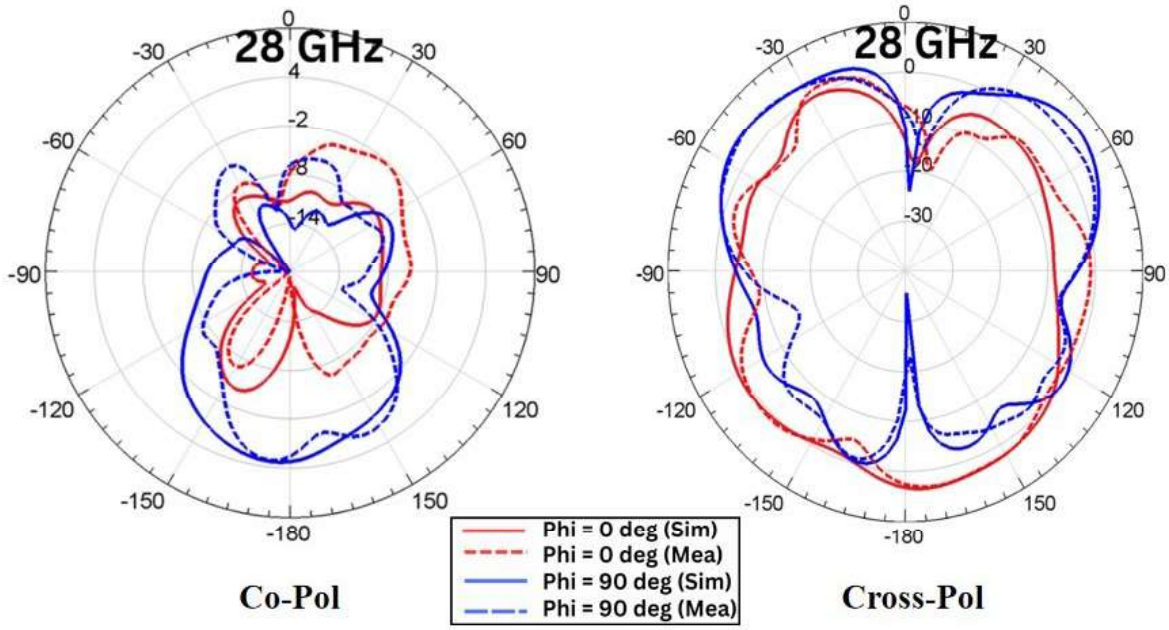

(b)

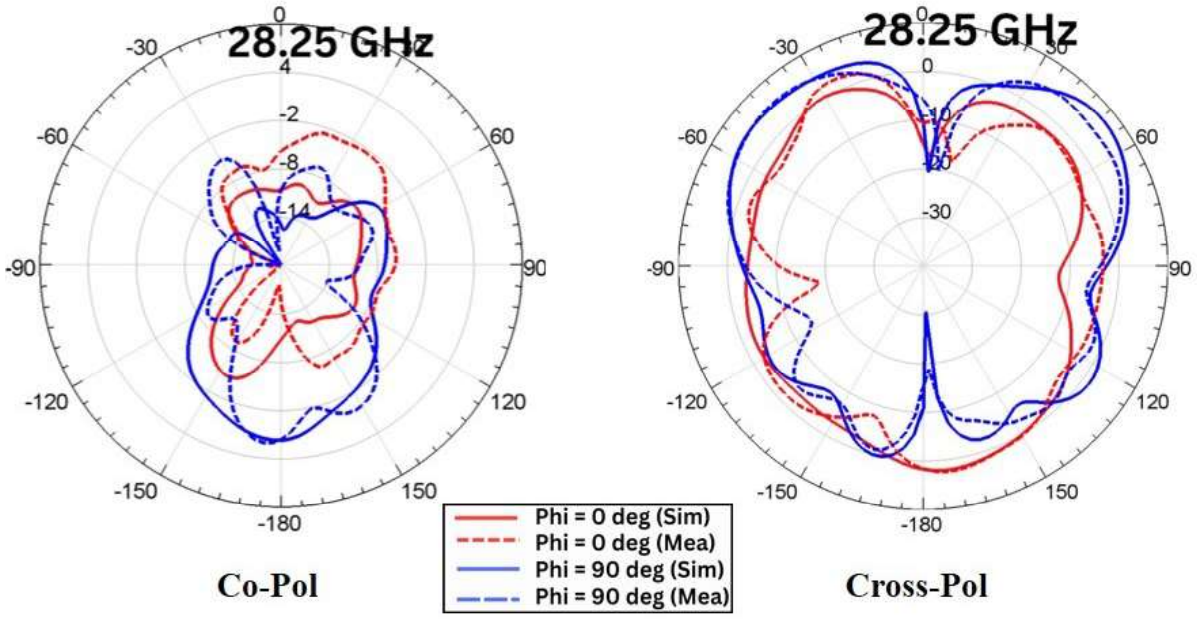

(c)

Fig. 5.7: Radiation pattern representing the Co and Cross-polarization behavior of Ant-1 at different frequency range (a) 27.7 GHz (b) 28 GHz (c) 28.25 GHz

- **Radaition Patterns of Antenna-2**

  The radiation patterns of Ant-2 at 27.7 GHz, 28 GHz, and 28.25 GHz as shown in Figure 5.12(a), (b), (c) illustrate the co and cross-polarization characteristics for both simulated and measured results at $\phi = 0^\circ$ and $\phi = 90^\circ$. In all three frequency scenarios, the co-polarization plots (left) exhibit stronger and more directional radiation compared to the cross-polarization plots (right). The cross-polarized levels remain relatively lower in terms of radiated power, indicating good polarization purity and minimal unwanted radiation. The measured results follow the simulated trends with minor variations, which may be attributed to fabrication tolerances or environmental influences during measurement. Overall, the consistent performance across the frequency range demonstrates the stable radiation behavior of Antenna-2.

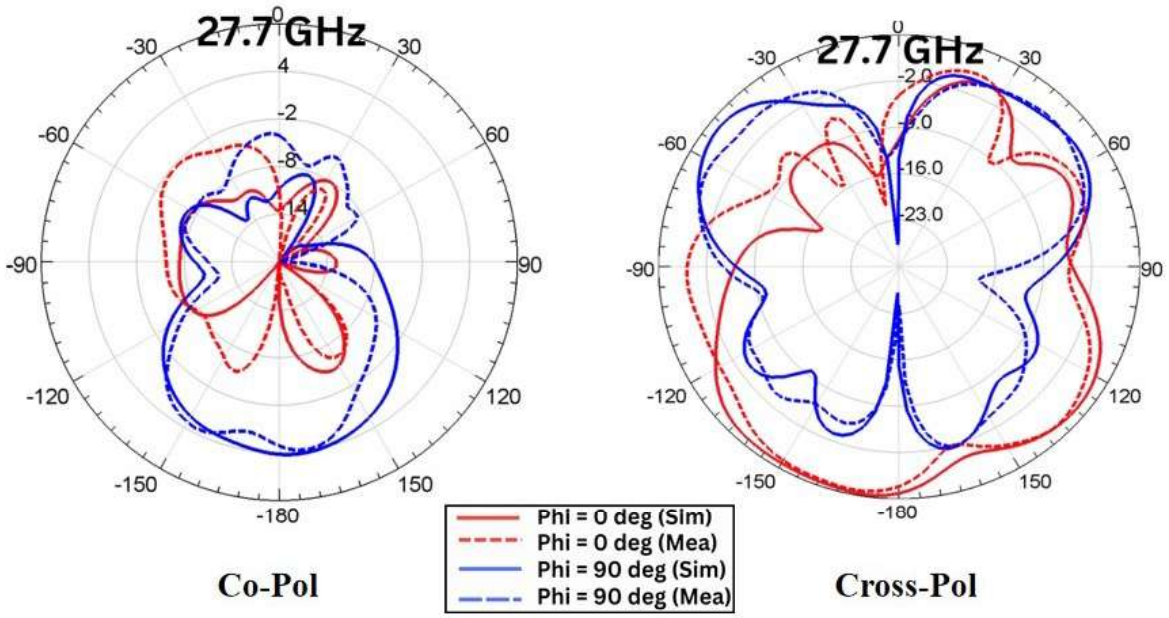

(a)

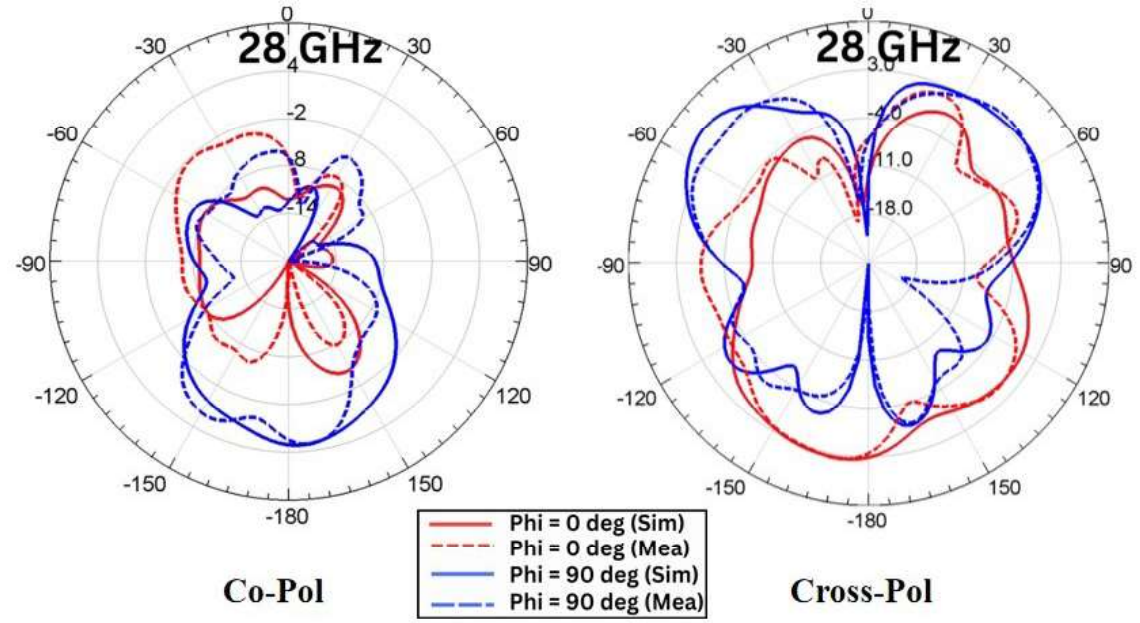

(b)

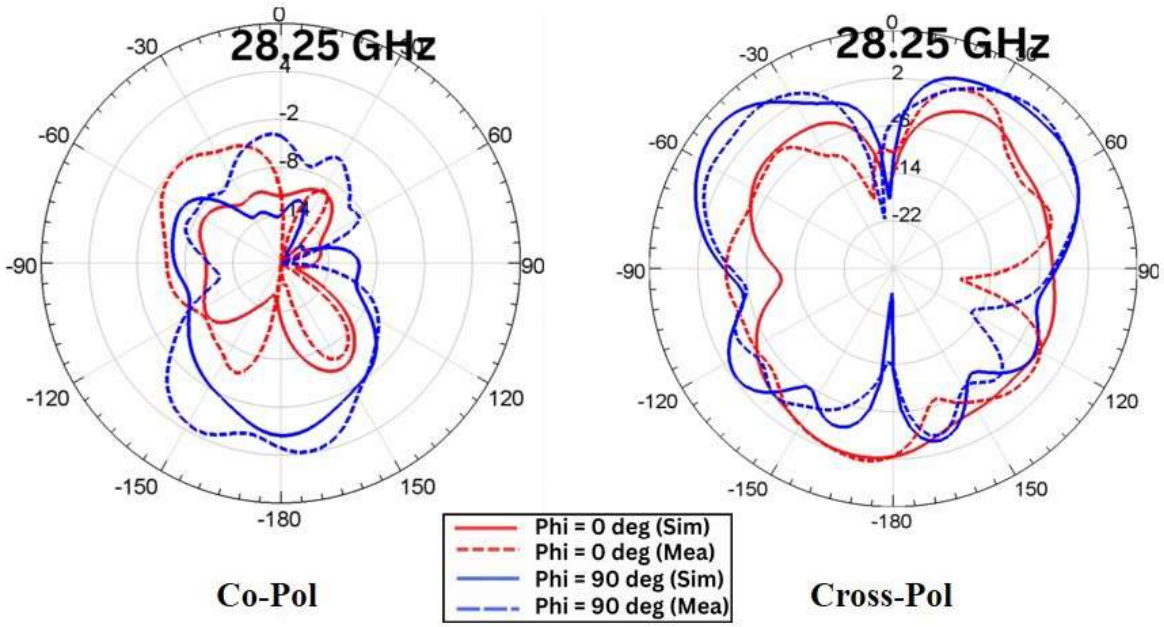

(c)

Fig. 5.8: Radiation pattern representing the Co and Cross-polarization behavior of Ant-2 at different frequency range (a) 27.7 GHz (b) 28 GHz (c) 28.25 GHz

- **Radaition Patterns of Antenna-3** As seen in Figure 5.13(a), (b), and (c), Ant-3's radiation patterns at 27.7 GHz, 28 GHz, and 28.25 GHz demonstrate the co-polarization and cross-polarization properties for both simulated and measured findings at $\phi = 0°$ and $\phi = 90°$..

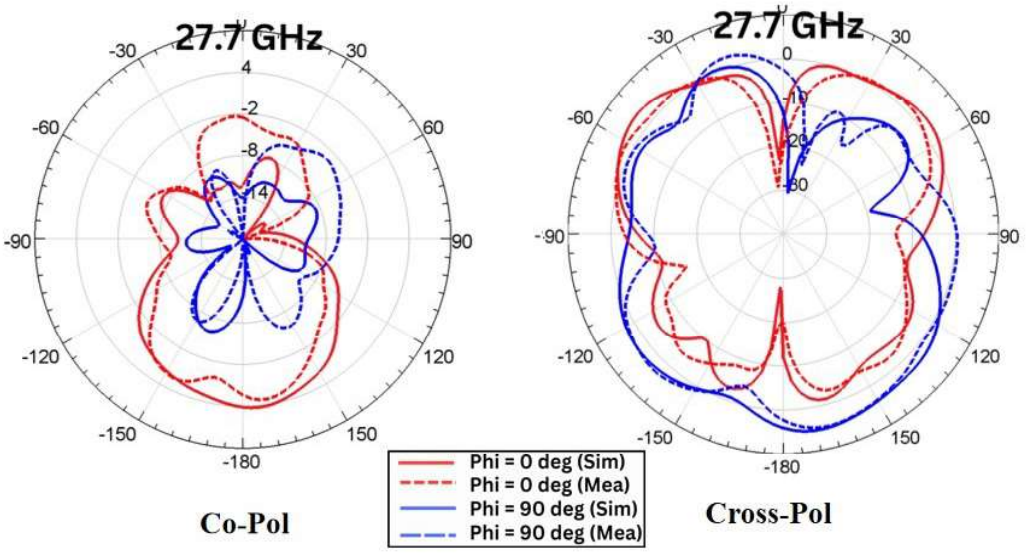

(a)

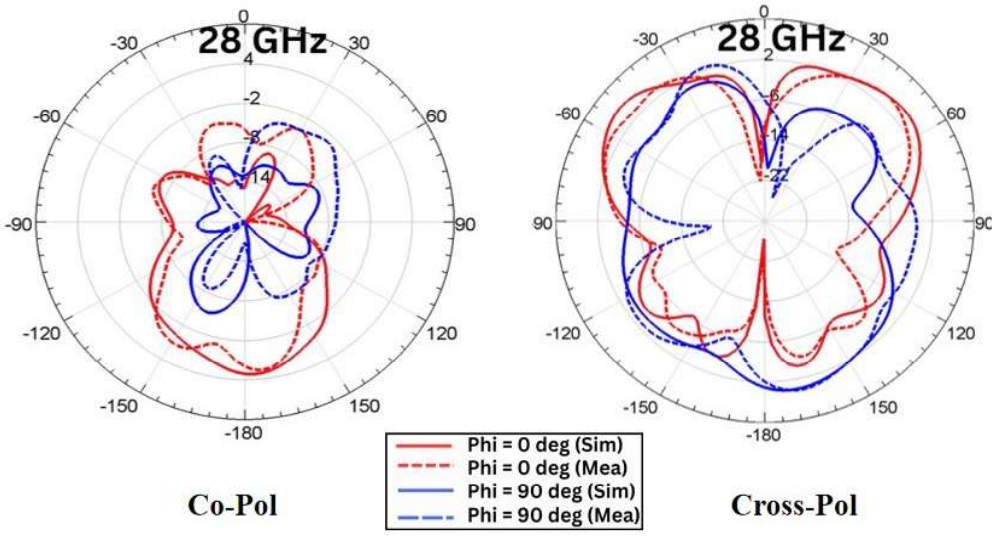

(b)

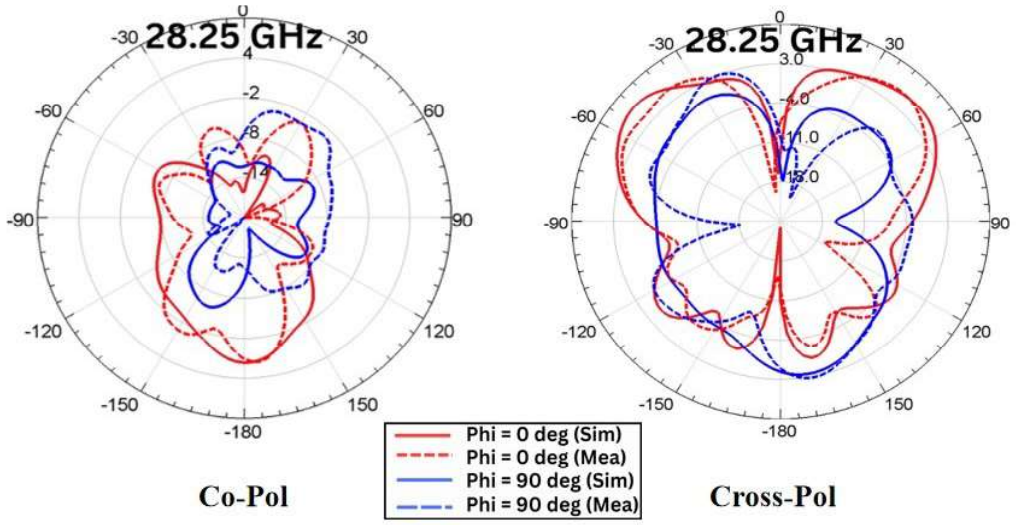

(c)

Fig. 5.9: Radiation pattern representing the Co and Cross-polarization behavior of Ant-3 at different frequency range (a) 27.7 GHz (b) 28 GHz (c) 28.25 GHz

- **Radaition Patterns of Antenna-4** As seen in Figure 5.14(a), (b), and (c), Ant-4's radiation patterns at 27.7 GHz, 28 GHz, and 28.25 GHz demonstrate the co-polarization and cross-polarization properties for both simulated and observed findings at $\phi = 0°$ and $\phi = 90°$..

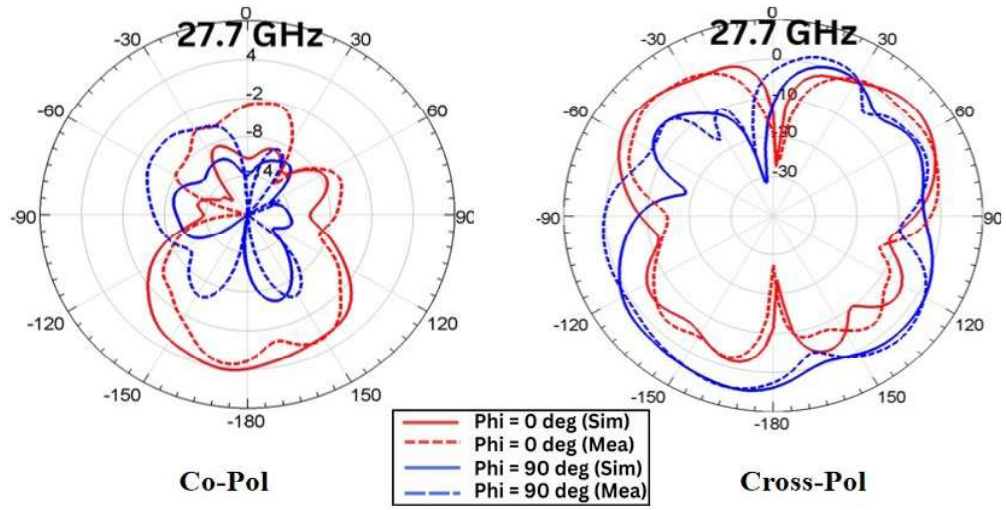

(a)

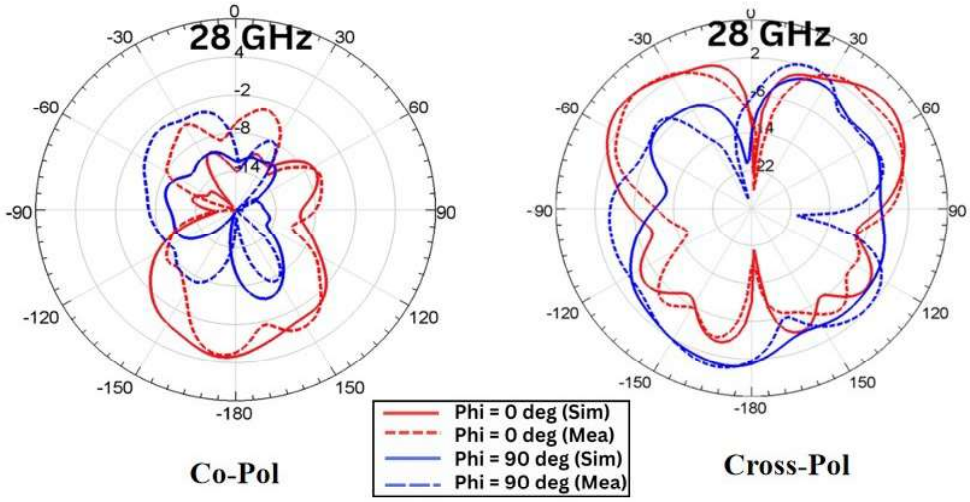

(b)

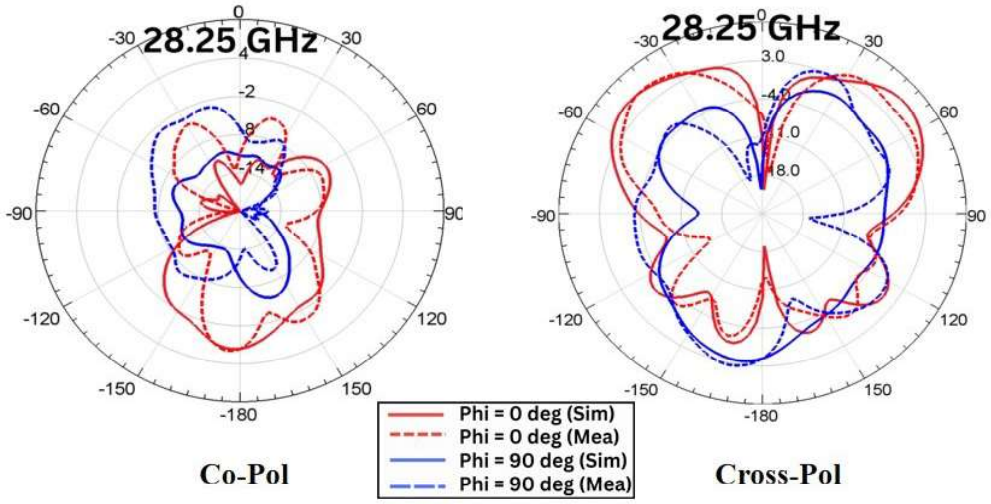

(c)

Fig. 5.10: Radiation pattern representing the Co and Cross-polarization behavior of Ant-4 at different frequency range (a) 27.7 GHz (b) 28 GHz (c) 28.25 GHz

5.4.3 MIMO Parameters

Diversity parameters play an important part in determining the performance of *MIMO* antennas.

- **Envelope Correlation Coefficient:** The degree of isolation between the *MIMO* antenna elements is evaluated using *ECC*. Although *ECC* should ideally be close to zero, numbers below 0.5 are acceptable in real-world applications. Using the formula in Equation (5.1), for *MIMO* antenna, the value of *ECC* can be calculated.from S-parameters.

$$\mathrm{ECC} = \frac{\left|S_{pq}^{*}S_{qp} + S_{qq}^{*}S_{pp}\right|^{2}}{\left(1-|S_{qq}|^{2}-|S_{qp}|^{2}\right)\left(1-|S_{pp}|^{2}-|S_{pq}|^{2}\right)} \tag{5.1}$$

where *Spp* and *Sqq* are reflection coefficients, and *Sqp* and *Spq* are transmission coefficients. As can be see from Figure 5.15 the simulated value of *ECC* falls below 0.011 within the necessary frequency range of n261.

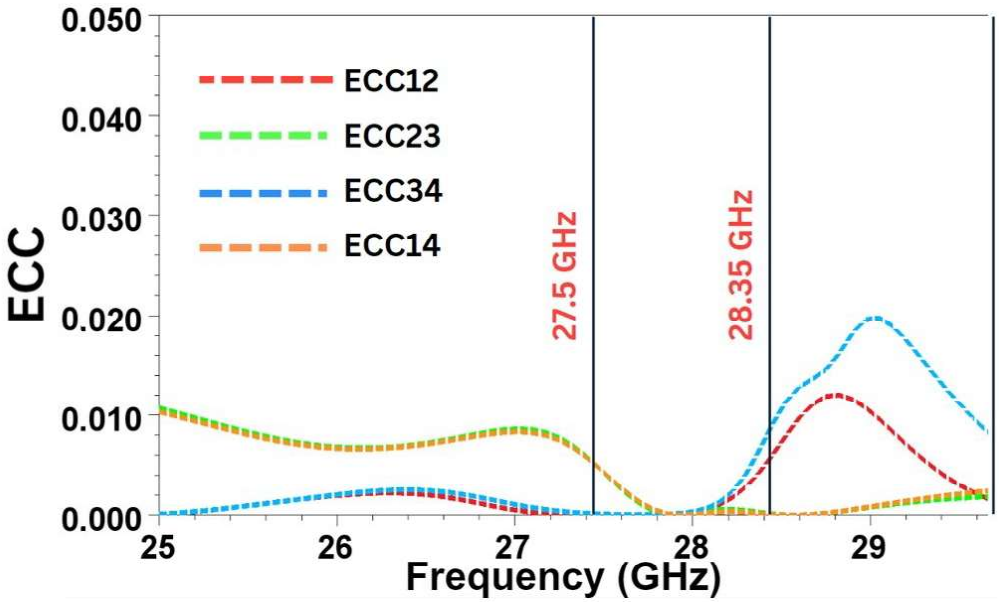

Fig. 5.11: Performance metrics of proposed MIMO antenna in terms of Envelope Correlation Coefficient (ECC)

Figure 5.15 illustrates the *Envelope Correlation Coefficient (ECC)* performance of the proposed 4-port *MIMO* antenna. The *ECC* values for different antenna port combinations: ECC12, ECC23, ECC34, and ECC14 are plotted as shown. Within the desired 27.5–28.35 GHz band, *ECC* values of all orthogonally placed antennas remain well below 0.005, indicating very low correlation between antenna elements. This demonstrates good diversity performance and minimal mutual coupling, which are desirable for efficient *MIMO* operation. The *ECC* values rise slightly outside the operating band, particularly

around 29 GHz for ECC34 and ECC12, but still remain below the acceptable threshold of 0.5.

- **Diversity Gain:** The expression provided in Equation (5.2) is used to calculate *Diversity Gain*, as outlined below.

$$DiversityGain = 10^{*}sqrt(1 - ECC^{2}) \tag{5.2}$$

Figure 5.16 illustrates that the value obtained for *DG* is more than 9.90dB.

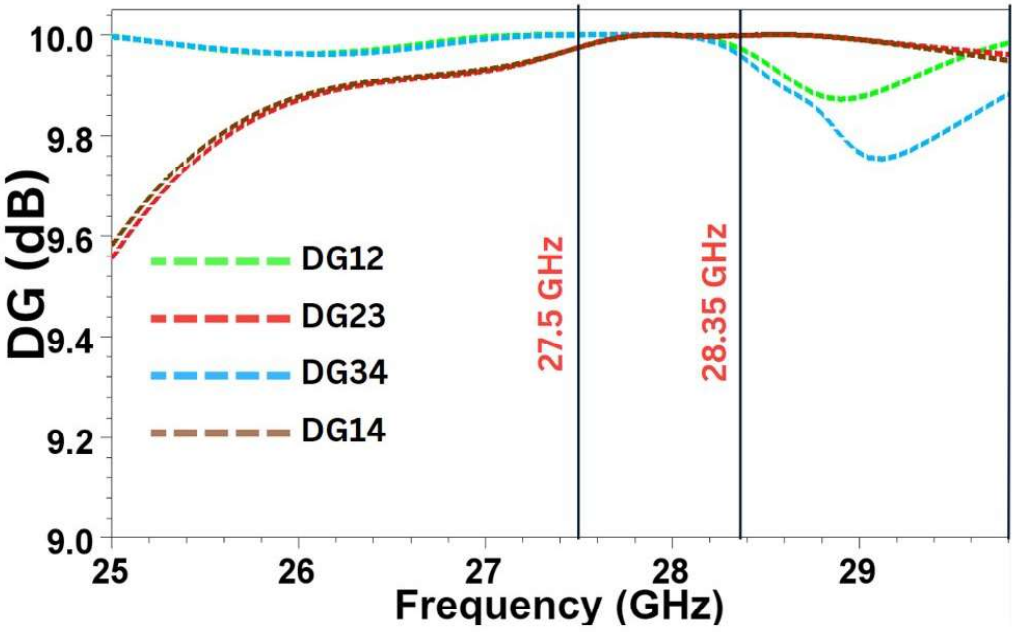

Fig. 5.12: Performance metrics of proposed MIMO antennain terms of Diversity Gain (DG)

Figure 5.16 presents the *Diversity Gain* performance for the proposed 4-port *MIMO* antenna across the 25–30 GHz range. The*DG* values for different antenna pairs: DG12, DG23, DG34, and DG14 are shown. All combinations maintain *DG* values close to 10 dB within the desired band of 27.5–28.35 GHz. DG12 and DG34 show minor variations, while DG23 and DG14 remain fairly stable. This indicates that the antenna maintains effective diversity performance across the target frequency band.

5.4.4 Surface Current

Figures 5.17 and 5.18 show the induced surface current of Antenna 1 and Antenna 2 at 27.8 GHz. As can be seen from these figures, large current is induced in dumbbell-shaped slot in ground plane when proposed antenna is excited from either antenna.

- **Antenna-1's surface current distribution** When Antenna 1 is excited at 27.8 GHz, the surface current distribution for the suggested 4×4 *MIMO* antenna is displayed. In the feed plane (top view), a strong current concentration is observed around the patch and feedline of Antenna 1, indicating effective excitation. The remaining antenna elements show minimal current presence, highlighting good isolation among the elements. In the ground plane (bottom view), current remains localized beneath Antenna 1, while the rest of the structure shows very low intensity. The use of slots and a *Defected Ground Structure* effectively limits current spread, thereby reducing coupling between antenna elements. These results confirm that the antenna structure maintains low mutual coupling through both the feed and ground planes.

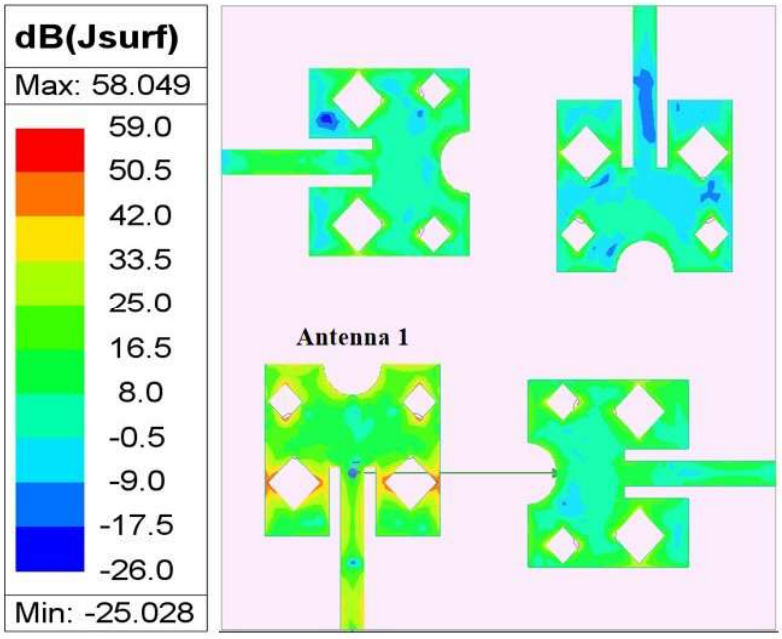

(a)

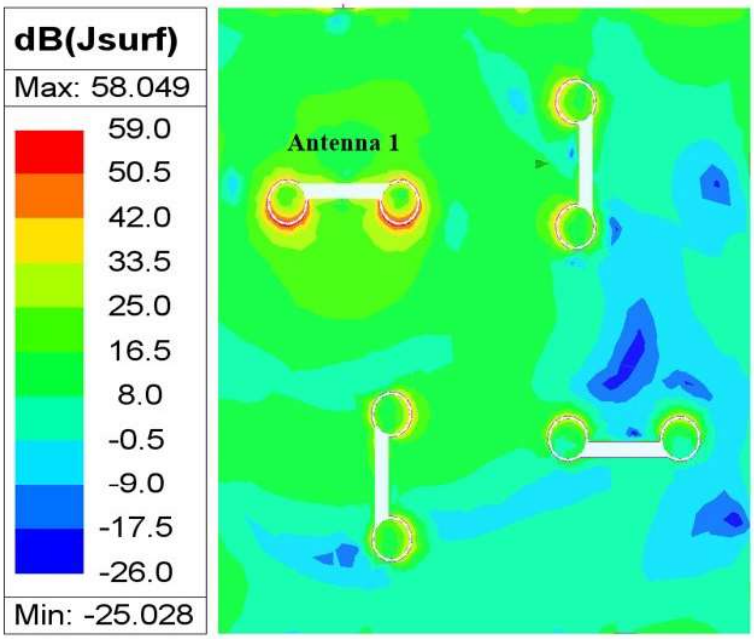

(b)

Fig. 5.13: The proposed MIMO antenna's surface current distribution at 27.8 GHz when Antenna-1 is excited (a) A feed plane that depicts the top view (b) The ground plane, which depicts the bottom view

- **Antenna-2's surface current distribution**

  The figure presents the surface current distribution of the proposed 4-port *MIMO* antenna at 27.8 GHz when Antenna-2 (Ant-2) is excited. In the feed plane (Figure 5.18 (a)), a strong current concentration is observed around the radiating patch and feed line of Antenna-2, indicating effective excitation. The ground plane top view (Figure 5.18 (b)) shows moderate current on adjacent elements, with limited spread, suggesting controlled mutual coupling. In the bottom view of the ground plane (Figure 5.18 (c)), the presence of the *Defected Ground Structure (DGS)* helps suppress unwanted surface currents, minimizing coupling between the ports. Overall, the current remains well-confined around the active element, supporting good isolation among antenna ports.

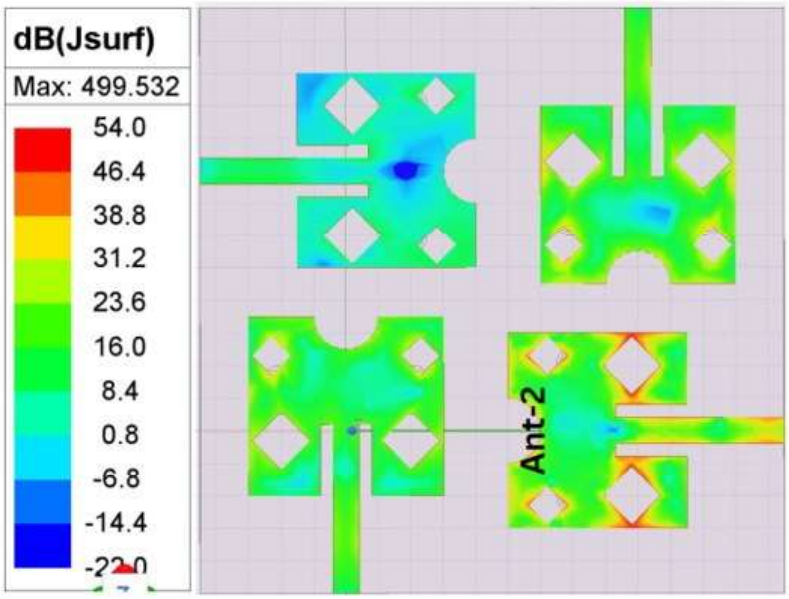

Feed Plane (top view)

(a)

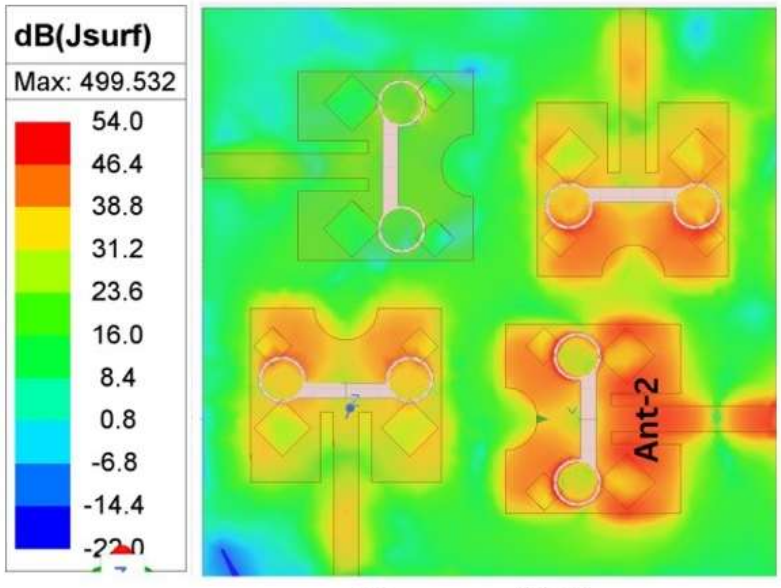

Ground Plane (top view)

(b)

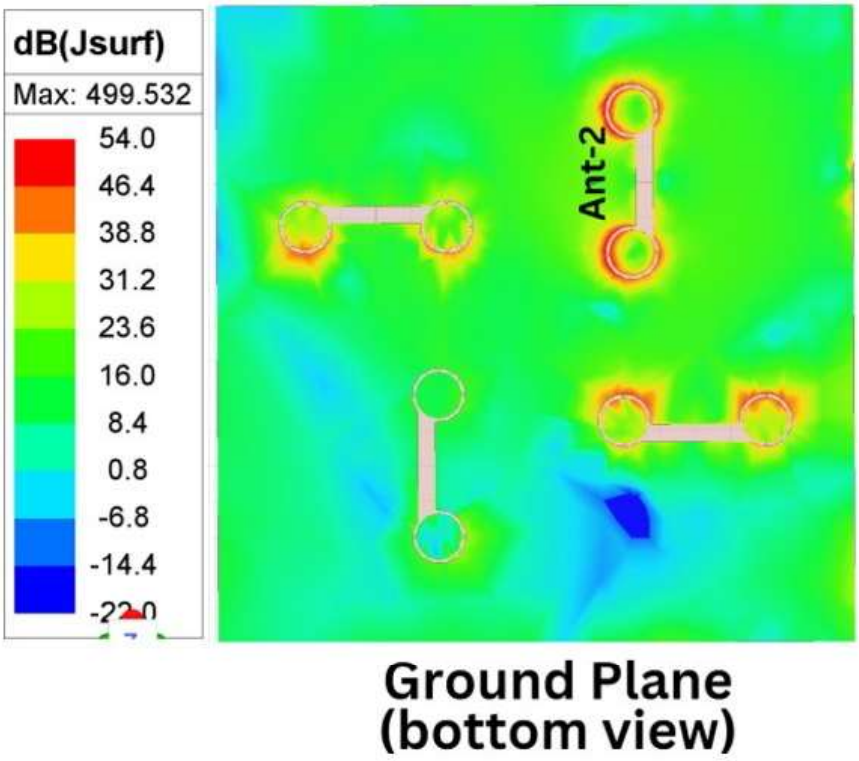

(c)

Fig. 5.14: Surface current distribution for the proposed MIMO antenna at 27.8 GHz when Antenna-2 is energized. Top view represents (a) the feed plane and (b) the ground plane. (c) Ground surface represents the bottom view.

This is consistent with what we talked about before in Section 4.4 of Chapter 4 where we notice substantial alteration in the resonant frequency when radius of the circular slot of dumbbell is changed. Also, the width of the horizontal rod of dumbbell was changed, and there was large variation in resonant frequency. So, we can clearly infer that the dumbbell-shaped slot in ground plane has substantial contribution in order to accomplish antenna response. Since the other antennas show a similar pattern, surface current for a single antenna is displayed.

Table 5.5 shows the comparison of earlier published articles related to four port *MIMO* structures with the proposed structures.

Table 5.5: Performance comparison of the proposed MIMO antenna with recent state-of-the-art designs

Ref.	Year	Centered Freq. (GHz)	BW (GHz)	Structure Shape	Size (mm)	No. of MIMO Ant.	DG (dB)	Peak Gain (dBi)	ECC	Min. Isolation (dB)
[147]	2024	28 (n257, n261)	4.87	Slotted Vivaldi Meander	50 x 20 x 1.6	1	na	6.65	na	na
[59]	2024	27 (n261) (Medical)	2	T-shaped Patch	22 x 17 x 0.5 (Single Element)	8	9.97	4.64	0.005	-22
[148]	2023	FR2, K, Ka, Ku, X (8.31 - 36.14)	27.83	Slotted Hexagonal Patch	20 x 20 x 0.254	4	> 9.99	7.17	< 0.01	na
[149]	2022	n257/n258/n261 (23 - 30.5)	7.5	Coplanar Feed Patch	26 x 5 x 1.524	4	na	9.76	na	>-16
[150]	2021	28	—	Rectangular slot in Feed and Ground plane	30 x 15 x 0.25	2	9.99	5.4	< 0.008	-35
[129]	2020	28 (26.71 - 28.91)	2.2	Metamaterial DRA	20 x 40 x 1.6	4	na	7	0.02	-29.34
[151]	2017	28	1.75	Cylindrical Dielectric Resonator (cDRA) based MIMO	40 x 10 x 1.6	2	na	7	< 0.4	-25
[102]	2021	28	1.5	Feedline with 3-circular shaped rings	30 x 30 x 0.78	4	9.87	6.1	< 0.16	-29
Our Work	2024	28 (n261)	0.85 (n261 exclusive)	Slotted Patch with Ground DGS	20 x 19 x 0.254	4	9.9	5.84	< 0.011	-19.5

5.5 SUMMARY

An antenna for the n261 mmWave band (27.5–28.35 GHz) with four ports is designed, simulated, fabricated, and tested in this chapter, targeting 5G applications. The antenna was optimized through parametric analysis and validated through measurements. Minor deviations in return loss and mutual coupling were observed but remained within acceptable limits. The radiation patterns confirmed good polarization diversity and balanced gain. Low *ECC* values and consistent *Diversity Gain* demonstrated strong *MIMO* performance. Surface current analysis showed effective isolation aided by the *DGS*. Overall, the design meets the objectives of compactness, isolation, and efficient operation for future wireless systems.

Chapter–6

Conclusions and Future Scope

This chapter provides an overview of the main conclusions of the study that concentrated on the design and fabrication of a planar *MIMO* antenna for mmWave applications.. The conclusions are presented in line with the research objectives, reflecting the progress made from literature review to simulation and experimental validation. It also highlights the major contributions of the work and suggests future directions to address remaining challenges in advancing *MIMO* antenna design for wireless systems of the next generation.

6.1 CONCLUSION

The thesis titled Design and Fabrication of MIMO Antenna for Millimeter Wave Applications systematically addressed the development of *MIMO* antennas for high-frequency wireless systems. In Chapter 1, the foundational aspects were established by presenting an overview of millimeter wave systems, the importance of *MIMO* technology in mmWave communication, and the key research gaps that prompted this investigation. Clearly defined objectives and methodology set the direction for the entire research work.

Chapter 2 reviewed extensive literature related to single-port, 2-port, 4-port *MIMO*and 8-port *MIMO* antennas designed for 5G applications. It also highlighted mutual coupling issues and methods used in past studies to minimize them, offering a strong background for the proposed designs.

In Chapter 3, a comprehensive comparative analysis of planar *MIMO* antennas operating in the millimeter frequency range was carried out. Performance metrics like *ECC*, *TARC*, *CCL*, and S-parameters were evaluated across different antenna types—slot, *DGS*, *DRA*s, and metasurface-based antennas—providing valuable insight into their relative advantages.

Chapter 4 focused on the design of a single antenna operating in the mmWave band. The design evolution, parametric studies, and simulation-based analysis (including gain, efficiency, and surface current) confirmed the structure's appropriateness for high-frequency uses.

In Chapter 5, a 4-port planar *MIMO* antenna was added to the design using the previously optimized single antenna element. Fabrication and testing confirmed the antenna's performance through real-time measurements, matching well with simulations. The proposed antenna exhibited improved gain, low mutual coupling, and good isolation, validating the research objectives.

The thesis's primary contributions can be summed up as follows:

- A detailed comparative study of various planar *MIMO* antenna configurations was carried out, highlighting key design trade-offs and performance metrics relevant to mmWave applications.
- To effectively improve isolation between elements, a *Defected Ground Structure (DGS)* was incorporated into a small planar *MIMO* antenna that was designed to operate at the 28 GHz millimeter wave band.
- Extensive parametric analysis of a single antenna element was conducted to optimize critical parameters, resulting in improved overall antenna performance.
- The successful fabrication and testing of a 4-port *MIMO* antenna prototype was accomplished. The effectiveness and practical viability of the suggested design were confirmed by the near match between the measured and simulated results.

6.2 FUTURE WORK

In the proposed work, a small planar *MIMO* antenna for millimeter wave applications was designed and constructed.. The research was carried out thoroughly, addressing key challenges identified from the existing literature. While the developed design meets the current objectives, several aspects remain open for future exploration to further improve antenna performance and adaptability in next-generation communication systems.

The following issues can be considered for future research:

- Enhancement of isolation techniques for more densely packed *MIMO* systems using advanced structures like *Electromagnetic Band Gap (EBG)* or Metamaterials.
- Development of reconfigurable or tunable *MIMO* antennas to support dynamic frequency bands and adaptive systems.
- Integration of conformal or flexible substrates to enable application in wearable and IoT-based platforms.
- Incorporation of beamforming or metasurface-based techniques for improved directionality and gain.
- Design of wideband or multiband antennas to support future 6G technologies requiring broader frequency operation.

.

List of Publications

JOURNAL PUBLICATIONS (SCOPUS)

1. Reena Aggarwal, Ajay Roy and Rajeev Kumar, "Millimeter Wave Antennas: a State-of-the-Art Survey of Recent Developments, Principles, and Applications," ***Progress In Electromagnetics Research B***, vol. 104, pp. 147-169, 2024.

   doi: https://doi:10.2528/PIERB23102401

2. Reena Aggarwal, Ajay Roy and Rajeev Kumar, "A Compact Four Port MIMO Antenna for n261 Millimeter Wave Band Applications," ***Progress In Electromagnetics Research M***, Vol. 129, 33-41, 2024. doi:10.2528/PIERM24080201

CONFERENCE PUBLICATIONS

1. Reena Aggarwal, Ajay Roy and Rajeev Kumar, "Comparative Analysis of Different Dielectric Substrate for the Design of Millimeter Wave Microstrip Patch Antenna. In: Singh, D., Chaudhary, R.K., Dev Kumar, K. (eds)," *Computer Aided Constellation Management and Communication Satellites. Lecture Notes in Electrical Engineering*, vol 987. Springer, Singapore. doi:https://doi.org/10.1007/978-981-19-8555-3_11

2. Reena Aggarwal, Ajay Roy. T.L. Singal and Rajeev Kumar, "(2024) Performance Analysis for Capacity Enhancement in Interference-limited Multi-User 5G Cellular System," in Proceedings of the International Conference on Emerging Technology and Sustainable Solutions- ICESS 2023, 040007. 10.1063/5.0228484.

References

[1] S. C. Shah, "Private mobile edge cloud for 5g network applications," *Internet Technology Letters*, vol. 2, no. 5, p. e124, 2019.

[2] P. R. Mane, P. Kumar, T. Ali, M. G. N. Alsath *et al.*, "Planar mimo antenna for mmwave applications: Evolution, present status & future scope," *Heliyon*, vol. 9, no. 2, 2023.

[3] H. Hanson and N. C. Kraus, "Long-term evolution of a long-term evolution model," *Journal of Coastal Research*, no. 59, pp. 118–129, 2011.

[4] D. Brenner, "Global 5g spectrum update," *Spectrum Strategy & Technology Poilcy*, 2020.

[5] S. Forge and K. Vu, "Forming a 5g strategy for developing countries: A note for policy makers," *Telecommunications Policy*, vol. 44, no. 7, p. 101975, 2020.

[6] Z. Pi and F. Khan, "An introduction to millimeter-wave mobile broadband systems," *IEEE communications magazine*, vol. 49, no. 6, pp. 101–107, 2011.

[7] J. Du and R. A. Valenzuela, "How much spectrum is too much in millimeter wave wireless access," *IEEE journal on selected areas in communications*, vol. 35, no. 7, pp. 1444–1458, 2017.

[8] C. Sudhamani, M. Roslee, J. J. Tiang, and A. U. Rehman, "A survey on 5g coverage improvement techniques: Issues and future challenges," *Sensors*, vol. 23, no. 4, p. 2356, 2023.

[9] R. Aggarwal, A. Roy, and R. Kumar, "Millimeter wave antennas: A state-of-the-art survey of recent developments, principles, and applications." *Progress in Electromagnetics Research B*, vol. 104, 2024.

[10] J. S. Cetnar, "Atmospheric effects on the propagation of mmw and sub-mmw radiation," Master's thesis, Wright State University, 2010.

[11] T. T. Oladimeji, P. Kumar, and N. O. Oyie, "Propagation path loss prediction modelling in enclosed environments for 5g networks: A review," *Heliyon*, vol. 8, no. 11, 2022.

[12] A. Kumar and M. Gupta, "A review on activities of fifth generation mobile communication system," *Alexandria Engineering Journal*, vol. 57, no. 2, pp. 1125–1135, June 2018.

[13] S. Parkvall, E. Dahlman, A. Furuskar, and M. Frenne, "Nr: The new 5g radio access technology," *IEEE Communications Standards Magazine*, vol. 1, no. 4, pp. 24–30, 2017.

[14] M. Zada, I. A. Shah, and H. Yoo, "Integration of sub-6-ghz and mm-wave bands with a large frequency ratio for future 5g mimo applications," *IEEE Access*, vol. 9, pp. 11 241–11 251, 2021.

[15] R. Dybdal, "Millimeter wave antenna technology," *IEEE Journal on Selected Areas in Communications*, vol. 1, no. 4, pp. 633–644, September 1983.

[16] M. S. Islam, M. Kamruzzaman, T. Jessy, M. S. Zahan, and M. S. Hassan, "Performance analysis of massive MIMO for 5G wireless communication systems," in *2016 International Conference on Computing, Communication and Automation (ICCCA)*, Apr. 2016, pp. 1579–1583.

[17] M. E. Shorbagy, R. M. Shubair, M. I. AlHajri, and N. K. Mallat, "On the design of millimetre-wave antennas for 5G," in *2016 16th Mediterranean Microwave Symposium (MMS)*, Nov. 2016, pp. 1–4.

[18] E. A. Abbas, M. Ikram, A. T. Mobashsher, and A. Abbosh, "Mimo antenna system for multi-band millimeter-wave 5g and wideband 4g mobile communications," *IEEE Access*, vol. 7, pp. 181 916–181 923, 2019.

[19] H. M. Marzouk, M. I. Ahmed, and A. A. Shaalan, "A novel dual-band 28/38 ghz slotted microstrip mimo antenna for 5g mobile applications," in *2019 IEEE International Symposium on Antennas and Propagation and USNC-URSI Radio Science Meeting*, Atlanta, GA, USA, Jul. 2019, pp. 607–608.

[20] M. Labidi and F. Choubani, "A design of metamaterials mimo antenna for millimeter wave application," in *2019 International Conference on Software, Telecommunications and Computer Networks (SoftCOM)*, Split, Croatia, Sep. 2019, pp. 1–4.

[21] X. Shen, Y. Liu, L. Zhao, G.-L. Huang, X. Shi, and Q. Huang, "A miniaturized microstrip antenna array at 5g millimeter-wave band," *IEEE Antennas and Wireless Propagation Letters*, vol. 18, no. 8, pp. 1671–1675, Aug. 2019.

[22] S. Zhang, Z. Ying, J. Xiong, and S. He, "Ultrawideband MIMO/diversity antennas with a tree-like structure to enhance wideband isolation," *IEEE Antennas Wireless Propag. Lett.*, vol. 8, pp. 1279–1282, 2009.

[23] C.-M. Luo, J.-S. Hong, and L.-L. Zhong, "Isolation enhancement of a very compact UWB-MIMO slot antenna with two defected ground structures," *IEEE Antennas Wireless Propag. Lett.*, vol. 14, pp. 1161–1164, 2015.

[24] C. R. Jetti and V. R. Nandanavanam, "A very compact MIMO antenna with triple band-notch function for portable UWB systems," *Prog. Electromagn. Res. C*, vol. 82, pp. 13–27, 2018.

[25] R. Chandel, A. K. Gautam, and K. Rambabu, "Tapered fed compact UWB MIMO-diversity antenna with dual band-notched characteristics," *IEEE Trans. Antennas Propag.*, vol. 66, no. 4, pp. 1677–1684, 2018.

[26] J. Zhu, B. Feng, B. Peng, S. Li, and L. Deng, "Compact CPW UWB diversity slot antenna with dual band-notched characteristics," *Microw. Opt. Technol. Lett.*, vol. 58, no. 4, pp. 989–994, 2016.

[27] H. Al-Saif, M. Usman, M. T. Chughtai, and J. Nasir, "Compact ultra-wide band MIMO antenna system for lower 5g bands," *Wirel. Commun. Mob. Comput.*, vol. 2018, p. 2396873, 2018.

[28] S. R. Patre and S. P. Singh, "Shared radiator MIMO antenna for broadband applications," *IET Microw. Antennas Propag.*, vol. 12, no. 7, pp. 1153–1159, 2018.

[29] B. Feng, J. Lai, Q. Zeng, and K. L. Chung, "A dual-wideband and high gain magneto-electric dipole antenna and its 3D MIMO system with metasurface for 5G/WiMAX/WLAN/X-band applications," *IEEE Access*, vol. 6, pp. 30 191–30 202, 2018.

[30] L. Chen, H. Wong, and K. M. Luk, "Compact 2×2 MIMO antenna for 28-GHz 5g applications with high isolation," *IEEE Antennas Wireless Propag. Lett.*, vol. 19, no. 6, pp. 1030–1034, 2020.

[31] A. Elfatimi, S. Bri, and A. Saadi, "Single feed compact millimeter wave antenna for future 5g applications," in *2018 International Conference on Intelligent Systems and Computer Vision (ISCV)*, 2018, pp. 1–4.

[32] S. Kumar and A. Kumar, "Design of circular patch antennas for 5g applications," in *2019 2nd International Conference on Innovations in Electronics, Signal Processing and Communication (IESC)*. IEEE, 2019, pp. 287–289.

[33] C. M. Saleh, E. Almajali, S. S. Alja'Afreh, and J. Yousaf, "Dual u-slot patch antenna for 5g applications," in *2021 IEEE International Symposium on Antennas and Propagation and USNC-URSI Radio Science Meeting (APS/URSI)*. IEEE, 2021, pp. 349–350.

[34] S. Pavithra and K. Vidhya, "Design of a circular microstrip patch antenna with high gain for 5g applications using 5g millimeter wave bands comparing to rectangular microstrip patch antenna," in *2022 2nd International Conference on Technological Advancements in Computational Sciences (ICTACS)*. IEEE, 2022, pp. 30–34.

[35] Y. Liu, X. Yang, Y. Jia, and Y. J. Guo, "A low correlation and mutual coupling mimo antenna," *IEEE Access*, vol. 7, pp. 127 384–127 392, 2019.

[36] M. Usman, E. Kobal, J. Nasir, and Y. Zhu, "Compact siw fed dual-port single element annular slot mimo antenna for 5g mmwave applications," *IEEE Access*, vol. 10, pp. 124 823–124 831, 2022.

[37] M. Ameen, R. K. Chaudhary, and S. Ghosh, "Millimeter-wave high-gain and highly isolated diversity mimo array antenna for 5g wireless applications," in *2022 IEEE Microwaves, Antennas, and Propagation Conference (MAPCON)*. IEEE, 2022, pp. 1203–1208.

[38] C. Manirathnam, S. Ghosh, and M. Swati, "A compact, two-port mimo antenna for mm-wave 5g application," in *2022 IEEE 11th International Conference on Communication Systems and Network Technologies (CSNT)*. IEEE, 2022, pp. 22–25.

[39] J. Jakhar, T. Jhajharia, and B. Gupta, "Asymmetric flare shape patch mimo antenna for millimeter wave 5g communication systems," *Prog. Electromagn. Res. C*, vol. 136, pp. 75–86, 2023.

[40] V. Koushick, D. R. Kumar, S. H. Basha, S. Asadh, and S. M. W. Khadri, "Design and analysis of wide-band 2-port mimo antenna for 5g wireless applications," in *2024 International Conference on Inventive Computation Technologies (ICICT)*. IEEE, 2024, pp. 1437–1445.

[41] S. Angadi, Y. Sharma, and N. Raghava, "A metasurface based close-proximity two-port circularly polarized mimo antenna for mid-band sub-6 ghz 5g applications," *AEU - International Journal of Electronics and Communications*, vol. 164, p. 155563, 2024, published August 1, 2024.

[42] M. S. Aung and T. Hla, "Two-port wideband mimo antenna for sub-6ghz 5g applications," *International Journal of Antennas and Propagation*, vol. 2024, pp. 1–6, 2024.

[43] C. Munusami and R. Venkatesan, "A compact boat shaped dual-band mimo antenna with enhanced isolation for 5g/wlan application," *International Journal of RF and Microwave Computer-Aided Engineering*, 2024, published online in 2024.

[44] T. Hlias and S. Koulouridis, "A two-port metamaterial antenna for mm-wave 5g mimo applications with enhanced bandwidth and gain," in *2024 18th European Conference on Antennas and Propagation (EuCAP)*. IEEE, 2024, pp. 1–5.

[45] H. Chattha, "4-port 2-element mimo antenna for 5g portable applications," *IEEE Access*, vol. 7, pp. 91 012–91 018, Jun 2019. [Online]. Available: https://ieeexplore.ieee.org/document/8759910

[46] M. Khalid, S. I. Naqvi, N. Hussain, M. Rahman, Fawad, S. S. Mirjavadi, M. J. Khan, and Y. Amin, "4-port mimo antenna with defected ground structure for 5g millimeter wave applications," *Electronics*, vol. 9, no. 1, p. 71, 2020. [Online]. Available: https://www.mdpi.com/2079-9292/9/1/71

[47] S. I. Naqvi and N. Hussain, "Integrated lte and millimeter-wave 5g mimo antenna system for 4g/5g wireless terminals," *Electronics*, vol. 9, no. 1, p. 69, 2020.

[48] A. Patel, A. Desai, I. Elfergani, A. Vala, H. Mewada, K. Mahant, S. Patel, C. Zebiri, J. Rodriguez, and E. Ali, "Uwb cpw fed 4-port connected ground mimo antenna for sub-millimeter-wave 5g applications," *Alexandria Engineering Journal*, vol. 61, no. 9, pp. 6645–6658, 2022.

[49] M. Bilal, S. I. Naqvi, N. Hussain, Y. Amin, and N. Kim, "High-isolation mimo antenna for 5g millimeter-wave communication systems," *Electronics*, vol. 11, no. 6, p. 962, 2022.

[50] C. Güler and S. E. Bayer Keskin, "A novel high isolation 4-port compact mimo antenna with dgs for 5g applications," *Micromachines*, vol. 14, no. 7, p. 1309, 2023.

[51] M. A. Abbas, A. Allam, A. Gaafar, H. M. Elhennawy, and M. F. A. Sree, "Compact uwb mimo antenna for 5g millimeter-wave applications," *Sensors*, vol. 23, no. 5, p. 2702, 2023.

[52] S. Ghosh, G. S. Baghel, and M. Swati, "Design of a highly-isolated, high-gain, compact 4-port mimo antenna loaded with csrr and dgs for millimeter wave 5g communications," *AEU-International Journal of Electronics and Communications*, vol. 169, p. 154721, 2023.

[53] C. Du, F. Zhang, and R. Li, "Design of tri-band flexible cpw 4-port slot mimo antenna for conformal 5g, wifi 6/6e and x-band applications," *Engineering Science and Technology, an International Journal*, vol. 62, p. 101937, 2025.

[54] M. Khalid, A. Manan, S. I. Naqvi, H. Zahra, C.-C. Chang, and S. M. Abbas, "5g millimeter-wave eight-port mimo antenna," in *2021 International Symposium on Antennas and Propagation (ISAP)*. IEEE, 2021, pp. 1–2.

[55] Y. Q. Hei, J. G. He, and W. T. Li, "Wideband decoupled 8-element mimo antenna for 5g mobile terminal applications," *IEEE Antennas and Wireless Propagation Letters*, vol. 20, no. 8, pp. 1448–1452, 2021.

[56] Y. Fawad, S. Ullah, M. Irfan, R. Ullah, S. Rahman, F. Muhammad, A. H. Almawgani, and S. N. F. Mursal, "Dual-polarized 8-port sub 6 ghz 5g mimo diamond-ring slot antenna for smart phone and portable wireless applications," *Plos one*, vol. 18, no. 11, p. e0288793, 2023.

[57] B. Mishra, V. Yadav, A. Pandey, C. Mh, R. SethuMadhavi, T. Satheesha, and P. Yadav, "High isolated 8-port mimo antenna and 16-port massive antenna for mm wave (5g nr-n260) applications in time division duplex mode," *Scientific Reports*, vol. 14, no. 1, p. 31023, 2024.

[58] M. Srinubabu and N. V. Rajasekhar, "A compact and highly isolated integrated 8-port mimo antenna for sub-6 ghz and mm-wave 5g-nr applications," *Results in Engineering*, p. 104068, 2025.

[59] A. Gupta, M. Kumari, M. Sharma, M. H. Alsharif, P. Uthansakul, M. Uthansakul, and S. Bansal, "8-port mimo antenna at 27 ghz for n261 band and exploring for body centric communication," *PLOS ONE*, vol. 19, no. 6, p. e0305524, 2024.

[60] J. Blanch, J. Romeu, and I. Corbella, "Exact representation of antenna system diversity performance from input parameter description," *Electronics Letters*, vol. 39, no. 9, pp. 705–707, 2003.

[61] S. Zhang, Z. N. Ying, J. Xiong, and S. He, "A novel formula for envelope correlation coefficient of multiport antennas including radiation efficiency," *IEEE Transactions on Antennas and Propagation*, vol. 64, no. 9, pp. 3943–3948, Sep 2016.

[62] Y.-S. Kim, H.-S. Kim, and Y.-J. Park, "Diversity gain and correlation coefficient of MIMO antennas," *IEICE Transactions on Communications*, vol. E88-B, no. 1, pp. 362–364, 2005. [Online]. Available: https://search.ieice.org/bin/summary.php?id=e88-b_1_362

[63] I. Szini, D. K. Karmokar, and K. Roy, "Diversity performance evaluation of MIMO antennas using ECC and DG," *IEEE Antennas and Propagation Magazine*, vol. 52, no. 6, pp. 232–243, 2010.

[64] J. W. Wallace and M. A. Jensen, "Mutual coupling in MIMO wireless systems: A rigorous network theory analysis," *IEEE Transactions on Wireless Communications*, vol. 3, no. 4, pp. 1316–1327, 2004.

[65] F. Zhao, W. Li, L. Qi, H. Zhang, and R. N. Simons, "TARC-based bandwidth definition for MIMO antennas," *IEEE Antennas and Wireless Propagation Letters*, vol. 16, pp. 2183–2186, 2017.

[66] W.-Q. Li, L.-L. Xiao, and J. Sun, "Compact UWB-MIMO antenna with high isolation and low CCL," *Progress in Electromagnetics Research C*, vol. 42, pp. 25–33, 2013. [Online]. Available: https://www.jpier.org/PIERC/pierc42/03.13053104.pdf

[67] C. A. Balanis, *Antenna theory: analysis and design*. John wiley & sons, 2016.

[68] M. S. Sharawi, "Current misuses and future prospects for printed multiple-input, multiple-output antenna systems [wireless corner]," *IEEE Antennas and Propagation Magazine*, vol. 59, no. 2, pp. 162–170, 2017.

[69] L. Zhong, R. Yu, and X. Hong, "Review of carbon-based electromagnetic shielding materials: film, composite, foam, textile," *Textile Research Journal*, vol. 91, p. 004051752096828, 10 2020.

[70] D. M. Pozar, *Microwave Engineering*, 4th ed. Hoboken, NJ, USA: Wiley, 2011.

[71] W. L. Stutzman and G. A. Thiele, *Antenna Theory and Design*, 3rd ed. Hoboken, NJ, USA: Wiley, 2012.

[72] R. Vaughan and J. Andersen, *Channels, Propagation and Antennas for Mobile Communications*. Stevenage, UK: Institution of Engineering and Technology (IET), 2003.

[73] G. F. Pedersen, J. B. Andersen, and H. S. Jensen, "MEG evaluation of small terminal antennas," *IEEE Transactions on Antennas and Propagation*, vol. 48, no. 5, pp. 713–721, 2000.

[74] H. Nakano and J. Yamauchi, "Printed slot and wire antennas: A review," *Proceedings of the IEEE*, vol. 100, no. 7, pp. 2158–2168, 2012.

[75] Y. Long, Z. Chen, and J. Fang, "Nonasymptotic analysis of capacity in massive mimo systems," *IEEE Wireless Communications Letters*, vol. 4, no. 5, pp. 541–544, 2015.

[76] A. A. Deshmukh and A. Rane, "Extc, svkm's djsce india."

[77] R. Kumar, G. S. Saini, and D. Singh, "Compact tri-band patch antenna for ku band applications," *Progress In Electromagnetics Research C*, vol. 103, pp. 45–58, 2020.

[78] A. Wa'il, R. M. Shaaban, and Z. A. Ahmed, "A modified e-shaped microstrip patch antenna for dual band in x-and ku-bands applications," in *Journal of Physics: Conference Series*, vol. 1234, no. 1. IOP Publishing, 2019, p. 012028.

[79] A. Dastranj and H. Abiri, "Bandwidth enhancement of printed e-shaped slot antennas fed by cpw and microstrip line," *IEEE Transactions on Antennas and Propagation*, vol. 58, no. 4, pp. 1402–1407, 2010.

[80] K.-F. Tong and T.-P. Wong, "Circularly polarized u-slot antenna," *IEEE Transactions on antennas and propagation*, vol. 55, no. 8, pp. 2382–2385, 2007.

[81] R. Xu, J.-Y. Li, J.-J. Yang, K. Wei, and Y.-X. Qi, "A design of u-shaped slot antenna with broadband dual circularly polarized radiation," *IEEE Transactions on Antennas and Propagation*, vol. 65, no. 6, pp. 3217–3220, 2017.

[82] Y. Sung, "Bandwidth enhancement of a wide slot using fractal-shaped sierpinski," *IEEE transactions on antennas and propagation*, vol. 59, no. 8, pp. 3076–3079, 2011.

[83] W.-L. Chen, G.-M. Wang, and C.-X. Zhang, "Bandwidth enhancement of a microstrip-line-fed printed wide-slot antenna with a fractal-shaped slot," *IEEE Transactions on Antennas and Propagation*, vol. 57, no. 7, pp. 2176–2179, 2009.

[84] E. Kobal, R.-J. Liu, C. Yu, and A. Zhu, "A high isolation, low-profile, triple-port siw based annular slot antenna for millimeter-wave 5g mimo applications," *IEEE Access*, vol. 10, pp. 89 458–89 464, 2022.

[85] J. Wang, Y. Li, and J. Wang, "A low-profile dual-mode slot-patch antenna for 5g millimeter-wave applications," *IEEE Antennas and Wireless Propagation Letters*, vol. 21, no. 3, pp. 625–629, 2022.

[86] C. R. Jetti, T. Addepalli, S. R. Devireddy, G. K. Tanimki, A. J. A. Al-Gburi, Z. Zakaria, and P. Sunitha, "Design and analysis of modified u-shaped four element mimo antenna for dual-band 5g millimeter wave applications," *Micromachines*, vol. 14, no. 8, p. 1545, 2023.

[87] S. Jabeen and Q. U. Khan, "An integrated mimo antenna design for sub-6ághz & millimeter-wave applications with high isolation," *AEU-International Journal of Electronics and Communications*, vol. 153, p. 154247, 2022.

[88] D. A. Sehrai, M. Abdullah, A. Altaf, S. H. Kiani, F. Muhammad, M. Tufail, M. Irfan, A. Glowacz, and S. Rahman, "A novel high gain wideband mimo antenna for 5g millimeter wave applications," *Electronics*, vol. 9, no. 6, p. 1031, 2020.

[89] A. Patel, A. Vala, A. Desai, I. Elfergani, H. Mewada, K. Mahant, C. Zebiri, D. Chauhan, and J. Rodriguez, "Inverted-l shaped wideband mimo antenna for millimeter-wave 5g applications," *Electronics*, vol. 11, no. 9, p. 1387, 2022.

[90] S. M. El-Nady and A. M. Attiya, "Periodically-stub-loaded microstrip line wideband circularly polarized millimeter wave mimo antenna," *IEEE Access*, vol. 10, pp. 20 465–20 472, 2022.

[91] W. Ali, S. Das, H. Medkour, and S. Lakrit, "Planar dual-band 27/39 ghz millimeter-wave mimo antenna for 5g applications," *Microsystem Technologies*, vol. 27, pp. 283–292, 2021.

[92] U. Farooq and A. Lokam, "A compact 26/39 ghz millimeter wave mimo antenna design for 5g iot applications," *Journal of Infrared, Millimeter, and Terahertz Waves*, vol. 44, no. 5, pp. 333–345, 2023.

[93] M. Khalid, S. Iffat Naqvi, N. Hussain, M. Rahman, Fawad, S. S. Mirjavadi, M. J. Khan, and Y. Amin, "4-port mimo antenna with defected ground structure for 5g millimeter wave applications," *Electronics*, vol. 9, no. 1, p. 71, 2020.

[94] A. Abdullah, H. Ahmad, M. Rahman, M. Haris, and M. Salman, "Wideband four-port compact millimeter-wave mimo antenna configuration through defected ground structure for forthcoming 5g handheld devices," *Progress In Electromagnetics Research C*, vol. 117, pp. 173–184, 2021.

[95] A. K. Dwivedi, N. K. Narayaswamy, V. Singh, and M. S. Darmanar, "Uwb-mimo dgs loaded patch antenna with low profile for millimeter-wave applications," *Journal of Electrical Engineering*, vol. 73, no. 1, pp. 28–35, 2022.

[96] S. Sharma and M. Arora, "A millimeter wave elliptical slot circular patch mimo antenna for future 5g mobile communication networks," *Progress In Electromagnetics Research M*, vol. 110, no. 13, 2022.

[97] J. Joseph, G. S. Let, C. B. Pratap, and J. J. Winston, "A miniaturized uniplanar mimo antenna for n79/n46/millimeter-wave applications," *International Journal of Communication Systems*, vol. 36, no. 9, p. e5477, 2023.

[98] A. Kumar and A. Kumar, "Defected ground structure based high gain, wideband and high diversity performance quad-element mimo antenna array for 5g millimeter-wave communication." *Progress In Electromagnetics Research B*, vol. 101, 2023.

[99] R. Hussain, M. Abou-Khousa, N. Iqbal, A. Algarni, S. I. Alhuwaimel, A. Zerguine, and M. S. Sharawi, "A multiband shared aperture mimo antenna for millimeter-wave and sub-6ghz 5g applications," *Sensors*, vol. 22, no. 5, p. 1808, 2022.

[100] A. Tahat, B. Ersan, L. Muhesen, Z. Shakhshir, and T. A. Edwan, "A compact 38 ghz millimetre-wave mimo antenna array for 5g mobile systems," *Journal of Telecommunications and the Digital Economy*, vol. 8, no. 3, pp. 44–59, 2020.

[101] B. Yang, Z. Yu, Y. Dong, J. Zhou, and W. Hong, "Compact tapered slot antenna array for 5g millimeter-wave massive mimo systems," *IEEE Transactions on Antennas and Propagation*, vol. 65, no. 12, pp. 6721–6727, 2017.

[102] M. M. Kamal, S. Yang, X.-c. Ren, A. Altaf, S. H. Kiani, M. R. Anjum, A. Iqbal, M. Asif, and S. I. Saeed, "Infinity shell shaped mimo antenna array for mm-wave 5g applications," *Electronics*, vol. 10, no. 2, p. 165, 2021.

[103] L. Malviya and P. Gupta, "Millimeter wave high-gain antenna array for wireless applications," *IETE Journal of Research*, vol. 69, no. 5, pp. 2645–2654, 2023.

[104] J. Khan, S. Ullah, U. Ali, F. A. Tahir, I. Peter, and L. Matekovits, "Design of a millimeter-wave mimo antenna array for 5g communication terminals," *Sensors*, vol. 22, no. 7, p. 2768, 2022.

[105] I. Ud Din, M. Alibakhshikenari, B. S. Virdee, R. K. R. Jayanthi, S. Ullah, S. Khan, C. H. See, L. Golunski, and S. Koziel, "Frequency-selective surface-based mimo antenna array for 5g millimeter-wave applications," *Sensors*, vol. 23, no. 15, p. 7009, 2023.

[106] M. S. Mandloi, P. Gupta, A. Parmar, P. Malviya, and L. Malviya, "Beamforming mimo array antenna for 5g-millimeter-wave application," *Wireless Personal Communications*, vol. 129, no. 1, pp. 153–172, 2023.

[107] S. Keyrouz and D. Caratelli, "Dielectric resonator antennas: basic concepts, design guidelines, and recent developments at millimeter-wave frequencies," *International Journal of Antennas and propagation*, vol. 2016, no. 1, p. 6075680, 2016.

[108] E. Erfani, T. Denidni, S. Tatu, and M. Niroo-Jazi, "A broadband and high gain millimeter-wave hybrid dielectric resonator antenna," in *2016 17th International Symposium on Antenna Technology and Applied Electromagnetics (ANTEM)*. IEEE, 2016, pp. 1–2.

[109] Q. Lai, C. Fumeaux, W. Hong, and R. Vahldieck, "60 ghz aperture-coupled dielectric resonator antennas fed by a half-mode substrate integrated waveguide," *IEEE Transactions on Antennas and Propagation*, vol. 58, no. 6, pp. 1856–1864, 2010.

[110] P. Bijumon, Y. Antar, A. Freundorfer, and M. Sayer, "Integrated dielectric resonator antennas for system on-chip applications," in *2007 Internatonal Conference on Microelectronics*. IEEE, 2007, pp. 275–278.

[111] ——, "Dielectric resonator antenna on silicon substrate for system on-chip applications," *IEEE Transactions on Antennas and Propagation*, vol. 56, no. 11, pp. 3404–3410, 2008.

[112] J. Joseph, G. S. Let, C. B. Pratap, and J. J. Winston, "A miniaturized uniplanar mimo antenna for n79/n46/millimeter-wave applications," *International Journal of Communication Systems*, vol. 36, no. 9, p. e5477, 2023.

[113] P. V. Bijumon, Y. M. M. Antar, A. P. Freundorfer, and M. Sayer, "Integrated dielectric resonator antennas for system on-chip applications," in *Proceedings of the International Conference on Microelectronics (ICM '07)*. Cairo, Egypt: IEEE, December 2007, pp. 275–278.

[114] A. A. Abdulmajid, S. Khamas, and S. Zhang, "Wideband high-gain millimetre-wave three-layer hemispherical dielectric resonator antenna," *Progress In Electromagnetics Research C*, vol. 103, pp. 225–236, 2020.

[115] I. A. Zubir, M. Othman, U. Ullah, S. Kamal, M. F. Ab Rahman, R. Hussin, M. F. B. M. Omar, A. S. Mohammed, M. F. B. Ain, Z. A. Ahmad *et al.*, "A low-profile hybrid multi-permittivity dielectric resonator antenna with perforated structure for ku and k band applications," *IEEE Access*, vol. 8, pp. 151 219–151 228, 2020.

[116] E. Baldazzi, A. Al-Rawi, R. Cicchetti, A. B. Smolders, O. Testa, C. d. J. van Coevorden Moreno, and D. Caratelli, "A high-gain dielectric resonator antenna with plastic-based conical horn for millimeter-wave applications," *IEEE Antennas and Wireless Propagation Letters*, vol. 19, no. 6, pp. 949–953, 2020.

[117] K. Gong and X. H. Hu, "Low-profile substrate integrated dielectric resonator antenna implemented with pcb process," *IEEE Antennas and Wireless Propagation Letters*, vol. 13, pp. 1023–1026, 2014.

[118] P. R. Meher, B. R. Behera, and S. K. Mishra, "Design and its state-of-the-art of different shaped dielectric resonator antennas at millimeter-wave frequency band," *International Journal of RF and Microwave Computer-Aided Engineering*, vol. 30, no. 7, p. e22221, 2020.

[119] W. M. A. Wahab, D. Busuioc, and S. Safavi-Naeini, "Low cost planar waveguide technology-based dielectric resonator antenna (dra) for millimeter-wave applications: Analysis, design, and fabrication," *IEEE Transactions on Antennas and Propagation*, vol. 58, no. 8, pp. 2499–2507, 2010.

[120] W. M. Abdel-Wahab, Y. Wang, and S. Safavi-Naeini, "Siw hybrid feeding network-integrated 2-d dra array: Simulations and experiments," *IEEE Antennas and Wireless Propagation Letters*, vol. 15, pp. 548–551, 2015.

[121] W. M. Abdel-Wahab, M. Abdallah, J. Anderson, Y. Wang, H. Al-Saedi, and S. Safavi-Naeini, "Siw-integrated parasitic dra array: Analysis, design, and measurement," *IEEE Antennas and Wireless Propagation Letters*, vol. 18, no. 1, pp. 69–73, 2018.

[122] W. Mazhar, D. M. Klymyshyn, G. Wells, A. A. Qureshi, M. Jacobs, and S. Achenbach, "Low-profile artificial grid dielectric resonator antenna arrays for mm-wave applications," *IEEE Transactions on Antennas and Propagation*, vol. 67, no. 7, pp. 4406–4417, 2019.

[123] W. M. Abdel-Wahab, D. Busuioc, and S. Safavi-Naeini, "Millimeter-wave high radiation efficiency planar waveguide series-fed dielectric resonator antenna (dra) array: analysis, design, and measurements," *IEEE Transactions on Antennas and Propagation*, vol. 59, no. 8, pp. 2834–2843, 2011.

[124] Y.-T. Liu, B. Ma, S. Huang, S. Wang, Z. J. Hou, and W. Wu, "Wideband low-profile connected rectangular ring dielectric resonator antenna array for millimeter-wave applications," *IEEE Transactions on Antennas and Propagation*, vol. 71, no. 1, pp. 999–1004, 2022.

[125] A. Dadgarpour, B. Zarghooni, B. S. Virdee, T. A. Denidni, and A. A. Kishk, "Mutual coupling reduction in dielectric resonator antennas using metasurface shield for 60-ghz mimo systems," *IEEE Antennas and Wireless Propagation Letters*, vol. 16, pp. 477–480, 2016.

[126] M. Farahani, J. Pourahmadazar, M. Akbari, M. Nedil, A. R. Sebak, and T. A. Denidni, "Mutual coupling reduction in millimeter-wave mimo antenna array using a metamaterial polarization-rotator wall," *IEEE Antennas and Wireless Propagation Letters*, vol. 16, pp. 2324–2327, 2017.

[127] Y. M. Pan, X. Qin, Y. X. Sun, and S. Y. Zheng, "A simple decoupling method for 5g millimeter-wave mimo dielectric resonator antennas," *IEEE Transactions on Antennas and Propagation*, vol. 67, no. 4, pp. 2224–2234, 2019.

[128] Y. Zhang, J.-Y. Deng, M.-J. Li, D. Sun, and L.-X. Guo, "A mimo dielectric resonator antenna with improved isolation for 5g mm-wave applications," *IEEE Antennas and Wireless Propagation Letters*, vol. 18, no. 4, pp. 747–751, 2019.

[129] N. Murthy, "Improved isolation metamaterial inspired mm-wave mimo dielectric resonator antenna for 5g application," *Progress In Electromagnetics Research C*, vol. 100, pp. 247–261, 2020.

[130] H. Chu and Y.-X. Guo, "A novel approach for millimeter-wave dielectric resonator antenna array designs by using the substrate integrated technology," *IEEE Transactions on Antennas and Propagation*, vol. 65, no. 2, pp. 909–914, 2016.

[131] A. Gaya, M. H. Jamaluddin, B. Alali, and A. A. Althuwayb, "A novel wide dual band circularly polarized dielectric resonator antenna for milli meter wave 5g applications," *Alexandria Engineering Journal*, vol. 61, no. 12, pp. 10 791–10 803, 2022.

[132] R.-Z. Huang, J.-W. Zhang, and C. Zhang, "Dual-band circularly polarized hybrid dielectric resonator antenna for 5g millimeter-wave applications," *Electronics*, vol. 11, no. 11, p. 1761, 2022.

[133] G. Zhao, Y. Zhou, J. R. Wang, and M. S. Tong, "A circularly polarized dielectric resonator antenna based on quasi-self-complementary metasurface," *IEEE Transactions on Antennas and Propagation*, vol. 70, no. 8, pp. 7147–7151, 2022.

[134] H. Xu, Z. Chen, H. Liu, L. Chang, T. Huang, S. Ye, L. Zhang, and C. Du, "Single-fed dual-circularly polarized stacked dielectric resonator antenna for k/ka-band uav satellite communications," *IEEE Transactions on Vehicular Technology*, vol. 71, no. 4, pp. 4449–4453, 2022.

[135] M. D. Alanazi, "A review of dielectric resonator antenna at mm-wave band," *Eng*, vol. 4, no. 1, pp. 843–856, 2023.

[136] S. Kumar and H. Singh, "A comprehensive review of metamaterials/metasurface-based mimo antenna array for 5g millimeter-wave applications," *Journal of Superconductivity and Novel Magnetism*, vol. 35, no. 11, pp. 3025–3049, 2022.

[137] M. Singh, S. Singh, and M. T. Islam, "Csrr loaded high gained 28/38ghz printed mimo patch antenna array for 5g millimeter wave wireless devices," *Microelectronic Engineering*, vol. 262, p. 111829, 2022.

[138] A. D. Tadesse, O. P. Acharya, and S. Sahu, "A compact planar four-port mimo antenna for 28/38 ghz millimeter-wave 5g applications," *Advanced Electromagnetics*, vol. 11, no. 3, pp. 16–25, 2022.

[139] B. A. Esmail and S. Koziel, "High isolation metamaterial-based dual-band mimo antenna for 5g millimeter-wave applications," *AEU-International Journal of Electronics and Communications*, vol. 158, p. 154470, 2023.

[140] S. Tariq, S. I. Naqvi, N. Hussain, and Y. Amin, "A metasurface-based mimo antenna for 5g millimeter-wave applications," *IEEE Access*, vol. 9, pp. 51 805–51 817, 2021.

[141] N. Hussain, M.-J. Jeong, A. Abbas, and N. Kim, "Metasurface-based single-layer wideband circularly polarized mimo antenna for 5g millimeter-wave systems," *Ieee Access*, vol. 8, pp. 130 293–130 304, 2020.

[142] S. Kumar and A. S. Dixit, "Wideband antipodal vivaldi antenna using metamaterial for micrometer and millimeter wave applications," *Journal of Infrared, Millimeter, and Terahertz Waves*, vol. 42, no. 9, pp. 974–985, 2021.

[143] S. Juneja, R. Pratap, and R. Sharma, "Design of a highly directive, wideband and compact endfire antenna array for 5g applications," in *2022 IEEE International Conference of Electron Devices Society Kolkata Chapter (EDKCON)*. IEEE, 2022, pp. 558–562.

[144] S. Juneja and R. Sharma, "Study of techniques to improve performance of patch antennas for 5g applications at millimeter wave (mmw) frequencies," in *IOP Conference Series: Materials Science and Engineering*, vol. 1022, no. 1. IOP Publishing, 2021, p. 012033.

[145] D. M. Pozar, "Design of aperture-coupled microstrip antennas," *IEEE Transactions on Antennas and Propagation*, vol. 37, no. 12, pp. 1534–1537, 1989.

[146] L. Liu, S. W. Cheung, and T. I. Yuk, "A review of millimeter-wave antennas for 5g applications," *Proceedings of the IEEE*, vol. 104, no. 10, pp. 2023–2035, 2016.

[147] N. R. Palepu, J. Kumar, S. Peddakrishna, and A. Ghosh, "Wideband meander-line-antipodal-vivaldi slot-antenna for millimeter-wave applications," *e-Prime-Advances in Electrical Engineering, Electronics and Energy*, vol. 9, p. 100641, 2024.

[148] M. Sharma, P. R. Kapula, S. Salagrama, K. Sharma, G. P. Pandey, D. K. Singh, M. Mahajan, and A. Gupta, "Miniaturized quad-port conformal multi-band (qpc-mb) mimo antenna for on-body wireless systems in microwave-millimeter bands," *IEEE access*, vol. 11, pp. 105 982–105 999, 2023.

[149] J.-J. Lo, Z. N. Chen *et al.*, "Design of a broadband millimeter-wave array antenna for 5g applications," *IEEE Antennas and Wireless Propagation Letters*, vol. 22, no. 5, pp. 1030–1034, 2022.

[150] N. Hussain, W. A. Awan, W. Ali, S. I. Naqvi, A. Zaidi, and T. T. Le, "Compact wideband patch antenna and its mimo configuration for 28 ghz applications," *AEU-International Journal of Electronics and Communications*, vol. 132, p. 153612, 2021.

[151] M. S. Sharawi, S. K. Podilchak, M. T. Hussain, and Y. M. Antar, "Dielectric resonator based mimo antenna system enabling millimetre-wave mobile devices," *IET Microwaves, Antennas & Propagation*, vol. 11, no. 2, pp. 287–293, 2017.